



universität
wien

MASTERARBEIT

Titel der Masterarbeit

„C-Parameter with Massive Quarks“

Verfasser

Moritz Preißer, BSc

angestrebter akademischer Grad

Master of Science (MSc)

Wien, 2014

Studienkennzahl lt. Studienblatt:

A 066 876

Studienrichtung lt. Studienblatt:

Masterstudium Physik UG2002

Betreuerin / Betreuer:

o.Univ.Prof. Dr. André Hoang

Abstract

In this thesis mass effects from primary bottom quark production in $e^+e^- \rightarrow \text{hadrons}$ are investigated. We focus on the differential cross-section of the C-parameter. Since the original definition of the C-parameter is not very sensitive to heavy quark masses, a suitable generalization, called the massive C-parameter, is defined. To resum large logarithms in a systematic way, soft-collinear effective theory (SCET) is used. In the dijet region, which corresponds to a minimal value of the C-parameter, this effective field theory (EFT) imposes a certain power counting by introducing a small parameter $\lambda \sim \sqrt{C}/6$, which separates the cross-section into a leading (called singular) and a subleading (called non-singular) part. In analogy with the massless C-parameter, we derive a factorization theorem for the singular cross-section, where each factor describes the dynamics at a different energy-scale. These factors are computed to $\mathcal{O}(\alpha_s)$, and by using standard renormalization-group (RG) methods we achieve the resummation of large logarithms to N²LL accuracy. Furthermore we determine the non-singular part of the cross-section by computing the full QCD result to $\mathcal{O}(\alpha_s)$, which up to now was only known through a parton level monte carlo generator. In addition, non-perturbative power corrections are treated by convoluting the perturbative cross-section with a non-perturbative shape function. To improve the convergence of the perturbative series the $\overline{\text{MS}}$ short-distance mass is used, and the leading renormalon of the soft function is removed. As a practical application we analyze primary bottom quark mass-effects at center-of-mass energies of 35 GeV and 91 GeV. This analysis is carried out for tagged $b\bar{b}$ -production and all-flavor production.

Zusammenfassung

In dieser Arbeit werden Masseneffekte von der Produktion primärer Bottom Quarks bei dem Prozess $e^+e^- \rightarrow \text{Hadronen}$ untersucht. Dabei betrachten wir im Speziellen den differentiellen Wirkungsquerschnitt des C-Parameters. Da die ursprüngliche Definition des C-Parameter nicht ausreichend sensitiv auf die untersuchten Masseneffekte ist, führen wir eine geeignete Verallgemeinerung, welche wir massiver C-Parameter nennen, ein. Weiters arbeiten wir im Rahmen der soft-collinear effective theory (SCET) um die auftretenden großen Logarithmen in einer systematischen Art und Weise zu resumieren. In der 2-Jet Region, welche einem minimalen C-Parameter Wert entspricht, führt diese effektive Feldtheorie (EFT) einen power-counting Parameter $\lambda \sim \sqrt{C}/6$ ein, welcher die Abspaltung eines führenden Terms (dieser wird singulär genannt) erlaubt. Analog zum masselosen C-Parameter, leiten wir ein Faktorisierungstheorem für den singulären Teil des Wirkungsquerschnitts her, wobei die auftretenden Faktoren jeweils die Dynamik an einer anderen Energie-Skala berücksichtigen. Anschließend werden diese Faktoren zu $\mathcal{O}(\alpha_s)$ berechnet und große Logarithmen mit Hilfe von Renormalisierungsgruppen-Gleichungen auf N²LL resummiert. Um den nicht-singulären Anteil des Wirkungsquerschnitts zu bestimmen wurden die Berechnungen auch in voller QCD zu $\mathcal{O}(\alpha_s)$ durchgeführt, wobei die Ergebnisse bisher nur mit Hilfe eines Parton-Level Monte Carlo Generators zugänglich waren. Weiters werden nicht-perturbative Effekte mittels einer Faltung zwischen perturbativen Wirkungsquerschnitt mit einer sogenannten shape-function berücksichtigt. Um die Konvergenz der Störungsreihe zu verbessern verwenden wir die $\overline{\text{MS}}$ -Masse und subtrahieren das führende Renormalon der soft function. Als praktische Anwendung analysieren wir primäre Bottom Quark Masseneffekte bei einer Schwerpunktsenergie von 35 GeV und 91 GeV. Dabei wird der Wirkungsquerschnitt von tagged $b\bar{b}$ Produktion und der Produktion aller Flavor untersucht.

Contents

1. Introduction	1
2. The C-parameter	3
3. Fixed-Order Calculations	5
3.1. General Considerations, Leptonic Tensor and Born Cross-Section	5
3.2. Radiative Part	7
3.3. Virtual Contributions	17
3.4. The Delta Coefficient and the Full FO Result	18
4. Soft-Collinear Effective Theory	20
4.1. Light Cone Coordinates and Mode Separation	20
4.2. SCET Fields and the Lagrangian	21
4.3. Wilson Lines	22
5. Factorization for the Massive c-Parameter	25
5.1. General Factorization Formula	25
5.2. Kinematic Considerations	26
5.3. Massive c-Parameter Factorization Formula	28
6. Resummed Cross-Section	30
6.1. Large Log Resummation and the Renormalization Group	30
6.2. Hard, Jet and Partonic Soft Function	33
6.3. Non-Singular Cross-Section	39
6.4. Non-Perturbative Corrections	41
6.5. Renormalons, $\overline{\text{MS}}$ Mass and Gap	43
6.6. Final Result	46
7. Analysis	48
7.1. Profile Function	48
7.2. Initial $b\bar{b}$ -Pair Production	51
7.3. All Flavor Production	54
8. Outlook	56
A. Radiative Contribution to the FO result	57
A.1. Reduction of Elliptic Integrals to Legendre's Normal Form	57
A.2. Radiative FO Result in Legendre's Normal Form	58
B. Distributions and useful Identities	60
C. Massive SCET Feynman Rules	62
D. Details on Hard-, Jet- and partonic Soft-Function Calculation	63
D.1. Jet Function	63
D.2. Hard Function	67
D.3. Partonic Soft Function	68
E. Evolution	69
E.1. Anomalous Dimensions and Evolution Kernels	69
E.2. R-Evolution	69
E.3. Evolution of α_s and the $\overline{\text{MS}}$ Mass	70

1. Introduction

In the modern era of particle physics the theoretical community is confronted with experimental collaborations which achieve more and more precise data measurements. To keep up with this development one of the major issues in theoretical particle physics is how to provide predictions with comparably small uncertainties. Concerning this issue and the particular case of QCD a class of observables, called *event-shapes* [1,2], has a long tradition. These observables were extensively used to test QCD as the theory of the strong interaction and also for high-precision determinations of its fundamental parameters. In general an event-shape e quantifies the geometrical shape of the final state 3-momentum distribution which is why these observables are well suited for investigating many-particle final states.

Some of the most commonly observed objects in modern high-energy experiments are hadronic jets, which are objects consisting of collimated high energetic hadrons. The amount of particles which are contained in a jet might be very large which is why event-shape variables are well suited to treat problems involving such objects. A special subclass, the so called 2-jet event shapes (e.g. thrust and C-parameter) are defined by the fact that they vanish (for massless particles) in the case of a so-called dijet configuration. This configuration is given by two strongly collimated (sometimes called pencil-like) jets and only additional soft radiation. In the dijet configuration each jet has a small invariant mass.

It is known that, close to the dijet region, the perturbative series for event-shape observables, such as thrust or the C-parameter, includes terms which are enhanced by large logarithms. These terms prohibit a good convergence of the fixed order series and therefore yield large uncertainties for this region. To get reliable predictions it is mandatory to resum these terms to all orders of perturbation theory. Then the remaining (unresummed) terms should only give small corrections as one would expect from higher order contributions. In the past this resummation was achieved by utilizing an *exponentiation* property of different event shapes, e.g. for thrust [3] and for the C-parameter [4].

In recent years a more systematic approach, using effective field theory (EFT) methods, was developed. Therefore *soft-collinear effective theory* (SCET) [5–9] was applied to calculate the differential cross-section for different 2-jet event-shape observables e including thrust [10,11] and the C-parameter [12]. In the dijet region SCET exploits the large scale hierarchies by imposing a certain power counting in terms of the small parameter $\lambda \sim \sqrt{e}$. This allows us to split the cross-section into a leading (called singular) and a subleading (called non-singular) part. Within the framework of SCET it is then possible to derive a factorization formula for the singular part where each factor accounts for the dynamics at a different energy scale. By using standard renormalization group (RG) methods it is then possible to resum large logarithms in a systematic way.

Except for the mentioned thrust analysis, earlier studies assumed that the produced primary quarks were massless. At large energies, mass effects are usually small and the assumption of massless partons simplifies the calculations significantly. However, mass effects play an important role in a number of cases and should therefore be studied in more detail. This is why recently an effort to further investigate and quantify these effects was made [13–15].

For the C-parameter study of [12], which aims for a precise determination of $\alpha_s(m_Z)$, also no quark mass effects were included. It is interesting whether mass effects have a sizable impact on this study and thereby cause larger errors in the final result. To clarify this and related issues we intend to study mass effects in the differential C-parameter cross-section.

The outline of this work is as follows. In Sec. 2 we introduce the original C-parameter and its generalization for treating massive partons. Throughout this work the generalization, which of course yields the correct massless limit, will be the used observable.

In Sec. 3 we compute the full QCD differential cross-section to $\mathcal{O}(\alpha_s)$, which up to now was only

accessible through a parton level Monte Carlo generator. This result is then used to calculate the non-singular contributions and for checking the FO limit of the singular cross-section.

In Sec. 4 and 5 we introduce SCET and related issues. We discuss the derivation of the massive SCET Lagrangian from which the massive SCET Feynman Rules can be obtained. Furthermore we derive a factorization theorem for the singular part of the massive C-parameter differential cross-section. This factorization theorem will later allow us to resum large logarithms in a systematic way.

In Sec. 6 the different contributions to the factorization theorem are computed to $\mathcal{O}(\alpha_s)$. Furthermore we calculate the so called *evolution kernels* which allow for a large log resummation to next-to-next-to-leading-logarithmic accuracy. In addition we treat non-perturbative hadronization effects using a so-called *shape function*. Afterwards we discuss the issue of *renormalons* which helps to improve the convergence of the perturbative series. This leads us to use the $\overline{\text{MS}}$ short-distance mass and to remove the leading renormalon in the soft function with a proper subtraction series for the associated gap parameter.

In Sec. 7 we turn towards practical applications. First we introduce the concept of *profile functions*, motivate their general behavior for the massless case and introduce a possible generalization for massive partons. Afterwards we investigate mass effects in the case of tagged $b\bar{b}$ -production. Therefore we compare the differential cross-section of the massless and the massive case with different order of log-resummation at center of mass (c.o.m.) energies of 35 GeV and 91 GeV. Furthermore we discuss the needed ingredients to modify our setup for the case of $t\bar{t}$ -production. Lastly we investigate bottom quark mass effects in the case of all flavor production as in [12].

2. The C-parameter

Since the late 1970s a class of observables called *event-shapes* was used to test and determine fundamental properties of QCD (for a review see [1, 2]). Their main field of application is e^+e^- annihilation and DIS but they have also been used in a variety of other processes. In the following we will concentrate on mass effects contributing to the measurement of a specific e^+e^- annihilation event-shape which was introduced by Ellis, Ross and Terrano in 1980 [16] called the *C-parameter*. The mass effects we intend to study are introduced by the initial production of a heavy quark antiquark pair (primary massive quarks) in the hard process. The purpose of this section is to define an observable which is well suited for treating mass effects and at the same time yields the correct massless result, hence we call it *massive C-parameter*.

To define the original C-parameter one looks at the so-called linearized momentum tensor which was introduced as [17, 18]:

$$\Theta^{kl} = \frac{1}{\sum_j |\vec{p}_j|} \sum_i \frac{p_i^k p_i^l}{|\vec{p}_i|}, \quad (2.1)$$

where p_i^k denotes the k -th spacial component of the i -th final state particle and the sum runs over all final state particles. In general this is a symmetric 3×3 matrix on which we impose energy and 3-momentum conservation. Overall this yields two degrees of freedom which can be written as parameters in the characteristic polynomial of the matrix. This defines the original C and D-parameter [16]:

$$\lambda^3 - \text{Tr}[\Theta] \lambda^2 + \frac{C}{3} \lambda - \frac{D}{27} = 0, \quad (2.2)$$

which in terms of the eigenvalues λ_i of the matrix read (it is easy to see that $\text{Tr}[\Theta] = 1$):

$$C = \frac{3}{2} (\text{Tr}[\Theta]^2 - \text{Tr}[\Theta^2]) = 3(\lambda_1 \lambda_2 + \lambda_1 \lambda_3 + \lambda_2 \lambda_3), \quad (2.3)$$

$$D = 27 \det(\Theta) = 27 \lambda_1 \lambda_2 \lambda_3. \quad (2.4)$$

As stated before we are interested in the original C-parameter which is then given by:

$$C = \frac{3}{2} \left[1 - \frac{1}{(\sum_j |\vec{p}_j|)^2} \sum_{i,j} \frac{(\vec{p}_i \cdot \vec{p}_j)^2}{|\vec{p}_i| |\vec{p}_j|} \right] = \frac{3}{2} \frac{\sum_{i,j} |\vec{p}_i| |\vec{p}_j| (1 - \cos^2(\theta_{ij}))}{(\sum_j |\vec{p}_j|)^2} = \frac{3}{2} \frac{\sum_{i,j} |\vec{p}_i| |\vec{p}_j| \sin^2(\theta_{ij})}{(\sum_j |\vec{p}_j|)^2}, \quad (2.5)$$

where θ_{ij} denotes the angle between the three-vectors of the i -th and j -th final state particle.

When treating mass effects the denominator involving moduli of three-momenta will make analytic calculations more difficult. To avoid this we want to define a new observable which yields the correct massless result. A suitable candidate is defined in terms of Lorentz invariants [16]:

$$C = \frac{3}{2} \left[2 - \sum_{i \neq j} \frac{(p_i \cdot p_j)^2}{(p_i \cdot q)(p_j \cdot q)} \right] \stackrel{(\text{c.o.m.})}{=} \frac{3}{2} \left[2 - \frac{1}{Q^2} \sum_{i \neq j} \frac{(p_i \cdot p_j)^2}{p_i^0 p_j^0} \right], \quad (2.6)$$

where p_i denotes the momentum of the i -th final state particle, $q = \sum_i p_i$ is the sum of all particle momenta and Q the total center of mass (c.o.m.) energy. If one compares Eq. (2.6) to Eq. (2.5) one can see that indeed they have the same massless limit since $p_i^0 = |\vec{p}_i|$ for $m = 0$. Although the definition of the original C-parameter involves the mentioned linearized momentum tensor it was not possible to relate the definition of the massive C-parameter to some kind of analogous quantity. However, this form of the C-parameter was already used in an earlier analysis involving massless quarks and an off-shell gluon [19] and will subsequently be the investigated observable.

Two Massive Quarks and a Massless Gluon

In the remainder of this work we will concentrate on the $\mathcal{O}(\alpha_s)$ contributions to the C-parameter cross-section. This involves two possible final states namely $Q\bar{Q}$ and $Q\bar{Q}g$. The first one is trivial and we therefore turn towards the second possibility. This final state represents a massive quark antiquark pair which emits a massless gluon. For convenience we will now (in analogy with [19]¹) rescale our observable to $c = C/6$ and call this the *c-parameter*.

Furthermore we define the variables x_i ($i = 1, 2, 3$) for the three particle final state $Q\bar{Q}g$ involving p_1, p_2, p_3 the quark, antiquark and gluon momentum, respectively. They are given by:

$$x_i = \frac{2p_i^0}{Q}. \quad (2.7)$$

Then energy momentum conservation takes the form:

$$2 = x_1 + x_2 + x_3, \quad \vec{0} = \hat{n}_1 \sqrt{x_1^2 - 4\hat{m}^2} + \hat{n}_2 \sqrt{x_2^2 - 4\hat{m}^2} + \hat{n}_3 x_3, \quad (2.8)$$

where \hat{n}_i is the direction of the 3-momentum of the corresponding particle and $\hat{m} = m/Q$ the Q-normalized quark (antiquark) mass. Using this we find:

$$\begin{aligned} (\vec{p}_1 + \vec{p}_2)^2 &= (\vec{p}_3)^2 = (\vec{p}_1)^2 + (\vec{p}_2)^2 + 2\vec{p}_1 \cdot \vec{p}_2 = (p_1^0)^2 + (p_2^0)^2 - 2m^2 + 2\vec{p}_1 \cdot \vec{p}_2 \equiv (p_3^0)^2 \\ \Rightarrow x_3^2 &= 4 + x_1^2 + x_2^2 - 4x_1 - 4x_2 + 2x_1x_2 = x_1^2 + x_2^2 - 8\hat{m}^2 + \frac{8}{Q^2}\vec{p}_1 \cdot \vec{p}_2 \\ \Rightarrow (4/Q^2)\vec{p}_1 \cdot \vec{p}_2 &= 2 + x_1x_2 + 4\hat{m}^2 - 2x_1 - 2x_2, \end{aligned} \quad (2.9)$$

and analogously:

$$(4/Q^2)\vec{p}_1 \cdot \vec{p}_3 = 2 + x_1x_3 - 2x_1 - 2x_3, \quad (2.10)$$

$$(4/Q^2)\vec{p}_2 \cdot \vec{p}_3 = 2 + x_2x_3 - 2x_2 - 2x_3. \quad (2.11)$$

With these relations it is easy to derive the following expressions which appear in the c-parameter definition:

$$\begin{aligned} p_1 \cdot p_2 &= p_1^0 p_2^0 - \vec{p}_1 \cdot \vec{p}_2 = (Q^2/2)(x_1 + x_2 - 1 - 2\hat{m}^2), \\ p_1 \cdot p_3 &= (Q^2/2)(x_1 + x_3 - 1), \\ p_2 \cdot p_3 &= (Q^2/2)(x_2 + x_3 - 1). \end{aligned} \quad (2.12)$$

Using this and simplifying the full expression one arrives at the final form of the $Q\bar{Q}g$ c-parameter in terms of the two independent phase space variables x_1 and x_2 :

$$c \equiv g(x_1, x_2, \hat{m}) = \frac{(1-x_1)(1-x_2)(x_1+x_2-1)}{x_1x_2(2-x_1-x_2)} + \frac{2\hat{m}^2}{x_1x_2}(x_1+x_2-1) - \frac{2\hat{m}^4}{x_1x_2}. \quad (2.13)$$

This formula is the foundation of the following analysis and of course also yields the correct massless result (see [16] and Eq. (2.12) therein).

¹In [12] the authors study the massless C-parameter and call the more convenient one $\tilde{c} = C/6$.

3. Fixed-Order Calculations

In this section we will calculate $\mathcal{O}(\alpha_s)$ QCD results for the differential massive c-parameter cross-section. Since we intend to sum up large logarithms to all orders in perturbation theory which are not contained in the $\mathcal{O}(\alpha_s)$ result (see Sec. 6.1) we may also refer to this as a fixed-order (FO) calculation. This means we study the production of a massive $Q\bar{Q}$ pair and add later a virtual or real gluon in QCD.

The real radiation part is calculated in $d = 4$ dimensions since the computation in $d = 4 - 2\epsilon$ dimensions is complicated and not necessarily needed (the calculations are performed in Sec. 3.2.1). Of course in four dimensions the singular cross-section is not properly regularized. However, since one knows the distributive structure of the cross-section one can extract the correctly regularized expression. To determine the delta function term $\sim \delta(c - c_{\min})$ we integrate the obtained result and subtract it from the integrated hadronic cross-section which is given in [20]. This yields a numeric coefficient for the delta term which is discussed in more detail in Sec. 3.4.

The virtual part of the cross-section is proportional to a delta function. Since the delta term will be evaluated numerically it is not needed to compute the full analytic expression. However, later we will switch to an effective field theory of QCD called *soft-collinear effective theory* (see Sec. 4) and therefore need virtual matrix elements (the calculations are done in Sec. 3.3) for the matching of SCET to QCD.

3.1. General Considerations, Leptonic Tensor and Born Cross-Section

We start by looking at the known formula for a general $e^+ + e^- \rightarrow X$ scattering cross-section formula:

$$\sigma = \frac{1}{2Q^2} \int \prod_{i \in X} \frac{d^{d-1}p_i}{(2\pi)^{d-1}} \frac{1}{2p_i^0} (2\pi)^d \delta^{(d)}\left(q - \sum_{i \in X} p_i\right) |\mathcal{M}(e^+e^- \rightarrow X)|^2, \quad (3.1)$$

where $q = k_1 + k_2$ is the momentum of the intermediate γ or Z with $q^2 = Q^2$ the squared center of mass energy, k_1 (k_2) the momentum of the electron (positron) and p_i the momentum of the i -th final state particle.

We will only look at the leading $\mathcal{O}(\alpha)$ contribution which is why the amplitude can be factorized as follows:

$$\begin{aligned} \mathcal{M} = \frac{i4\pi\alpha\tilde{\mu}^{2\epsilon}}{Q^2} \left\{ \left[\left(Q_e Q_f + \frac{v_e v_f}{1 - \hat{m}_z^2} \right) \langle X | \mathcal{J}_v^\mu | 0 \rangle + \left(\frac{v_e a_f}{1 - \hat{m}_z^2} \right) \langle X | \mathcal{J}_a^\mu | 0 \rangle \right] [\bar{v}(k_1) \gamma_\mu u(k_2)] \right. \\ \left. + \left[\left(\frac{a_e v_f}{1 - \hat{m}_z^2} \right) \langle X | \mathcal{J}_v^\mu | 0 \rangle + \left(\frac{a_e a_f}{1 - \hat{m}_z^2} \right) \langle X | \mathcal{J}_a^\mu | 0 \rangle \right] [\bar{v}(k_1) \gamma_\mu \gamma_5 u(k_2)] \right\}. \end{aligned} \quad (3.2)$$

The v and a factors from the coupling of fermions to the Z -boson are given by:

$$v_f = \frac{T_{3,L}^f - 2Q_f \sin^2(\theta_w)}{\sin(2\theta_w)}, \quad a_f = -\frac{T_{3,L}^f}{\sin(2\theta_w)}, \quad (3.3)$$

where $T_{3,L}^f$ denotes the weak isospin, Q_f stands for the electric charge of the produced fermion and θ_w is the weak mixing angle (also called Weinberg angle). Furthermore we introduced vector and axial-vector currents which are given by:

$$\mathcal{J}_i^\mu(x) = \bar{\psi}(x) \Gamma_i^\mu \psi(x), \quad \Gamma_v^\mu = \gamma^\mu, \quad \Gamma_a^\mu = \gamma^\mu \gamma_5. \quad (3.4)$$

The next step is to square the amplitude and take the spin sums. Since we consider the electron and positron to be massless the involved tensor structures on the leptonic side are given by:

$$\begin{aligned}
 s_{\mu\nu}^{(1)} &= \sum_{\text{spins}} [\bar{v}(k_1)\gamma_\mu u(k_2)]^\dagger [\bar{v}(k_1)\gamma_\nu u(k_2)] = \text{Tr}[\not{k}_1\gamma_\nu\not{k}_2\gamma_\mu] = 4g_{\mu\alpha}g_{\nu\beta}(k_1^\beta k_2^\alpha + k_1^\alpha k_2^\beta) - 4g_{\mu\nu}k_1 \cdot k_2, \\
 s_{\mu\nu}^{(2)} &= \sum_{\text{spins}} [\bar{v}(k_1)\gamma_\mu\gamma_5 u(k_2)]^\dagger [\bar{v}(k_1)\gamma_\nu\gamma_5 u(k_2)] = 4g_{\mu\alpha}g_{\nu\beta}(k_1^\beta k_2^\alpha + k_1^\alpha k_2^\beta) - 4g_{\mu\nu}k_1 \cdot k_2, \\
 s_{\mu\nu}^{(3)} &= \sum_{\text{spins}} [\bar{v}(k_1)\gamma_\mu\gamma_5 u(k_2)]^\dagger [\bar{v}(k_1)\gamma_\nu u(k_2)] = -4i\epsilon_{\alpha\nu\beta\mu}k_1^\alpha k_2^\beta, \\
 s_{\mu\nu}^{(4)} &= \sum_{\text{spins}} [\bar{v}(k_1)\gamma_\mu u(k_2)]^\dagger [\bar{v}(k_1)\gamma_\nu\gamma_5 u(k_2)] = -4i\epsilon_{\alpha\mu\beta\nu}k_1^\alpha k_2^\beta.
 \end{aligned} \tag{3.5}$$

Since we are only interested in a differential treatment of the final state we do not care about the orientation of final-state particles w.r.t. the beam axis, hence we average over all beam directions (directions of the incoming leptons). To do this we make the most general ansatz and afterwards demand the averaged tensor structures of Eq. (3.5) to take this form:

$$l_{\mu\nu} = A \cdot \frac{q_\mu q_\nu}{Q^2} + B \cdot g_{\mu\nu} \quad \Rightarrow \quad \int \frac{d^{d-2}\Omega}{\Omega_{\text{tot}}^{d-2}} s_{\mu\nu}^{(i)} \stackrel{!}{=} l_{\mu\nu}, \tag{3.6}$$

where we used the total solid angle in $(d-2)$ -dimensions (with $d = 4 - 2\epsilon$) $\Omega_{\text{tot}}^{d-2} = \Omega_{\text{tot}}^{2-2\epsilon} = \frac{2\pi^{1-\epsilon}}{\Gamma(1-\epsilon)}$. Next we determine the coefficients A and B by looking at the contractions with k^μ , k^ν and $g^{\mu\nu}$. Since $s_{\mu\nu}^{(3)}$ and $s_{\mu\nu}^{(4)}$ are antisymmetric while the used ansatz is symmetric we find the coefficients in this case to be zero. For $s_{\mu\nu}^{(1)}$ and $s_{\mu\nu}^{(2)}$ we find the following coefficients:

$$A = \left(\frac{d/2 - 1}{d - 1} \right) = \left(\frac{1 - \epsilon}{3 - 2\epsilon} \right), \quad B = -A, \tag{3.7}$$

and afterwards define the leptonic tensor structure as:

$$\tilde{l}_{\mu\nu} = \frac{q_\mu q_\nu}{Q^2} - g_{\mu\nu}. \tag{3.8}$$

The leptonic tensor structure is therefore symmetric under exchange of μ and ν . To get a non-zero contribution to the cross-section the hadronic structure should also be symmetric. This results in the fact that when squaring the amplitude we also get no mixing of vector and axial-vector contributions on the hadronic side.

Furthermore the full cross-section might receive contributions from more than one final state configuration, thus we sum over different final states X . This yields the final form of our cross-section formula (where we define the leptonic and hadronic tensor)²:

$$\begin{aligned}
 \sigma &= \sum_X \int d\Pi_X (2\pi)^d \delta^{(d)}(q - P_X) \sum_{i=a,v} L_{\mu\nu}^i \langle 0 | \mathcal{J}_i^{\mu\dagger}(0) | X \rangle \langle X | \mathcal{J}_i^\nu(0) | 0 \rangle \\
 &= \sum_X \int d\Pi_X (2\pi)^d \delta^{(d)}(q - P_X) \sum_{i=a,v} L_{\mu\nu}^i H_i^{\mu\nu}.
 \end{aligned} \tag{3.9}$$

Since the intended analysis might also involve higher energies, close to m_Z , we have to modify the leptonic tensor to incorporate the full Z propagator which involves a non-zero width. The leptonic

²Note that the spin and polarization sums are omitted. Since we have unpolarized electron (positron) beams we have to average over the incoming spin configurations where we get another factor of $1/4$.

tensor is then given by:

$$L_{\mu\nu}^v = c_{lep}^v \cdot \tilde{l}_{\mu\nu} \quad (3.10)$$

$$= \tilde{\mu}^{4\epsilon} \left(\frac{1-\epsilon}{3-2\epsilon} \right) \frac{8\pi^2\alpha^2}{Q^4} \left(Q_e^2 Q_f^2 + \frac{v_f^2(v_e^2 + a_e^2)}{(1-\hat{m}_Z^2)^2 + (\frac{\Gamma_Z}{m_Z})^2} + \frac{2Q_e Q_f v_e v_f (1-\hat{m}_Z^2)}{(1-\hat{m}_Z^2)^2 + (\frac{\Gamma_Z}{m_Z})^2} \right) \tilde{l}_{\mu\nu} ,$$

$$L_{\mu\nu}^a = c_{lep}^a \cdot \tilde{l}_{\mu\nu} = \tilde{\mu}^{4\epsilon} \left(\frac{1-\epsilon}{3-2\epsilon} \right) \frac{8\pi^2\alpha^2}{Q^4} \left(\frac{a_f^2(v_e^2 + a_e^2)}{(1-\hat{m}_Z^2)^2 + (\frac{\Gamma_Z}{m_Z})^2} \right) \tilde{l}_{\mu\nu} . \quad (3.11)$$

Born Cross-Section

To get the Born cross-section of the process $e^+e^- \rightarrow \text{hadrons}$ we use Eq. (3.9) with a $Q\bar{Q}$ -pair in the final state. Doing some manipulations and calculating the phase space integral over the quark and antiquark momentum yields the Born cross-section. In $d = 4 - 2\epsilon$ it reads:

$$\sigma_{\text{born}}^{i,\epsilon} = \frac{N_c Q^2 c_{lep}^i}{2\pi} \frac{\Gamma(1-\epsilon)}{\Gamma(2-2\epsilon)} \left(\frac{4\pi}{Q^2} \right)^\epsilon v^{1-2\epsilon} c_m^{i,\epsilon} , \quad (3.12)$$

which involves the Q-normalized quark (antiquark) mass $\hat{m} = m/Q$ and the quark (antiquark) velocity $v = \sqrt{1-4\hat{m}^2}$. Furthermore there are two factors which distinguish the vector and the axial-vector case where one was already defined in Eq. (3.10) and (3.11) and the other one is given by:

$$c_m^{i,\epsilon} = \begin{cases} (1-\epsilon) + 2\hat{m}^2 & \text{vec} \\ (1-\epsilon)(1-4\hat{m}^2) & \text{ax} \end{cases} , \quad \xrightarrow{\epsilon \rightarrow 0} \quad c_m^i = \begin{cases} 1 + 2\hat{m}^2 & \text{vec} \\ 1 - 4\hat{m}^2 & \text{ax} \end{cases} . \quad (3.13)$$

There are two important limits which should be considered. First the $\epsilon \rightarrow 0$ limit:

$$\sigma_{\text{born}}^i = \frac{N_c Q^2 c_{lep}^i}{2\pi} v c_m^i , \quad (3.14)$$

and second the massless limit:

$$\sigma_0^{i,\epsilon} = \frac{N_c Q^2 c_{lep}^i}{2\pi} \frac{\Gamma(1-\epsilon)}{\Gamma(2-2\epsilon)} \left(\frac{4\pi}{Q^2} \right)^\epsilon , \quad \xrightarrow{\epsilon \rightarrow 0} \quad \sigma_0^i = \frac{N_c Q^2 c_{lep}^i}{2\pi} . \quad (3.15)$$

The massless $\epsilon \rightarrow 0$ Born cross-section is important since it will be used as a normalization factor.

3.2. Radiative Part

3.2.1. Radiative FO Cross-Section

In this subsection we will calculate the radiative contributions to the massive c-parameter differential cross-section (the same was done for massless particles and the case of massless quarks and an off-shell gluon in [19]). We start by calculating the hadronic tensor which is related to the diagrams shown in Fig. 1. After that we calculate the double differential cross-section with respect to the variables x_1 and x_2 which are related to the quark (antiquark) energy. With this and the relation to the c-parameter (which we know from Eq. (2.13)) we can calculate the desired quantity.

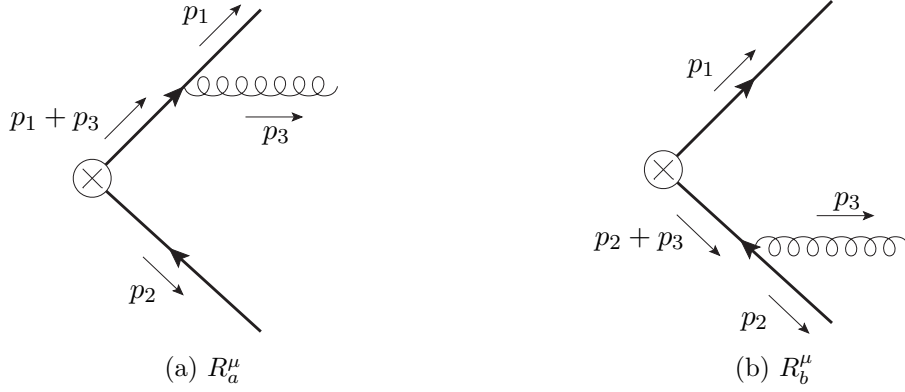


Figure 1: QCD diagrams which contribute to the radiative cross-section

The diagrams are evaluated using QCD Feynman rules. For example Fig. 1a yields:

$$R_a^\mu = \bar{u}(p_1, s_1) \left((ig_s \tilde{\mu}^\epsilon T^A \gamma^\lambda) \frac{i(\not{p}_1 + \not{p}_3 + m)}{(p_1 + p_3)^2 - m^2 + i0} \Gamma_i^\mu \right) v(p_2, s_2) \epsilon(p_3, \lambda). \quad (3.16)$$

Using the two contributing diagrams and evaluating the spin and polarization sums we get:

$$\begin{aligned} H_i^{\mu\nu} &= (-1) g_s^2 \tilde{\mu}^{2\epsilon} C_F \\ &\times \text{Tr} \left[(\not{p}_2 - m) \left(\Gamma^\mu \frac{(\not{p}_1 + \not{p}_3 + m)}{(p_1 + p_3)^2 - m^2 + i0} \gamma^\lambda - \gamma^\lambda \frac{\not{p}_2 + \not{p}_3 - m}{(p_2 + p_3)^2 - m^2 + i0} \Gamma^\mu \right) \right. \\ &\quad \left. \times (\not{p}_1 + m) \left(\gamma_\lambda \frac{(\not{p}_1 + \not{p}_3 + m)}{(p_1 + p_3)^2 - m^2 + i0} \Gamma^\nu - \Gamma^\nu \frac{\not{p}_2 + \not{p}_3 - m}{(p_2 + p_3)^2 - m^2 + i0} \gamma_\lambda \right) \right]. \end{aligned} \quad (3.17)$$

As mentioned before we set $d = 4$ to simplify the calculations and insert the above expression into our cross-section formula given in Eq. (3.9):

$$\sigma_{\text{rad}}^i = \int \frac{d^3 \vec{p}_1}{(2\pi)^5} \frac{d^3 \vec{p}_2}{(2\pi)^5} \frac{d^3 \vec{p}_3}{(2\pi)^5} \frac{1}{8 p_1^0 p_2^0 p_3^0} \delta(Q - p_1^0 - p_2^0 - p_3^0) \delta^{(3)}(\vec{p}_1 + \vec{p}_2 + \vec{p}_3) c_{lep}^i \tilde{l}_{\mu\nu} H_i^{\mu\nu}. \quad (3.18)$$

In the next step we carry out the $d^3 \vec{p}_3$ integration using the delta function. Therefore we use the following relations (where $\cos \theta_{12} = u = \frac{\vec{p}_1 \vec{p}_2}{|\vec{p}_1| |\vec{p}_2|}$ and $\theta_{12} \in [0, \pi]$):

$$d^3 \vec{p}_1 d^3 \vec{p}_2 = \Omega_{\text{tot}}^3 \Omega_{\text{tot}}^2 dp_1^0 dp_2^0 p_1^0 p_2^0 |\vec{p}_1| |\vec{p}_2| d(\cos \theta_{12}) = 8\pi^2 dp_1^0 dp_2^0 p_1^0 p_2^0 |\vec{p}_1| |\vec{p}_2| du, \quad (3.19)$$

$$\frac{1}{2p_3^0} \delta(Q - p_1^0 - p_2^0 - p_3^0) = \delta((Q - p_1^0 - p_2^0)^2 - (p_3^0)^2) - \frac{1}{2p_3^0} \delta(Q - p_1^0 - p_2^0 + p_3^0), \quad (3.20)$$

$$(p_3^0)^2 = (\vec{p}_3)^2 = (\vec{p}_1 + \vec{p}_2)^2 = (p_1^0)^2 + (p_2^0)^2 - 2m^2 + 2|\vec{p}_1| |\vec{p}_2| u. \quad (3.21)$$

Note that the kinematic situation associated with the second term of Eq. (3.20) is not within the phase space boundaries and can therefore be omitted. Using these relations we get:

$$\begin{aligned} \sigma_{\text{rad}}^i &= \int \frac{dp_1^0 dp_2^0 du}{2(2\pi)^3} |\vec{p}_1| |\vec{p}_2| \left[c_{lep}^i \tilde{l}_{\mu\nu} H_i^{\mu\nu} \right]_{\vec{p}_3 = -(\vec{p}_1 + \vec{p}_2)} \\ &\quad \times \frac{1}{Q^2} \delta \left(1 - \frac{2p_1^0}{Q} - \frac{2p_2^0}{Q} + \frac{1}{2} \frac{2p_1^0}{Q} \frac{2p_2^0}{Q} + 2 \frac{m^2}{Q^2} - 2 \frac{|\vec{p}_1| |\vec{p}_2|}{Q^2} u \right) \\ &= \frac{Q^2}{4} \int \frac{dx_1 dx_2 du}{4(2\pi)^3} \left[c_{lep}^i \tilde{l}_{\mu\nu} H_i^{\mu\nu} \right]_{\vec{p}_3 = -(\vec{p}_1 + \vec{p}_2)} \\ &\quad \times \delta \left(u - \frac{Q^2}{2|\vec{p}_1| |\vec{p}_2|} \left[1 - x_1 - x_2 + \frac{1}{2} x_1 x_2 + 2\hat{m}^2 \right] \right), \end{aligned} \quad (3.22)$$

where we used the variables x_1 and x_2 which were defined in Eq. (2.7). Next we carry out the u integration which corresponds to a replacement for u due to the delta function. This replacement reflects the known kinematic relations of Eq. (2.12). Together with $\vec{p}_3 = -(\vec{p}_1 + \vec{p}_2)$ this yields a set of relations which we will label *rules*. In the next step we put everything together and get:

$$\sigma_{\text{rad}}^i = \frac{Q^2 c_{\text{lep}}^i}{2(4\pi)^3} \int dx_1 dx_2 \left[\tilde{l}_{\mu\nu} H_i^{\mu\nu} \right]_{\text{rules}}. \quad (3.23)$$

Now we use the *Mathematica* package *FeynCalc* [21] to carry out the contraction and the trace in Eq. (3.17) while implementing *rules*. Afterwards the obtained result is differentiated w.r.t. x_1 and x_2 which yields the desired radiative double differential cross section for the production of one massive quark flavor (where we used the massless $d = 4$ Born cross-section for normalization):

$$\begin{aligned} \frac{1}{\sigma_0^v} \frac{d^2 \sigma_{\text{rad}}^v}{dx_1 dx_2} &= \frac{\alpha_s(\mu) C_F}{2\pi} \left[\frac{x_1^2 + x_2^2}{(1-x_1)(1-x_2)} - 2\hat{m}^2 \left(\frac{2}{1-x_1} + \frac{2}{1-x_2} + \frac{1}{(1-x_1)^2} + \frac{1}{(1-x_2)^2} \right) \right. \\ &\quad \left. - 4\hat{m}^4 \left(\frac{1}{1-x_1} + \frac{1}{1-x_2} \right)^2 \right] \end{aligned} \quad (3.24)$$

$$\begin{aligned} &\equiv \frac{\alpha_s(\mu) C_F}{2\pi} f^v(x_1, x_2, \hat{m}), \\ \frac{1}{\sigma_0^a} \frac{d^2 \sigma_{\text{rad}}^a}{dx_1 dx_2} &= \frac{\alpha_s(\mu) C_F}{2\pi} \left[\frac{x_1^2 + x_2^2}{(1-x_1)(1-x_2)} - 2\hat{m}^2 \left(\frac{2}{1-x_1} + \frac{2}{1-x_2} + \frac{1}{(1-x_1)^2} + \frac{1}{(1-x_2)^2} \right) \right. \\ &\quad \left. + 2\hat{m}^2 \frac{(2-x_1-x_2)^2 + 6(1-x_1-x_2)}{(1-x_1)(1-x_2)} + 8\hat{m}^4 \left(\frac{1}{1-x_1} + \frac{1}{1-x_2} \right)^2 \right] \end{aligned} \quad (3.25)$$

$$\equiv \frac{\alpha_s(\mu) C_F}{2\pi} f^a(x_1, x_2, \hat{m}).$$

Note that this result agrees with literature [22]. Since we are rather interested in the differential c -parameter cross section we use Eq. (2.13) by inserting:

$$\mathbb{1} = \int dc \delta(c - g(x_1, x_2, \hat{m})). \quad (3.26)$$

Afterwards we differentiate with respect to c . Carrying out the phase space (PS) integrals over x_1 and x_2 yields the desired result:

$$\frac{1}{\sigma_0^i} \frac{d\sigma_{\text{rad}}^i}{dc} \equiv \frac{\alpha_s(\mu) C_F}{2\pi} f_{\text{rad}}^i(c, \hat{m}) = \frac{\alpha_s(\mu) C_F}{2\pi} \int_{PS} dx_1 dx_2 \delta(c - g(x_1, x_2, \hat{m})) f^i(x_1, x_2, \hat{m}). \quad (3.27)$$

Phase Space and Substitution

To get the phase space boundaries we have to analyze the kinematic situation. We know and already used that we look at a three particle system in the c.o.m. frame. Energy-momentum conservation yields Eq. (2.8) and from this the relations for the phase space endpoints directly follow:

- (A) Point of minimal gluon energy: $x_1 = x_2 = 1$
- (B) Point of maximal gluon energy: $x_1 = x_2 = \frac{1}{2}(1 + 4\hat{m}^2)$
- (C₁) Point of minimal quark energy: $x_1 = 2\hat{m}$; $x_2 = \frac{1+2\hat{m}^2-2\hat{m}}{1-\hat{m}}$
- (C₂) Point of minimal antiquark energy: $x_1 = \frac{1+2\hat{m}^2-2\hat{m}}{1-\hat{m}}$; $x_2 = 2\hat{m}$

Next we determine the boundaries of the phase space which can be obtained by looking at the kinematical endpoints and the transition between them. We find two restricting curves where both

start at (A) and end at (B). These curves either go through (C₁) or (C₂). Using

$$b(x_i, \hat{m}) = \frac{1}{2(1 - \hat{m}^2 - x_i)} \left(2 + 4\hat{m}^2 - 3x_i - 2\hat{m}^2 x_i + x_i^2 + (x_i - 1) \sqrt{x_i^2 - 4\hat{m}^2} \right), \quad (3.28)$$

the boundaries are given by:

- AC₁B : $x_1 = b(x_2, \hat{m})$
- AC₂B : $x_2 = b(x_1, \hat{m})$

In the next step we introduce a convenient substitution using the new variable z [19]:

$$\begin{aligned} x_3 &= 2 - x_1 - x_2, & z &= (1 - x_2)/x_3 \\ \Rightarrow x_1 &= 1 - x_3(1 - z), & x_2 &= 1 - x_3 z & \Rightarrow dx_1 dx_2 &= x_3 dx_3 dz. \end{aligned} \quad (3.29)$$

The change of the phase space boundaries is illustrated in Fig. 2 where one can see that the new variables are well suited for this phase space. Note that the endpoint (A) does not translate to a single point but to the boundary of $x_3 = 0$ and that therefore the boundaries AC₁ and AC₂ vanish.

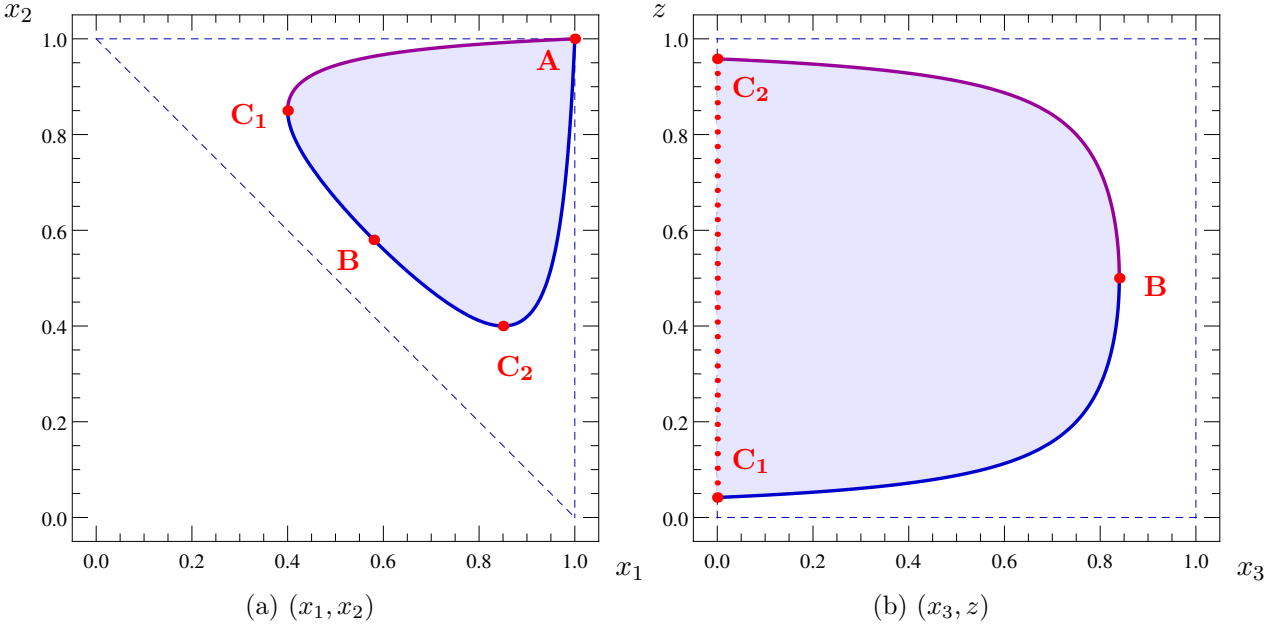


Figure 2: Phase space with boundaries in the used variables. The solid lines show the boundaries for $\hat{m} = 0.2$ and the dashed lines show the massless case

Furthermore we introduce the function $\tilde{f}^i(x_3, z, \hat{m}) = f^i(1 - x_3(1 - z), 1 - x_3 z, \hat{m})$ as well as $\tilde{g}(x_3, z, \hat{m})$ and make use of the symmetry of $z \leftrightarrow 1 - z$ (which corresponds to the symmetry $x_1 \leftrightarrow x_2$ in the old coordinates). This yields the expression:

$$f_{\text{rad}}^i(c, \hat{m}) = 2 \int_0^{1-4\hat{m}^2} dx_3 x_3 \int_{z_l}^{\frac{1}{2}} dz \delta \left[c - \tilde{g}(x_3, z, \hat{m}) \right] \tilde{f}^i(x_3, z, \hat{m}), \quad (3.30)$$

involving $z_l = \frac{1}{2} \left(1 - \sqrt{1 - \frac{4\hat{m}^2}{1-x_3}} \right)$. Performing one last substitution $z \rightarrow \frac{1}{2} - \sqrt{\tilde{z}}$ we arrive at:

$$f_{\text{rad}}^i(c, \hat{m}) = \int_0^{1-4\hat{m}^2} dx_3 x_3 \int_0^{\frac{1}{4}(1-\frac{4\hat{m}^2}{1-x_3})} \frac{d\tilde{z}}{\sqrt{\tilde{z}}} \delta \left[c - \tilde{g}(x_3, \frac{1}{2} - \sqrt{\tilde{z}}, \hat{m}) \right] \tilde{f}^i \left(x_3, \frac{1}{2} - \sqrt{\tilde{z}}, \hat{m} \right). \quad (3.31)$$

In the next step we would like to integrate over z by using the delta function. For the argument of the delta function one can observe:

$$c - \tilde{g}\left(x_3, \frac{1}{2} - \sqrt{\tilde{z}}, \hat{m}\right) \equiv \tilde{g}_c(x_3, \tilde{z}, \hat{m}, c) = (\tilde{z} - \tilde{z}_0) \left(\frac{4x_3[x_3(1+c) - 1]}{4x_3^2\tilde{z} - (x_3 - 2)^2} \right), \quad (3.32)$$

with

$$\tilde{z}_0 = \frac{x_3^2(1+c) + x_3(8\hat{m}^2 - 4c - 1) + 8\hat{m}^4 - 8\hat{m}^2 + 4c}{4x_3[x_3(1+c) - 1]}. \quad (3.33)$$

Now we can carry out the z integration and get:

$$f_{\text{rad}}^i(c, \hat{m}) = \int_0^{1-4\hat{m}^2} dx_3 \frac{x_3}{\sqrt{\tilde{z}_0}} \frac{\tilde{f}^i(x_3, \frac{1}{2} - \sqrt{\tilde{z}_0}, \hat{m})}{\left| \frac{d}{d\tilde{z}} \tilde{g}_c(x_3, \tilde{z}, \hat{m}, c) \right|_{\tilde{z}=\tilde{z}_0}} \theta(\tilde{z}_0) \theta \left[\frac{1}{4} \left(1 - \frac{4\hat{m}^2}{1-x_3} \right) - \tilde{z}_0 \right]. \quad (3.34)$$

After this step the integrand takes its final form. The differential massive c-parameter cross-section then reads:

$$\frac{1}{\sigma_0^i} \frac{d\sigma_{\text{rad}}^i}{dc} = \frac{\alpha_s(\mu) C_F}{2\pi} \int_0^{1-4\hat{m}^2} dx_3 \theta(\tilde{z}_0) \theta \left[\frac{1}{4} \left(1 - \frac{4\hat{m}^2}{1-x_3} \right) - \tilde{z}_0 \right] \mathcal{F}_i(x_3, c, \hat{m}), \quad (3.35)$$

where the integrand for the vector and axial-vector case is given by:

$$\begin{aligned} \mathcal{F}_v(x_3, c, \hat{m}) &= \frac{2\{1 + 2(-1 - \hat{m}^2 + \hat{m}^4)x_3 + (1 + 2\hat{m}^2)x_3^2\}}{[x_3(1+c) - 1][c(-1+x_3) - 2\hat{m}^2(-1 + \hat{m}^2 + x_3)]^2} \\ &\times \left\{ [x_3(1+c) - 1]x_3[4(c - 2\hat{m}^2 + 2\hat{m}^4) - (1 + 4c - 8\hat{m}^2)x_3 + (1+c)x_3^2] \right\}^{-\frac{1}{2}} \\ &\times \{ 2(1 + 2\hat{m}^2)(c - 2\hat{m}^2 + 2\hat{m}^4) + x_3^4 \cdot [c + c^2 - 2\hat{m}^2 - 2c\hat{m}^2] \\ &\quad - x_3^3 \cdot [(4c + 5c^2 - 6\hat{m}^2 - 6c\hat{m}^2 + 6c^2\hat{m}^2 + 6\hat{m}^4 + 2c\hat{m}^4 + 4c^2\hat{m}^4)] \\ &\quad + x_3^2 \cdot [7c + 8c^2 - 10\hat{m}^2 - 8c\hat{m}^2 + 8c^2\hat{m}^2 + 6\hat{m}^4 + 4c\hat{m}^4 - 8\hat{m}^6 + 8c\hat{m}^6] \\ &\quad - x_3 \cdot 2[3c + 2c^2 - 5\hat{m}^2 + 2c^2\hat{m}^2 - 2\hat{m}^4 + 2c\hat{m}^4 + 4c\hat{m}^6 + 4\hat{m}^8] \}, \end{aligned} \quad (3.36)$$

$$\begin{aligned} \mathcal{F}_a(x_3, c, \hat{m}) &= \frac{2\{1 + 2(-1 - \hat{m}^2 + \hat{m}^4)x_3 + (1 + 2\hat{m}^2)x_3^2\}}{[x_3(1+c) - 1][c(-1+x_3) - 2\hat{m}^2(-1 + \hat{m}^2 + x_3)]^2} \\ &\times \left\{ [x_3(1+c) - 1]x_3[4(c - 2\hat{m}^2 + 2\hat{m}^4) - (1 + 4c - 8\hat{m}^2)x_3 + (1+c)x_3^2] \right\}^{-\frac{1}{2}} \\ &\times \{ 2(1 - 4\hat{m}^2)(c - 2\hat{m}^2 + 2\hat{m}^4) + x_3^4 \cdot [c + c^2 - 2\hat{m}^2 - 2c\hat{m}^2][1 + 2\hat{m}^2] \\ &\quad - x_3^3 \cdot [(4c + 5c^2 - 6\hat{m}^2 - 14c\hat{m}^2 - 4c^2\hat{m}^2 + 10\hat{m}^4 - 2c\hat{m}^4 - 8c^2\hat{m}^4 + 4\hat{m}^6 + 4c\hat{m}^6)] \\ &\quad + x_3^2 \cdot [7c + 8c^2 - 10\hat{m}^2 - 42c\hat{m}^2 - 16c^2\hat{m}^2 + 50\hat{m}^4 + 28c\hat{m}^4 + 28\hat{m}^6 - 16c\hat{m}^6] \\ &\quad - x_3 \cdot 2[3c + 2c^2 - 5\hat{m}^2 - 18c\hat{m}^2 - 4c^2\hat{m}^2 + 28\hat{m}^4 + 14c\hat{m}^4 - 24\hat{m}^6 - 8c\hat{m}^6 + 4\hat{m}^8] \}. \end{aligned} \quad (3.37)$$

Case Analysis and x_3 Boundaries

Now we would like to determine how the theta functions in Eq. 3.35 influences the integration bounds of the x_3 integral. When we integrated over \tilde{z} we restricted ourselves to curves of equal c-parameter which are parametrized by x_3 . Therefore the remaining integration involves an integrand

which depends on the position on the curve. To find the boundaries of the remaining integral one has to find the interval on which the curves of equal c -parameter are within the physical phase space. This requires a thorough analysis of the involved theta functions. In Fig. 3 we illustrated the situation for a specific mass value. One finds three different types of equal c -parameter curves:

- curves which start ($\tilde{z} = 0$ and small x_3) and end ($\tilde{z} = 0$ and larger x_3) within the phase space.
- curves which start and end within but partially lie outside the phase space.
- curves which start within and end outside the phase space.

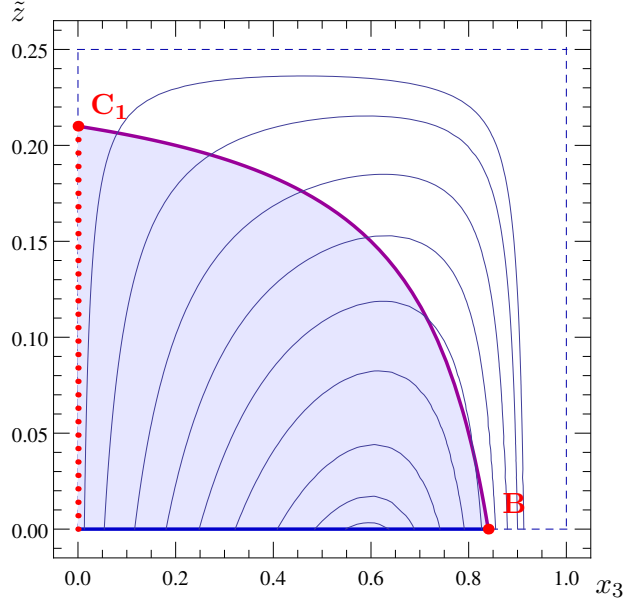


Figure 3: Phase space with boundaries and curves of equal c -parameter. The solid lines show the boundaries for $\hat{m} = 0.2$ and the dashed lines show the massless case

If one increases the mass one finds additional cases. When the mass exceeds $\hat{m} = \hat{m}_m$ it happens that the curves either lie completely within the phase space or start within and end outside the phase space. The third type of curve does not exist anymore. Further increasing the mass yields the third mass case valid for $\hat{m} \geq \hat{m}_p$. There only one type of curve, namely the one which starts within and ends outside of the phase space, is left. The mentioned $\hat{m} = m/Q$ thresholds read:

$$\hat{m}_m = \sqrt{\frac{1}{6} \left\{ 1 - \sqrt{19} \cos \left(\frac{1}{3} \left[\pi + \arctan \left(\frac{3\sqrt{687}}{26} \right) \right] \right) \right\}} = 0.299135, \quad (3.38)$$

$$\hat{m}_p = \frac{1}{2} \sqrt{\frac{1}{2} (\sqrt{5} - 1)} = 0.393076. \quad (3.39)$$

The different types of curves are characterized by a specific c -parameter interval. Overall this yields six cases which are summarized in Tab. 1. Therein one can see the three different mass cases and the different types of equal c -parameter curves. The different curves start and end at the point where $\tilde{z} = 0$. The related x_3 value is of course \hat{m} - and c -dependent and given by:

$$y_{m,p} = \frac{1 + 4c - 8\hat{m}^2 \mp \sqrt{1 + 16\hat{m}^2 + 32\hat{m}^4 - 8c(1 + 2\hat{m}^2)^2}}{2(1 + c)}. \quad (3.40)$$

case 1		$c_{\min} \leq c \leq c_m$	$x_3 \in [y_m, y_{\tilde{m}}]$
2	$0 \leq \hat{m} \leq \hat{m}_m$	$c_m \leq c \leq c_p$	$x_3 \in [y_m, y_{\tilde{m}}] \cup [y_{\tilde{p}}, y_p]$
3		$c_p \leq c \leq c_{\max}$	$x_3 \in [y_m, y_p]$
4	$\hat{m}_m \leq \hat{m} \leq \hat{m}_p$	$c_{\min} \leq c \leq c_m$	$x_3 \in [y_m, y_{\tilde{m}}]$
5		$c_m \leq c \leq c_{\max}$	$x_3 \in [y_m, y_p]$
6	$\hat{m}_p \leq \hat{m} \leq 0.5$	$c_{\min} \leq c \leq c_m$	$x_3 \in [y_m, y_{\tilde{m}}]$

Table 1: Final case structure for the phase space boundaries of the x_3 integration

The boundaries of the c -parameter intervals which characterize the different types of curves are given by:

$$\begin{aligned}
c_{\min} &= 2\hat{m}^2(1 - \hat{m}^2) , \\
c_m &= \frac{4\hat{m}^2(1 + 2\hat{m}^2)}{(1 + 4\hat{m}^2)^2} , \\
c_p &= \hat{m}^2 - \hat{m}^4 + \frac{1}{2}\sqrt{\hat{m}^2 - 4\hat{m}^6 + 4\hat{m}^8} , \\
c_{\max} &= \frac{1 + 16\hat{m}^2 + 32\hat{m}^4}{8(1 + 2\hat{m}^2)^2} .
\end{aligned} \tag{3.41}$$

Except for the type of curve which completely lies within the phase space the curves intersect with the phase space boundaries which happens at the following x_3 values:

$$y_{\hat{m}, \tilde{p}} = \frac{2c - 3\hat{m}^2 + 2\hat{m}^4 \mp \hat{m}\sqrt{-4c^2 + (1 - 8c)\hat{m}^2 - 4(1 + 2c)\hat{m}^4 + 4\hat{m}^6}}{2[c + (c - 1)\hat{m}^2]} . \tag{3.42}$$

Note that the maximal c -parameter is not always given by c_{\max} but sometimes by c_m . This happens when \hat{m} becomes larger than \hat{m}_p since then the configuration which corresponds to a c -parameter value c_{\max} does not lie within the physical phase space anymore. The maximal C -parameter is therefore given by:

$$c_{\text{top}} = \begin{cases} c_{\max} & 0 \leq \hat{m} \leq \hat{m}_p \\ c_p & \hat{m}_p < \hat{m} \leq 0.5 \end{cases} , \tag{3.43}$$

This concludes the discussion about the case structure needed for the x_3 integration of Eq. (3.35). In fact we did not get into detail how to compute the involved quantities but after realizing the case structure one can obtain the given expressions straightforwardly.

Reduction to Legendre's Normal Form

The next important observation is that the integral given in Eq. (3.35) is a so-called *elliptic integral*. These are the ones which can be reduced to the form:

$$\int dx R_1(x) + \int dx \frac{R_2(x)}{\sqrt{p(x)}} , \tag{3.44}$$

where $R_i(x)$ are rational functions and $p(x)$ is a polynomial of order $n \leq 4$. For these integrals there exists no general theory how to solve them and it is usually not possible to find a solution

in form of elementary functions. However, there is a theorem due to Legendre that one can reduce (or rather express) them as a linear combination of an integral of a rational function and three standard elliptic integrals which are called *Legendre's normal form* of elliptic integrals. For these standard integrals one can find Taylor expansions to any order and numerical implementations with arbitrary precision. The (incomplete) elliptic integrals of first, second and third kind are given by:

$$\begin{aligned} F(\theta, m) &= \int_0^{\sin(\theta)} dy \frac{1}{\sqrt{(1-y^2)(1-my^2)}} , & E(\theta, m) &= \int_0^{\sin(\theta)} dy \sqrt{\frac{1-my^2}{1-y^2}} , \\ \Pi(n; \theta, m) &= \int_0^{\sin(\theta)} dy \frac{1}{(1-ny^2)\sqrt{(1-y^2)(1-my^2)}} , \end{aligned} \quad (3.45)$$

where $k = \sqrt{m}$ is called the *elliptic modulus* and n is the so-called *characteristic* of the elliptic integrals of the 3rd kind Π .

To achieve the form which is convenient to start the reduction with (which requires $p(x)$ to be factorized) one should observe that (involving $y_0 \geq y_1 \geq y_2 \geq y_3$):

$$\begin{aligned} &\left\{ [x_3(1+c) - 1]x_3[4(c - 2\hat{m}^2 + 2\hat{m}^4) - (1 + 4c - 8\hat{m}^2)x_3 + (1+c)x_3^2] \right\}^{\frac{1}{2}} = \\ &= (1+c) \left\{ (x_3 - y_0)(x_3 - y_1)(x_3 - y_2)(x_3 - y_3) \right\}^{\frac{1}{2}} , \end{aligned} \quad (3.46)$$

where the y_i 's are given by:

$$y_0 = \frac{1}{1+c} , \quad y_1 = y_p , \quad y_2 = y_m , \quad y_3 = 0 . \quad (3.47)$$

After this observation we can start the reduction procedure. Therefore it is convenient to break the whole cross-section into smaller pieces. The cases given in Tab. 1 involve sums of elliptic integrals which look like (with some generic upper bound \tilde{y}):

$$\tilde{\mathcal{F}}_i(c, \hat{m}, \theta(\tilde{y})) = \int_{y_m}^{\tilde{y}} dx_3 \mathcal{F}_i(x_3, c, \hat{m}) , \quad i = a, v . \quad (3.48)$$

This kind of integrals can be reduced to Legendre normal form. We present the procedure and all the necessary formulas in Sec. A.1. A more general treatment and an overview is given in [23].

As stated above after the reduction process we should arrive at a linear combination of an integral over a rational function and the elliptic standard integrals. In fact for our case we can solve the integral over the rational function and the result then takes the form:

$$\begin{aligned} \tilde{\mathcal{F}}_i(c, \hat{m}, \theta) &= c_i(c, \hat{m}) + f_i(c, \hat{m}) F(\theta, m) + e_i(c, \hat{m}) E(\theta, m) \\ &+ p_{n,i}(c, \hat{m}) \Pi(n; \theta, m) + p_{h,i}(c, \hat{m}) \Pi(h; \theta, m) . \end{aligned} \quad (3.49)$$

The involved coefficients, elliptic moduli and characteristics are rather long expressions, thus we present them in Sec. A.2.

As one can see by looking at the explicit calculations the boundaries of the integration were transformed during the reduction process. In the end we only have two c - and \hat{m} -dependent boundaries

which are given by:

$$\theta_m = \arcsin \left(\sqrt{\frac{y_1 \cdot (y_{\hat{m}} - y_2)}{y_{\hat{m}} \cdot (y_1 - y_2)}} \right), \quad \theta_p = \arcsin \left(\sqrt{\frac{y_1 \cdot (y_{\hat{p}} - y_2)}{y_{\hat{p}} \cdot (y_1 - y_2)}} \right). \quad (3.50)$$

Involving these new boundaries the whole cross section result which is valid for $c > c_{\min}$ can then be written in a very nice way:

$$\frac{1}{\sigma_0^i} \frac{d\sigma_{\text{rad}}^i}{dc} = \frac{\alpha_s(\mu) C_F}{2\pi} \begin{cases} \tilde{\mathcal{F}}_i(c, \hat{m}, \theta_m) & \text{case 1} \\ \tilde{\mathcal{F}}_i(c, \hat{m}, \pi/2) - \tilde{\mathcal{F}}_i(c, \hat{m}, \theta_p) + \tilde{\mathcal{F}}_i(c, \hat{m}, \theta_m) & 2 \\ \tilde{\mathcal{F}}_i(c, \hat{m}, \pi/2) & 3 \\ \tilde{\mathcal{F}}_i(c, \hat{m}, \theta_m) & 4 \\ \tilde{\mathcal{F}}_i(c, \hat{m}, \pi/2) & 5 \\ \tilde{\mathcal{F}}_i(c, \hat{m}, \theta_m) & 6 \end{cases}. \quad (3.51)$$

This is the most convenient way for expressing our final result which is also well suited for a numerical treatment.

3.2.2. Series Expansions

In this subsection we will take the radiative FO result from Eq. (3.51) and expand it in different limits. First we will calculate the divergent behavior by performing a threshold expansion which will then be used to manually regularize our radiative FO result. This is done by subtracting the divergent pieces and adding them back in terms of plus distribution (which are defined in Sec. B). This yields the regularized radiative FO result which is then valid for $c \geq c_{\min}$.

The second expansion is in the SCET limit where we expand the FO result in the limit which is inferred by the SCET power counting (see Sec. 4). This result will then be used to check the unresummed SCET result and also for determining the non-singular contributions to our SCET cross-section (see Sec. 6.3).

Threshold Expansion

To calculate the threshold expansion we have to expand around the minimal c -parameter value $c_{\min} = 2\hat{m}^2(1 - \hat{m}^2)$. A straightforward expansion of the elliptic standard integrals and the coefficients at the point $c = c_{\min}$ yields the divergent term of the threshold expansion (c_m^i was defined in Eq. (3.13)):

$$f_{\text{rad}}^i(c, \hat{m}) = f_{\text{div}}^i(c, \hat{m}) + f_{\text{ndiv}}^i(c, \hat{m}) = f_{\text{div}}^i(c, \hat{m}) + \mathcal{O}((c - c_{\min})^0),$$

$$f_{\text{div}}^i(c, \hat{m}) = \frac{4c_m^i}{c - c_{\min}} \left[2(1 - 2\hat{m}^2) \ln \left(\frac{1 + \sqrt{1 - 4\hat{m}^2}}{2\hat{m}} \right) - \sqrt{1 - 4\hat{m}^2} \right] \equiv f_+^i(\hat{m}) \frac{1}{c - c_{\min}}. \quad (3.52)$$

To regularize the radiative FO result we will subtract the divergent part which is proportional to $(c - c_{\min})^{-1}$ and add it back as a plus distribution. This is the reason why we defined the coefficient function $f_+^i(\hat{m})$.

Furthermore we would like to have some information about the non-divergent contributions to the threshold expansion. This might become handy when dealing with the numerical implementation of the full QCD cross-section minus the divergent part which is part of the non-singular contributions

to the cross-section (see Sec. 6.3). Since close to threshold one subtracts very large numbers this might give rise to numeric instabilities which could be cured (at least approximately) by switching to an expansion within a small vicinity of the threshold. The expansion of this non-divergent contribution to some order N takes the form:

$$f_{\text{ndiv}}^i(c, \hat{m}) \approx a_0^i(\hat{m}) + \sum_j^N a_j^i(\hat{m}) \cdot (c - c_{\text{min}})^j. \quad (3.53)$$

Except for the constant term the expansion using the elliptic integrals and their coefficients does not work anymore. In fact when doing the integral reduction one introduced a singularity at $c = 2\hat{m}^2$ which is canceled exactly between the different terms (note that this divergence has no connection with the SCET threshold - see Eq. (5.25) - which is located at the same c -parameter value). Although this singularity cancels numerically we still subtract very large numbers which yields to instabilities at this c value and spoils the threshold expansion. To get rid of this problem we use the expression given in Eq. (3.35) and try to expand the whole integral (since we are close to threshold we are in cases 1,4,6 and therefore look always at the same integral). The expansion is simplified when doing the substitution of Eq. (A.4) because then the divergent behavior factorizes out of the integral. Now we can Taylor expand the integral which is multiplied with the divergent factor $(c - c_{\text{min}})^{-1}$. With this method one can derive the constant coefficient which is given by:

$$a_0^i(\hat{m}) = \frac{4c_m^i}{\hat{m}^6(1-8\hat{m}^4)^{3/2}} \left[(1 - \hat{m}^2 - 11\hat{m}^4 + 8\hat{m}^6 + 20\hat{m}^8 - 8\hat{m}^{10}) \text{artanh}\left(\sqrt{\frac{1-4\hat{m}^2}{1-8\hat{m}^4}}\right) \right. \\ \left. - (1 - 8\hat{m}^4)^{3/2}(1 - \hat{m}^2 + \hat{m}^4) \text{artanh}(\sqrt{1-4\hat{m}^2}) \right. \\ \left. - \hat{m}^2 \sqrt{(1-4\hat{m}^2)(1-8\hat{m}^4)}(1 + \hat{m}^2 - 5\hat{m}^4) \right]. \quad (3.54)$$

Note that for very small masses the above expressions also involve subtractions of very large terms which is numerically unstable, hence one has to switch to an expansion in \hat{m} .

For the higher order terms the analytic calculation involves handling very large expressions. Therefore these coefficients should be determined numerically. Since the derivation is an ordinary Taylor expansion we do not get into details.

SCET expansion

The second expansion we are interested in is the so-called SCET expansion. SCET imposes a certain power counting in some (at this point generic) parameter λ which is used as an expansion parameter. SCET is derived from QCD by using this power counting and a leading order approximation. Therefore an appropriate expansion which implements the correct power counting can be used to cross check the SCET result (see Sec. 6.3).

The power counting (see Sec. 4) results in a certain scaling for different variables. Since we are interested in the expansion of the c - and \hat{m} -dependent QCD result one should note that $c \sim \lambda^2$ and for a collinear particle $\hat{m} \sim \lambda$. To get a correct leading order expansion we replace $c \rightarrow x^2 c$ as well as $\hat{m} \rightarrow x \hat{m}$ and expand around $x = 0$. This realizes $c \sim \hat{m}^2$ while expanding for small values of both. Expanding the elliptic standard integrals and their coefficients yields:

$$f_{\text{rad}}^i(c, \hat{m}) \stackrel{c \sim \hat{m}^2}{=} -\frac{4[1 + \ln(c - \hat{m}^2)]}{c - 2\hat{m}^2} + \frac{c - 2\hat{m}^2}{(c - \hat{m}^2)^2} + \mathcal{O}(c^0, \hat{m}^0) \xrightarrow{\hat{m} \rightarrow 0} -\frac{3 + 4 \ln(c)}{c} + \mathcal{O}(c^0). \quad (3.55)$$

Note that this expansion gives the correct singular contribution to the massless QCD result (see [4]) which emphasizes that it implements an expansion in c and \hat{m} simultaneously and therefore does not lose track of the correct massless limit.

3.3. Virtual Contributions

Although it is not needed for the FO cross-section we have to compute the $\mathcal{O}(\alpha_s)$ virtual diagram (see Fig. 4) for the matching of SCET to QCD which is done in Sec. 6.2.1. In fact we need physical matrix elements at $\mathcal{O}(\alpha_s)$ which are obtained from the virtual diagram by applying the LSZ formula.

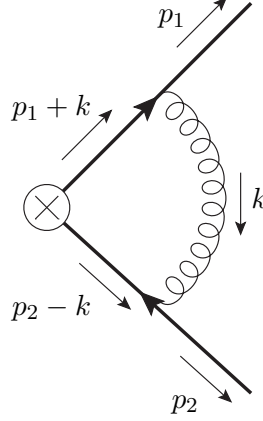


Figure 4: Virtual QCD diagram V_i^μ

Using QCD Feynman rules the virtual diagram is given by:

$$V_i^\mu = \bar{u}(p_1, s_1) \int \frac{d^d k}{(2\pi)^d} (ig_s \gamma^\alpha T^A \tilde{\mu}^\epsilon) \frac{i(\not{p}_1 + \not{k} + m)}{(p_1 + k)^2 - m^2 + i0} \Gamma_i^\mu \frac{i(-\not{p}_2 + \not{k} + m)}{(p_2 - k)^2 - m^2 + i0} \\ \times (ig_s \gamma_\alpha T^A \tilde{\mu}^\epsilon) \frac{-i}{k^2 + i0} v(p_2, s_2). \quad (3.56)$$

Next we again use *FeynCalc* [21] to do the tensor reduction and results from [24] for the 1-, 2- and 3-point functions. Since we are interested in the physical S-matrix element we have to use the LSZ formula. In this case we simply have to multiply a factor $(Z_\psi^{\text{OS}})^{-1/2}$ per external line where the wave-function renormalization factor in the on-shell scheme is given by [6]:

$$Z_\psi^{\text{OS}} = 1 + \frac{\alpha_s(\mu) C_F}{4\pi} \left\{ -\frac{3}{\epsilon} + 3 \ln \left(\frac{m^2}{\mu^2} \right) - 4 \right\}. \quad (3.57)$$

Note that after including the wave-function renormalization factor all the divergences which arise are of IR type which can be seen by using an IR regulator like a massive gluon or an off-shellness. The desired one loop matrix element (involving $v = \sqrt{1 - 4\hat{m}^2}$) is then given by:

$$\langle Q\bar{Q} | \mathcal{J}_i^\mu | 0 \rangle_{\text{QCD}} = \bar{u}(p_1, s_1) \Gamma_i^\mu \frac{\alpha_s(\mu) C_F}{4\pi} \left\{ -\frac{2}{\epsilon} - \frac{1+v^2}{v\epsilon} \ln \left(\frac{v-1}{1+v} \right) - \ln \left(\frac{m^2}{\mu^2} \right) \right. \\ + 3 \ln \left(\frac{-m^2}{\mu^2} \right) - 3v \ln \left(\frac{1-v}{1+v} \right) - 4 + \frac{1+v^2}{v} \left[\ln \left(\frac{m^2}{\mu^2} \right) \ln \left(\frac{v-1}{1+v} \right) + \frac{\pi^2}{6} \right. \\ + 2 \text{Li}_2 \left(\frac{1-v}{1+v} \right) + 2 \ln \left(\frac{2v}{1+v} \right) \ln \left(\frac{v-1}{1+v} \right) - \frac{1}{2} \ln^2 \left(\frac{v-1}{1+v} \right) \left. \right] \left. \right\} v(p_2, s_2) \\ + \mathcal{O}(\alpha_s m, \alpha_s^2). \quad (3.58)$$

This result will be used to do the matching calculation of SCET to QCD (see Sec. 6.2.1). We can also compare this result with the literature [25] and find agreement for $d = 4 - 2\epsilon$. Although the $\mathcal{O}(\alpha_s m)$ terms (which are different for the vector and axial-vector current) clearly contribute to the one loop matrix element we do not write them down explicitly. Since leading SCET only involves terms up to $\mathcal{O}(\hat{m}^0)$ it happens that it cannot reproduce the IR divergences which behave like $(1/\epsilon_{IR})\mathcal{O}(\hat{m})$ although they are involved in the full mass dependent QCD result. This forces us to use an expansion of Eq. (3.58) when calculating the matching coefficient and later account for the error. A more detailed discussion of this subtlety and how we deal with it is given in Sec. 6.2.1.

3.4. The Delta Coefficient and the Full FO Result

In this subsection we will show how to derive the numerical coefficient for the delta part of the FO cross-section. The strategy to determine the coefficient is to integrate the radiative result over the full c -parameter range and subtracting it from the integrated hadronic cross-section. The remainder should then correspond to the delta function coefficient.

The integrated hadronic cross-section at $\mathcal{O}(\alpha_s)$ can be found in [20] and reads:

$$\sigma_{\text{tot}} = \sigma_{\text{tot}}^v + \sigma_{\text{tot}}^a = \sigma_{\text{born}}^v \left[1 + \frac{\alpha_s(\mu)C_F}{\pi} K^v(v) \right] + \sigma_{\text{born}}^a \left[1 + \frac{\alpha_s(\mu)C_F}{\pi} K^a(v) \right], \quad (3.59)$$

involving σ_{born}^i defined in Eq. (3.14). The coefficient functions which depend on $v = \sqrt{1 - 4\hat{m}^2}$ read:

$$K^v(v) = \frac{1}{v} \left[A(v) + \frac{P^v(v)}{(1 - v^2/3)} \ln \left(\frac{1 + v}{1 - v} \right) + \frac{Q^v(v)}{(1 - v^2/3)} \right], \quad (3.60)$$

$$K^a(v) = \frac{1}{v} \left[A(v) + \frac{P^a(v)}{v^2} \ln \left(\frac{1 + v}{1 - v} \right) + \frac{Q^a(v)}{v^2} \right], \quad (3.61)$$

$$A(v) = (1 + v^2) \left[\text{Li}_2 \left(\left[\frac{1 - v}{1 + v} \right]^2 \right) + 2\text{Li}_2 \left(\frac{1 - v}{1 + v} \right) + \ln \left(\frac{1 + v}{1 - v} \right) \ln \left(\frac{(1 + v)^3}{8v^2} \right) \right], \quad (3.62)$$

$$P^v(v) = \frac{33}{24} + \frac{22}{24}v^2 - \frac{7}{24}v^4, \quad Q^v(v) = \frac{5}{4}v - \frac{3}{4}v^3, \quad (3.63)$$

$$P^a(v) = \frac{21}{32} + \frac{59}{32}v^2 - \frac{19}{32}v^4 - \frac{3}{32}v^6, \quad Q^a(v) = -\frac{21}{16}v + \frac{30}{16}v^3 + \frac{3}{16}v^5. \quad (3.64)$$

On the other hand side the total hadronic cross-section has to be the same as the integrated differential cross section. With the definition from Eq. (3.41) and (3.43) we can write the total hadronic cross-section as:

$$\begin{aligned} \sigma_{\text{tot}}^i &= \int_{c_{\text{min}}}^{c_{\text{top}}} dc \frac{d\sigma}{dc} = \sigma_{\text{born}}^i \left\{ 1 + \frac{\alpha_s(\mu)C_F}{\pi} \frac{1}{2} \frac{\sigma_0^i}{\sigma_{\text{born}}^i} \int_{c_{\text{min}}}^{c_{\text{top}}} dc \left[\left(f_{\text{rad}}^i(c, \hat{m}) - \frac{f_+^i(\hat{m})}{c - c_{\text{min}}} \right) \right. \right. \\ &\quad \left. \left. + f_+^i(\hat{m}) \left[\frac{\theta(c - c_{\text{min}})}{c - c_{\text{min}}} \right]_+ + f_{\delta}^i(\hat{m}) \delta(c - c_{\text{min}}) \right] \right\} \\ &= \sigma_{\text{born}}^i \left[1 + \frac{\alpha_s(\mu)C_F}{\pi} \frac{1}{2v} \frac{1}{c_m^i} \left(f_{\delta}^i(\hat{m}) + f_+^i(\hat{m}) \ln(c_{\text{top}} - c_{\text{min}}) + \int_{c_{\text{min}}}^{c_{\text{top}}} dc f_{\text{ndiv}}^i(c, \hat{m}) \right) \right], \quad (3.65) \end{aligned}$$

where we introduced the coefficient function of the delta function $f_{\delta}^i(\hat{m})$ and used the non divergent part of the radiative FO cross-section which was introduced in Eq. (3.52). By comparing Eq. (3.59)

and (3.65) we can numerically calculate the $\mathcal{O}(\alpha_s)$ coefficient function of the delta function for the vector and axial-vector case. It is given by:

$$f_{\delta}^i(\hat{m}) = 2 v c_m^i K^i(v) - \left(f_+^i(\hat{m}) \ln(c_{\text{top}} - c_{\text{min}}) + \int_{c_{\text{min}}}^{c_{\text{top}}} dc f_{\text{ndiv}}^i(c, \hat{m}) \right). \quad (3.66)$$

This result will contribute to the delta coefficient of the non-singular cross-section (see Sec. 6.3) which is shown in Fig. 10a.

The Full FO Result

In this and the previous subsections we calculated all the contributions to the FO QCD cross-section. Afterwards we properly regularized the radiative contributions and thereby arrived at an integrable result. Then we used this feature to calculate the FO delta coefficient and thereby the last ingredient to the full FO cross-section. The final result to $\mathcal{O}(\alpha_s)$ reads:

$$\frac{d\sigma_{\text{QCD}}}{dc} = \sum_{i=v,a} \frac{d\sigma_{\text{QCD}}^i}{dc} \quad (3.67)$$

$$\begin{aligned} \frac{d\sigma_{\text{QCD}}^i}{dc} = & \sigma_{\text{born}}^i \delta(c - c_{\text{min}}) \\ & + \sigma_0^i \frac{\alpha_s(\mu) C_F}{2\pi} \left[f_{\delta}^i(\hat{m}) \delta(c - c_{\text{min}}) + f_+^i(\hat{m}) \left[\frac{\theta(c - c_{\text{min}})}{c - c_{\text{min}}} \right]_+ + f_{\text{ndiv}}^i(c, \hat{m}) \right] \\ & + \mathcal{O}(\alpha_s^2), \end{aligned} \quad (3.68)$$

where the different coefficients are defined in Eq. (3.52) and (3.66).

4. Soft-Collinear Effective Theory

The *soft-collinear effective theory* (SCET) [5–9] is an effective field theory (EFT) of QCD which was introduced in the context of a heavy meson decaying into a jet.

Motivated by the scale hierarchy of particles within jets one first decomposes QCD into modes with different momentum scaling, then integrates out the modes which are far off-shell. Afterwards one uses a power counting to determine the relevancy of the remaining modes and thereby constructs an EFT which exactly reproduces the IR degrees of freedom of full QCD. Furthermore SCET simplifies the derivation of factorization theorems and the resummation of large logarithms [10,26,27]. Overall it is an optimal framework to study event-shape distributions at high energies as we intend to do.

4.1. Light Cone Coordinates and Mode Separation

In our case where we study hadron production from e^+e^- annihilation the c.o.m. frame is most convenient to describe the relevant kinematics. Since we want to describe jets which consist of highly boosted hadrons, hence particles which live almost on the light cone, we use so-called *light cone coordinates*. Therefore we change from x^μ to a new basis which reads:

$$\begin{aligned} n^\mu &= (1, 0, 0, -1) , & \bar{n}^\mu &= (1, 0, 0, 1) , \\ x_1^\mu &= (0, 1, 0, 0) , & x_2^\mu &= (0, 0, 1, 0) , \end{aligned} \quad (4.1)$$

where trivially $n \cdot \bar{n} = 2$. In this new basis we look at a general vector p^μ and for this define

$$p^- = p^0 - p^3 , \quad p^+ = p^0 + p^3 , \quad p_\perp^\mu = (0, p^1, p^2, 0) = (0, \vec{p}_\perp) . \quad (4.2)$$

Then we can decompose a momentum p^μ as follows:

$$p^\mu = p^- \frac{n^\mu}{2} + p^+ \frac{\bar{n}^\mu}{2} + p_\perp^\mu , \quad p^2 = p^+ p^- - (\vec{p}_\perp)^2 . \quad (4.3)$$

Now we identify the for our problem relevant modes of the theory. Since we want to describe jets we need to include close to on-shell particles which have high momenta in a specific direction. Therefore we look at an energetic particle which (without loss of generality) moves in $-x_3$ direction. It is easy to see that $m \ll p^0 \approx |p^3|$, hence the light cone coordinates are widely separated $p^- \approx 2p^0$ and $p^+ \approx 0$. If Q denotes the total c.o.m. energy, then:

$$Q^2 \gg p^2 = (p^0)^2 - (p^3)^2 + (p_\perp)^2 \quad \Rightarrow \quad p_\perp \equiv |\vec{p}_\perp| \ll Q^2 . \quad (4.4)$$

Furthermore the large component should be of the same size as the total center of mass energy i.e. $p^- \sim Q$. With the small parameter $\lambda \sim p_\perp/p^-$ one can write $p_\perp \sim Q\lambda$ and since $p^+ p^- \approx (p_\perp)^2 \sim Q^2 \lambda^2$ the small component scales like $p^+ \sim Q\lambda^2$. Particles which light cone components scale like $p_n = (p^+, p^-, p_\perp) \sim Q(\lambda^2, 1, \lambda)$ are called *n-collinear*. Similar particles which move in the opposite direction and therefore fulfill $p_{\bar{n}} \sim Q(1, \lambda^2, \lambda)$ are called *\bar{n} -collinear*.

The other relevant modes which will appear are induced by the radiation of a gluon. While staying close to its mass-shell a *n-collinear* quark can only emit a gluon which is either ultra-soft (usoft) i.e. $k_{us} \sim Q(\lambda^2, \lambda^2, \lambda^2)$ or again *n-collinear* $k_n \sim Q(\lambda^2, 1, \lambda)$. Together with the corresponding *\bar{n} -collinear* particles we identified all the relevant modes we want to include in SCET³. All other modes are far off-shell and therefore integrated out.

³Note that if one is interested in an $\mathcal{O}(\alpha_s^2)$ analysis one has to deal with secondary massive quarks which forces us to include mass modes with a soft scaling - see [13].

4.2. SCET Fields and the Lagrangian

Now we look at the QCD quark field and separate it in an n -, \bar{n} -collinear and usoft part i.e. $\psi(x) = \psi_n(x) + \psi_{\bar{n}}(x) + \psi_{us}(x)$. Since the large components of collinear momenta can only be changed by collinear particles we can separate the interactions of collinear and usoft particles. Therefore we decompose momenta in a large *label*-momentum and a small residual momentum⁴:

$$p^\mu = \tilde{p}^\mu + k^\mu, \quad \tilde{p}^\mu = p^- \frac{n^\mu}{2} + p_\perp^\mu. \quad (4.5)$$

Next we restrict the momentum of the Fourier integral of the n -collinear quark field to the scaling of a n -collinear particle. Together with the above decomposition this yields the following:

$$\begin{aligned} \psi_n(x) &= \int \frac{d^4 p}{(2\pi)^3} \delta(p^2 - m^2) \theta(p^0 - m) \left[u(p) a(p) e^{-ip \cdot x} + v(p) b^\dagger(p) e^{ip \cdot x} \right] \\ &= \sum_{\tilde{p}} e^{-i\tilde{p} \cdot x} \int \frac{d^4 k}{(2\pi)^3} \delta(p^2 - m^2) \theta(p^-) \left[u_{\tilde{p}}(k) a_{\tilde{p}}(k) e^{-ik \cdot x} + v_{-\tilde{p}}(k) b_{-\tilde{p}}^\dagger(k) e^{ik \cdot x} \right] \\ &\equiv \sum_{\tilde{p}} e^{-i\tilde{p} \cdot x} \left[\psi_{n,\tilde{p}}^+ + \psi_{n,-\tilde{p}}^- \right] = \sum_{\tilde{p}} e^{-i\tilde{p} \cdot x} \psi_{n,\tilde{p}}, \end{aligned} \quad (4.6)$$

where we omit an implicit sum over spins and use that for a collinear particle $p^2 = m^2 \sim \lambda^2$ which corresponds to $m_c \sim \lambda$. Next we introduce projection operators:

$$P_n = \frac{\not{n} \not{\bar{n}}}{4}, \quad P_{\bar{n}} = \frac{\not{\bar{n}} \not{n}}{4}, \quad (P_n + P_{\bar{n}}) = \mathbb{1}, \quad (4.7)$$

which are used to separate the quark field into two parts:

$$\psi_{n,\tilde{p}} = (P_n + P_{\bar{n}}) \psi_{n,\tilde{p}} \equiv \xi_{n,\tilde{p}} + \hat{\xi}_{n,\tilde{p}}. \quad (4.8)$$

Using the definition of the projection operators in Eq. (4.7) one can derive the following relations:

$$\begin{aligned} \not{n} \xi_{n,\tilde{p}} &= 0, & \not{\bar{n}} \hat{\xi}_{n,\tilde{p}} &= 0, \\ P_n \xi_{n,\tilde{p}} &= \xi_{n,\tilde{p}}, & P_{\bar{n}} \hat{\xi}_{n,\tilde{p}} &= \hat{\xi}_{n,\tilde{p}}. \end{aligned} \quad (4.9)$$

Note that derivatives of these new fields give $\mathcal{O}(\lambda^2)$ contributions. To obtain the SCET Lagrangian we start with the n -collinear quark part of the QCD Lagrangian and use the relations of Eq. (4.9). Then we get:

$$\begin{aligned} \mathcal{L}_{q,n} &= \bar{\psi} (i \not{D} - m) \psi = \sum_{\tilde{p}, \tilde{p}'} e^{i\tilde{p}' \cdot x} \left[\bar{\xi}_{n,\tilde{p}'} + \bar{\hat{\xi}}_{n,\tilde{p}'} \right] \left(i D^- \frac{\not{n}}{2} + i D^+ \frac{\not{\bar{n}}}{2} + i \not{D}_\perp - m \right) e^{-i\tilde{p} \cdot x} \left[\xi_{n,\tilde{p}} + \hat{\xi}_{n,\tilde{p}} \right] \\ &= \sum_{\tilde{p}, \tilde{p}'} e^{-i(\tilde{p} - \tilde{p}') \cdot x} \left[\bar{\xi}_{n,\tilde{p}'} (i D^+) \frac{\not{n}}{2} \xi_{n,\tilde{p}} + \bar{\hat{\xi}}_{n,\tilde{p}'} (\tilde{p}^- + i D^-) \frac{\not{n}}{2} \hat{\xi}_{n,\tilde{p}} \right. \\ &\quad \left. + \bar{\hat{\xi}}_{n,\tilde{p}'} (\not{p}_\perp + i \not{D}_\perp - m) \xi_{n,\tilde{p}} + \bar{\xi}_{n,\tilde{p}'} (\not{p}_\perp + i \not{D}_\perp - m) \hat{\xi}_{n,\tilde{p}} \right]. \end{aligned} \quad (4.10)$$

In the second term of the above result one can see that D^- is of order λ^2 and therefore suppressed w.r.t. p^- . In the leading Lagrangian, which is $\mathcal{O}(\lambda^4)$, the field $\hat{\xi}_{n,\tilde{p}}$ is therefore not dynamical and can be integrated out using the equation of motion [6, 28]:

$$(\tilde{p}^- + i D^-) \hat{\xi}_{n,\tilde{p}} = (\not{p}_\perp + i \not{D}_\perp + m) \frac{\not{n}}{2} \xi_{n,\tilde{p}}. \quad (4.11)$$

⁴To separate the dynamics of the label and the residual momentum components is already known from other EFTs and illustrated for SCET in [7].

Applying the same procedure to the \bar{n} -collinear quark Lagrangian one finds a corresponding expression. One can determine the power counting of the different fields by looking at their kinetic term. By imposing that the kinetic term in the action is of $\mathcal{O}(\lambda^0)$ and the fact that the final fields only contain residual dynamics, which is the reason that the derivatives count as λ^2 , we can easily determine the power counting of the fields. Then it is easy to argue that the usoft quark Lagrangian is suppressed in λ .

Now one decomposes the gluon field, in analogy with the quark field, in an n -, \bar{n} -collinear and usoft part i.e. $A^\mu = A_n^\mu + A_{\bar{n}}^\mu + A_{us}^\mu$. Their power counting is obtained the same way as for the quark fields [6].

Then we expand the n -collinear quark Lagrangian to $\mathcal{O}(\lambda^4)$. Involving an implicit sum over all labels the Lagrangian reads:

$$\begin{aligned} \mathcal{L}_{q,n} = & \bar{\xi}_{n,p} \left[iD^+ + \frac{p_\perp^2}{\bar{n} \cdot p} \right] \frac{\not{n}}{2} \xi_{n,p} \\ & + g_s \bar{\xi}_{n,p'} \left[A_{n,r}^+ + A_{n,r}^\perp \frac{(\not{p}_\perp + m)}{\bar{n} \cdot p} + \frac{(\not{p}'_\perp - m)}{\bar{n} \cdot p'} A_{n,r}^\perp - \frac{(\not{p}'_\perp - m)(\not{p}_\perp + m)}{\bar{n} \cdot p' \bar{n} \cdot p} A_{n,r}^- \right] \frac{\not{n}}{2} \xi_{n,\tilde{p}} \\ & + g_s^2 \bar{\xi}_{n,p'} \left[\frac{1}{\bar{n} \cdot (p - q)} \left\{ A_{n,q}^\perp A_{n,r-q}^\perp - A_{n,q}^- \frac{(\not{p}'_\perp - m)}{\bar{n} \cdot p'} A_{n,r-q}^\perp - A_{n,q}^\perp \frac{(\not{p}_\perp + m)}{\bar{n} \cdot p} A_{n,r-q}^- \right. \right. \\ & \quad \left. \left. + \frac{(\not{p}'_\perp - m)(\not{p}_\perp + m)}{\bar{n} \cdot p' \bar{n} \cdot p} A_{n,q}^- A_{n,r-q}^- \right\} \right] \frac{\not{n}}{2} \xi_{n,\tilde{p}} + \mathcal{O}(g_s^3, \lambda^5), \end{aligned} \quad (4.12)$$

where $r \equiv p' - p$ and $D^\mu = \partial^\mu - ig_s A_{us}^\mu$. Together with the Lagrangian of \bar{n} -collinear quarks and the Lagrangian of collinear and usoft gluons [8] this yields the whole $\mathcal{O}(\lambda^4)$ SCET Lagrangian. From this one can obtain the effective theory Feynman rules which are given in Sec. C.

Remark: Here one can also see the origin of the so-called *zero bin subtractions* [29]. First we divided the gluon field into collinear and usoft fields, then we separated the label from the residual momentum dynamics in the collinear fields. If we calculate Feynman diagrams involving collinear and usoft gluons we double count the usoft region since the label $\tilde{p} = 0$ corresponds to an usoft gluon. This means we did not achieve complete separation between these modes which has to be compensated by an explicit subtraction of the $\tilde{p} = 0$ bin, i.e. the *zero bin*.

4.3. Wilson Lines

4.3.1. Collinear Wilson Lines

In a full QCD calculation the interactions between \bar{n} -collinear antiquarks with n -collinear gluons is of course not prohibited. Since it would push the antiquark far off-shell these contributions are integrated out in SCET. To reproduce also these contributions they are expected to reappear in the matching calculations. In fact so-called collinear Wilson lines [6, 8] which arise in the matching will account for these contributions.

The discussed QCD process is illustrated in Fig. 5. To determine the contribution to the SCET current we change to collinear fields and expand in λ using the SCET power counting. Involving a collinear (anti)quark and several collinear gluon fields we get⁵:

$$\bar{\xi}_n \Gamma^\mu \frac{i(-\not{p}_2 - \sum_i \not{q}_i + m)}{(p_2 + \sum_i q_i)^2 - m^2 + i0} (ig_s \gamma_{\mu_m} A_{n,q_m}^{\mu_m} \tilde{\mu}^\epsilon) \times \dots \times \frac{i(-\not{p}_2 - \not{q}_1 + m)}{(p_2 - q_1)^2 - m^2 + i0} (ig_s \gamma_{\mu_1} A_{n,q_1}^{\mu_1} \tilde{\mu}^\epsilon) \xi_{\bar{n}}.$$

⁵We use the notation $A_\mu := T_\mu^a A^a$.

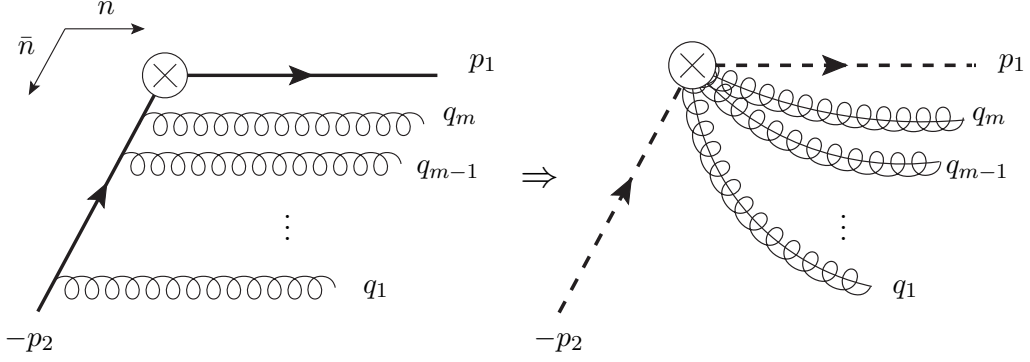


Figure 5: Collinear Wilson lines (all gluon momenta are outgoing)

(4.13)

In the next step we apply the power counting where the antiquark is \bar{n} -collinear and the quark and gluons are n -collinear. Furthermore we use the gamma matrix decomposition

$$\gamma^\mu = \frac{\not{n}}{2} n^\mu + \frac{\not{\bar{n}}}{2} \bar{n}^\mu + \gamma_\perp^\mu, \quad (4.14)$$

and the relations of Eq. (4.9) to obtain:

$$\bar{\xi}_n \Gamma^\mu \frac{-i(p_2^+ \bar{n}_{\mu_m} + (\sum_i q_i^-) \frac{\not{n}}{2} \gamma_{\mu_m}^\perp)}{(p_2^+)(\sum_i q_i^-) + i0 + \mathcal{O}(\lambda^2)} (ig_s A_{n,q_m}^{\mu_m} \tilde{\mu}^\epsilon) \cdots \frac{-i(p_2^+ \bar{n}_{\mu_1} + q_1^- \frac{\not{n}}{2} \gamma_{\mu_1}^\perp)}{(p_2^+)(q_1^-) + i0 + \mathcal{O}(\lambda^2)} (ig_s A_{n,q_1}^{\mu_1} \tilde{\mu}^\epsilon). \quad (4.15)$$

Since the second term of each numerator is suppressed when the contraction with the collinear gluon field is carried out we arrive at the result:

$$(g_s \tilde{\mu}^\epsilon)^m \frac{\bar{n}_{\mu_1} \cdots \bar{n}_{\mu_m}}{(q_1^- + i0) \cdots (\sum_i q_i^- + i0)} \left[\bar{\xi}_n \Gamma^\mu A_{n,q_m}^{\mu_m} \cdots A_{n,q_1}^{\mu_1} \xi_{\bar{n}} \right] + \mathcal{O}(\lambda). \quad (4.16)$$

Of course the same considerations are valid for \bar{n} -collinear gluons radiated by a n -collinear quark. The calculations are in complete analogy with the previous ones and are therefore omitted. Furthermore at leading order in λ arbitrary many of these (identical) gluons can be emitted which tells us to sum over the number of gluons m and the permutations of their occurrence which yields the n and \bar{n} -collinear Wilson lines in momentum space:

$$W_n = \sum_m \sum_{perm.} (g_s \tilde{\mu}^\epsilon)^m \frac{\bar{n}_{\mu_1} \cdots \bar{n}_{\mu_m}}{(q_1^- + i0) \cdots (\sum_i q_i^- + i0)} A_{n,q_m}^{\mu_m} \cdots A_{n,q_1}^{\mu_1}, \quad (4.17)$$

$$W_{\bar{n}}^\dagger = \sum_m \sum_{perm.} (-g_s \tilde{\mu}^\epsilon)^m \frac{n_{\mu_1} \cdots n_{\mu_m}}{(q_1^+ + i0) \cdots (\sum_i q_i^+ + i0)} A_{\bar{n},q_1}^{\mu_1} \cdots A_{\bar{n},q_m}^{\mu_m}. \quad (4.18)$$

These Wilson lines effectively account for the interaction of any number of $\bar{n}(n)$ -collinear gluons with a $n(\bar{n})$ -collinear quark (antiquark) in SCET. Next we perform the Fourier transform of these Wilson lines to position space. The position space gluon is connected to an outgoing gluon in momentum space via $\bar{n} \cdot A_n(x) = \int \frac{d^d q}{(2\pi)^d} \exp(iq \cdot x) \bar{n} \cdot A_{n,q}$. This yields:

$$W_n(x) = \bar{P} \exp \left[-ig \tilde{\mu}^\epsilon \int_0^\infty ds \bar{n} \cdot A_n(s \bar{n} + x) \right],$$

$$W_{\bar{n}}^\dagger(x) = P \exp \left[ig \tilde{\mu}^\epsilon \int_0^\infty ds n \cdot A_{\bar{n}}(s n + x) \right], \quad (4.19)$$

where $P(\bar{P})$ denotes path(antipath) ordering of the involved fields. Then the full SCET current which is important for the matching on QCD reads $\bar{\chi}_n \Gamma^\mu \chi_{\bar{n}}$ involving the $n(\bar{n})$ -collinear jet field $\chi_{n(\bar{n}),P} = W_{n(\bar{n})}^\dagger \xi_{n(\bar{n}),p}$ and $P = p + \sum_i q_i$ the jet momentum (also see [9]).

4.3.2. Usoft Wilson Lines

Next let's look at the interactions between usoft gluons and collinear (anti)quarks. In fact these interactions can also be summed in a so-called usoft Wilson line [8]. In analogy with the collinear case we calculate these usoft Wilson lines by looking at contributions like the ones illustrated in Fig. 6. We find:

$$Y_n^\dagger = \sum_m \sum_{\text{perm}} (-g_s \tilde{\mu}^\epsilon)^m \frac{n_{\mu_1} \cdots n_{\mu_m}}{(\sum q_i^+ + i0) \cdots (\sum_i q_i^+ + i0)} A_{us}^{\mu_1} \cdots A_{us}^{\mu_m}, \quad (4.20)$$

$$Y_{\bar{n}} = \sum_m \sum_{\text{perm}} (g_s \tilde{\mu}^\epsilon)^m \frac{n_{\mu_1} \cdots n_{\mu_m}}{(\sum q_i^+ - i0) \cdots (\sum_i q_i^+ - i0)} A_{us}^{\mu_m} \cdots A_{us}^{\mu_1}. \quad (4.21)$$



Figure 6: Usoft gluons interacting with a collinear (anti)quark to give an usoft Wilson lines (all gluon momenta are outgoing)

When taking the Fourier transform of these usoft Wilson lines one obtains:

$$Y_n^\dagger(x) = P \exp \left[ig \tilde{\mu}^\epsilon \int_0^\infty ds \, n \cdot A_{us}(s n + x) \right],$$

$$Y_{\bar{n}}(x) = \bar{P} \exp \left[-ig \tilde{\mu}^\epsilon \int_0^\infty ds \, \bar{n} \cdot A_{us}(s \bar{n} + x) \right]. \quad (4.22)$$

Furthermore the interaction of usoft gluons with collinear (anti)quarks can be removed from the Lagrangian by performing a field redefinition [8] of the form:

$$\begin{aligned} \xi_n &\rightarrow Y_n \xi_n^{(0)} & \xi_{\bar{n}} &\rightarrow Y_{\bar{n}} \xi_{\bar{n}}^{(0)}, \\ A_n &\rightarrow Y_n A_n^{(0)} Y_n^\dagger, & A_{\bar{n}} &\rightarrow Y_{\bar{n}} A_{\bar{n}}^{(0)} Y_{\bar{n}}^\dagger, \end{aligned} \quad (4.23)$$

where the fields with the “0” label are new collinear fields which no longer interact with usoft gluons. This effectively rewrites the current as:

$$\bar{\xi}_n \Gamma^\mu \xi_{\bar{n}} \rightarrow \bar{\xi}_n^{(0)} Y_n^\dagger \Gamma^\mu Y_{\bar{n}} \xi_{\bar{n}}^{(0)}. \quad (4.24)$$

Together with the change from the collinear Wilson lines and secondary massive particles which give rise to soft Wilson lines [27] the full SCET current is then given by Eq. (5.4).

5. Factorization for the Massive c-Parameter

In this section we want to show that starting with the QCD cross-section in the dijet limit and rewriting it in terms of SCET expressions one can arrive at a factorized cross-section formula. This factorization separates the cross-section in three factors and reads:

$$\sigma = H \cdot J \otimes S. \quad (5.1)$$

The first factor, called hard function, is basically the squared Wilson coefficient between SCET and QCD and therefore encodes hard physics. In addition one encounters a convolution between the so-called jet and soft functions. The jet function accounts for the dynamics within the jet(s) while the soft function takes care of the soft radiation and soft cross talk between them.

We will start by deriving a general factorized SCET cross-section. After that we will use our findings regarding the massive c-parameter kinematics to impose certain kinematic constraints. In the end we simplify the result and thereby arrive at our final formula for the differential c-parameter cross-section.

5.1. General Factorization Formula

In this derivation we will follow [26] and therefore omit some of the intermediate steps. To derive a general factorized SCET cross-section one starts with the full QCD cross-section of the process $e^+e^- \rightarrow \gamma^*, Z^* \rightarrow Q\bar{Q} + X$ which we already know from Eq. (3.9)⁶:

$$\sigma = \sum_X^{res} (2\pi)^4 \delta^{(4)}(q - P_X) \sum_{i=a,v} L_{\mu\nu}^i \langle 0 | \mathcal{J}_i^{\nu\dagger}(0) | X \rangle \langle X | \mathcal{J}_i^\mu(0) | 0 \rangle. \quad (5.2)$$

For our purposes we assume the production of two particles which are back to back (namely the $Q\bar{Q}$ pair) and only collinear and soft gluon radiation. This is implemented by the restricted sum which only includes states which involve a n -collinear and a \bar{n} -collinear jet together with soft radiation. In this context one also calls this configuration the *dijet-limit*. For this setup SCET is applicable and we switch from the current in QCD to the one in SCET J_i^μ . Already in Sec. 4.3 we saw how Wilson lines arise and modify the current in SCET. This and its connection to special gauge transformations is discussed in more detail in [8, 9]. The matching to QCD is then given by:

$$\mathcal{J}_i^\mu(0) = \int d\omega d\bar{\omega} C(\omega, \bar{\omega}, \mu) J_i^{(0)\mu}(\omega, \bar{\omega}, \mu), \quad (5.3)$$

with:

$$J_i^{(0)\mu} = (\bar{\chi}_{n,\omega} Y_n^\dagger S_n^\dagger \Gamma_i^\mu S_{\bar{n}} Y_{\bar{n}} \chi_{\bar{n},\bar{\omega}})(0), \quad (5.4)$$

involving the jet field χ_n , usoft and mass mode Wilson lines Y_n and S_n (see Sec. 4.3).

On top of that we impose the factorization of the final state and the phase space into collinear and soft contributions which makes sense since a final state particle belongs unambiguously either to one of the jets or to soft radiation⁷:

$$|X\rangle = |X_n\rangle |X_{\bar{n}}\rangle |X_s\rangle. \quad (5.5)$$

⁶The sum over all final state configurations also contains the integration over the phase space. It is omitted for convenience.

⁷In [30] this assumption is criticized and shown to be unnecessary. The authors discuss a method to derive a factorized formula without final state factorization which should lack several drawbacks of the presented one. The argument is shown for a class of massless e^+e^- event-shapes and it is not obvious that it also applies for our massive c-parameter. Nevertheless one should be able to generalize their argument by using methods from [31].

Using this and a generalized fierz formula⁸ one can write the cross-section formula as three factors where each one accounts for a different kinematic region. Note that color and spin traces are implied for each factor separately, hence these factors are singlets with respect to color and spin transformations. The cross-section is now given by:

$$\sigma^i = \frac{K_0^i}{16N_c^2} \mathcal{M}(m, \mu) \sum_{\vec{n}} \sum_{X_n, X_{\bar{n}}, X_s}^{res} (2\pi)^4 \delta^{(4)}(q - P_{X_n} + P_{X_{\bar{n}}} + P_{X_s}) \int d\omega d\bar{\omega} |C(\omega, \bar{\omega})|^2 \quad (5.6)$$

$$\times \langle 0 | \bar{Y}_{\vec{n}}^{bd} Y_n^{be} | X_s \rangle \langle X_s | Y_n^{\dagger ec} \bar{Y}_{\vec{n}}^{\dagger dc} | 0 \rangle \langle 0 | \bar{\chi}_{\vec{n}} | X_{\bar{n}} \rangle \langle X_{\bar{n}} | \not{n} \chi_{\vec{n}, \bar{\omega}} | 0 \rangle \langle 0 | \not{n} \chi_n | X_n \rangle \langle X_n | \bar{\chi}_{n, \omega} | 0 \rangle ,$$

where a normalization factor $K_0 = 2(d-2)c_{lep}^i$ and the vacuum mass mode matrix element \mathcal{M} was introduced⁹. Momentum conservation implies that $C(\omega, \bar{\omega}, \mu) = C(Q, -Q, \mu) \equiv C(Q, \mu)$. Furthermore we introduced *barred* usoft Wilson lines which arise since the matrix elements are in fact time-ordered (respectively antitime-ordered). By switching to these barred Wilson lines this ordering becomes redundant [26]. The involved barred Wilson lines are given by:

$$\bar{Y}_{\vec{n}} = T(Y_{\vec{n}})^T = \bar{P} \exp \left[-ig\tilde{\mu}^\epsilon \int_0^\infty ds \bar{n} \cdot \bar{A}_{us}(s\bar{n} + x) \right] ,$$

$$\bar{Y}_{\vec{n}}^\dagger = \bar{T}(Y_{\vec{n}}^\dagger)^T = P \exp \left[ig\tilde{\mu}^\epsilon \int_0^\infty ds \bar{n} \cdot \bar{A}_{us}(s\bar{n} + x) \right] , \quad (5.7)$$

where $\bar{A}_{us} = A_{us}^A \bar{T}^A$ with $\bar{T}^A = -(T^A)^T$. The unbarred usoft Wilson lines are given in Eq. (4.22).

In the next step of the derivation most of the kinematic constraints are implemented by introducing corresponding delta functions and utilizing SCET properties. The remaining delta functions are then turned into integrals over exponentials [26]. Some further manipulations yield the general factorized SCET cross-section formula:

$$\sigma^i = \sigma_0^i |C(Q, \mu)|^2 \int dk_n^+ dk_{\bar{n}}^- dk_s^+ dk_s^- \quad (5.8)$$

$$\times \sum_{X_n}^{res} \frac{1}{2\pi} \int d^4x e^{\frac{i}{2}k_n^+ x^-} \text{Tr} \langle 0 | \left(\frac{\not{n}}{4N_c} \right) \chi_n(x) | X_n \rangle \langle X_n | \bar{\chi}_{n, Q}(0) | 0 \rangle$$

$$\times \sum_{X_{\bar{n}}}^{res} \frac{1}{2\pi} \int d^4y e^{\frac{i}{2}k_{\bar{n}}^- y^+} \text{Tr} \langle 0 | \bar{\chi}_{\bar{n}}(y) | X_{\bar{n}} \rangle \langle X_{\bar{n}} | \left(\frac{\not{\bar{n}}}{4N_c} \right) \chi_{\bar{n}, -Q}(0) | 0 \rangle$$

$$\times \sum_{X_s}^{res} \frac{1}{4N_c(2\pi)^2} \int dz^+ dz^- e^{\frac{i}{2}(k_s^+ z^- + k_s^- z^+)} \text{Tr} \langle 0 | \bar{Y}_{\vec{n}}(z^+) Y_n(z^-) | X_s \rangle \langle X_s | Y_n^\dagger(0) \bar{Y}_{\vec{n}}^\dagger(0) | 0 \rangle .$$

5.2. Kinematic Considerations

In this subsection we take a closer look into the kinematics of the massive c-parameter in the dijet limit. We would like to show that it can be written as a sum of contributions from the different kinematic regions, hence one from each collinear and a soft contribution:

$$c_{dijet} = c_{ss} + c_{ns} + c_{\bar{n}s} + c_{sn} + c_{s\bar{n}} + c_{nn} + c_{\bar{n}\bar{n}} + c_{n\bar{n}} + c_{\bar{n}n}$$

$$= c_{ss} + 2(c_{sn} + c_{s\bar{n}}) + c_{nn} + c_{\bar{n}\bar{n}} + 2c_{n\bar{n}}$$

$$= c_s + c_n + c_{\bar{n}} . \quad (5.9)$$

⁸This fierz formula can be derived by using SCET power counting and Eq. (33) from [32].

⁹The mass modes only contribute in higher orders (see the discussion in [26]) thus $\mathcal{M} = 1 + \mathcal{O}(\alpha_s^2)$. This is the reason why we can drop this factor.

The first step is to rewrite our massive c-parameter definition in a way which is useful for showing that Eq. (5.9) holds (we use $q^2 = (\sum_i p_i)^2 = \sum_{i,j} (p_i \cdot p_j) = Q^2$):

$$c = \frac{1}{4Q^2} \left[2Q^2 - \sum_{i \neq j} \frac{(p_i \cdot p_j)^2}{p_i^0 p_j^0} \right] = \frac{1}{4Q^2} \sum_{i,j} \frac{1}{p_i^0 p_j^0} \left[2(p_i \cdot p_j) p_i^0 p_j^0 - (p_i \cdot p_j)^2 (1 - \delta_{ij}) \right]. \quad (5.10)$$

Rearranging it as a sum of the different kinematic regions yields:

$$c = \frac{1}{4Q^2} \sum_{a,b} \sum_{\substack{i \in a \\ j \in b}} \frac{1}{p_i^0 p_j^0} \left[(p_i \cdot p_j) (p_i^0 p_j^0 - p_i \cdot p_j) + \delta_{ab} \delta_{ij} m_i^4 \right]. \quad (5.11)$$

Now we use relations for light cone coordinates $2p_i^0 = p_i^+ + p_i^-$ and $2(p_i \cdot p_j) = p_i^+ p_j^- + p_i^- p_j^+ + p_i^\perp \cdot p_j^\perp$ and note that the last factor of Eq. (5.11) is always $\mathcal{O}(\lambda^4)$ since for a collinear particle $m_c \sim \lambda$ and for a soft particle $m_s \sim \lambda^2$ holds. By simplifying our last result one obtains:

$$c = \frac{1}{4Q^2} \sum_{a,b} \sum_{\substack{i \in a \\ j \in b}} \frac{(p_i^+ p_j^- + p_i^- p_j^+ + 2p_i^\perp \cdot p_j^\perp) (p_i^+ p_j^+ + p_i^- p_j^- + 2p_i^\perp \cdot p_j^\perp)}{(p_i^+ + p_i^-) (p_j^+ + p_j^-)} + \mathcal{O}(\lambda^4). \quad (5.12)$$

In the following we will look in the different kinematic regions and show that the relation of Eq. (5.9) indeed holds.

soft-soft and soft-collinear contributions

Contributions to the c-parameter involving soft particles read:

$$c_{ss} = \mathcal{O}(\lambda^4) \quad \Rightarrow \quad \text{subleading}, \quad (5.13)$$

$$c_{sn} = \frac{1}{4Q^2} \sum_{\substack{i \in s \\ j \in n}} \frac{p_i^+ p_i^- (p_j^-)^2}{(p_i^+ + p_i^-) p_j^-} + \mathcal{O}(\lambda^4) = \frac{1}{4Q^2} \left(\sum_{j \in n} p_j^- \right) \sum_{i \in s} \frac{p_i^+ p_i^-}{p_i^+ + p_i^-} + \mathcal{O}(\lambda^4). \quad (5.14)$$

For collinear particles $m_c \sim \lambda$ holds. From this we get the following relations:

$$\begin{aligned} |\vec{p}_i| &= \sqrt{(p_i^0)^2 - m_c^2} = \frac{1}{2} \sqrt{(p_i^+ + p_i^-)^2 - 4m_c^2} = \frac{1}{2} p_i^- + \mathcal{O}(\lambda^2), \\ \sum_{i \in n} |\vec{p}_i| &= \sum_{i \in \bar{n}} |\vec{p}_i| + \mathcal{O}(\lambda^2), \\ \sum_{i \in c} |\vec{p}_i| &= Q + \mathcal{O}(\lambda^2) = 2 \sum_{i \in n} |\vec{p}_i| + \mathcal{O}(\lambda^2). \end{aligned}$$

For convenience we also define \mathbb{P}_a^μ and note:

$$\begin{aligned} \mathbb{P}_a^\mu &\equiv \sum_{i \in a} p_i^\mu, \\ \mathbb{P}_n^- &= 2 \mathbb{P}_n^0 + \mathcal{O}(\lambda^2) = 2 \sum_{i \in n} |\vec{p}_i| + \mathcal{O}(\lambda^2) = Q + \mathcal{O}(\lambda^2), \\ \mathbb{P}_{\bar{n}}^+ &= Q + \mathcal{O}(\lambda^2) \quad \Rightarrow \quad \mathbb{P}_n^- = \mathbb{P}_{\bar{n}}^+ + \mathcal{O}(\lambda^2), \\ \mathbb{P}_n^\perp &= \mathbb{P}_{\bar{n}}^\perp = \mathcal{O}(\lambda^2), \end{aligned}$$

where the last relation is true since the total transverse momentum in one hemisphere adds up to 0 with respect to the thrust axis. Using these relations one is now able to write all c-parameter contributions involving soft particles as:

$$\begin{aligned} c_{sn} &= \frac{\mathbb{P}_n^-}{4Q^2} \sum_{i \in s} \frac{p_i^+ p_i^-}{p_i^+ + p_i^-} + \mathcal{O}(\lambda^4) = \frac{1}{4Q} \sum_{i \in s} \frac{p_i^+ p_i^-}{p_i^+ + p_i^-} + \mathcal{O}(\lambda^4) = c_{s\bar{n}} , \\ c_s &= 2(c_{sn} + c_{s\bar{n}}) = \frac{1}{Q} \sum_{i \in s} \frac{p_i^+ p_i^-}{p_i^+ + p_i^-} + \mathcal{O}(\lambda^4) . \end{aligned} \quad (5.15)$$

collinear-collinear contributions

The contributions involving only collinear particles can be derived by simple power counting and read:

$$\begin{aligned} c_{nn} &= \frac{1}{4Q^2} \sum_{i,j \in n} \frac{(p_i^+ p_j^- + p_i^- p_j^+) p_i^- p_j^-}{p_i^- p_j^-} + \mathcal{O}(\lambda^4) = \frac{1}{2Q} \mathbb{P}_n^+ + \mathcal{O}(\lambda^4) , \\ c_{\bar{n}\bar{n}} &= \frac{1}{4Q^2} \sum_{i,j \in \bar{n}} \frac{(p_i^+ p_j^- + p_i^- p_j^+) p_i^+ p_j^+}{p_i^+ p_j^+} + \mathcal{O}(\lambda^4) = \frac{1}{2Q} \mathbb{P}_{\bar{n}}^- + \mathcal{O}(\lambda^4) , \\ c_{n\bar{n}} &= \frac{1}{4Q^2} \sum_{\substack{i \in n \\ j \in \bar{n}}} \frac{p_i^- p_j^+ (p_i^+ p_j^+ + p_i^- p_j^-)}{p_i^- p_j^+} + \mathcal{O}(\lambda^4) = \frac{1}{4Q} (\mathbb{P}_n^+ + \mathbb{P}_{\bar{n}}^-) + \mathcal{O}(\lambda^4) . \end{aligned} \quad (5.16)$$

Now it directly follows that:

$$c_{nn} + c_{\bar{n}\bar{n}} + 2c_{n\bar{n}} = \frac{1}{Q} \left\{ \mathbb{P}_n^+ + \mathbb{P}_{\bar{n}}^- \right\} + \mathcal{O}(\lambda^4) , \quad (5.17)$$

$$c_n = \frac{1}{Q} \mathbb{P}_n^+ + \mathcal{O}(\lambda^4) , \quad (5.18)$$

$$c_{\bar{n}} = \frac{1}{Q} \mathbb{P}_{\bar{n}}^- + \mathcal{O}(\lambda^4) . \quad (5.19)$$

This shows that Eq. (5.9) indeed holds.

5.3. Massive c-Parameter Factorization Formula

Now we want to exploit the results of the previous subsection. By inserting the identity operator we implement our c-parameter prescription:

$$\mathbb{1} = \int dc \, \delta(c - c_n - c_{\bar{n}} - c_s) \int dc_n \, \delta\left(c_n - \frac{k_n^+}{Q}\right) \int dc_{\bar{n}} \, \delta\left(c_{\bar{n}} - \frac{k_{\bar{n}}^-}{Q}\right) \int dc_s \, \delta\left(c_s - \frac{k_s^+ k_s^-}{Q(k_s^+ + k_s^-)}\right) . \quad (5.20)$$

After the insertion of the above relation we work through the integrals, take a derivative with respect to c and arrive at the final differential cross-section for the c-parameter. Since we have imposed all of the kinematic constraints we were able to sum over the n - and \bar{n} -collinear final states and arrive at:

$$\begin{aligned} \frac{1}{\sigma_0^i} \frac{d\sigma^i}{dc} &= |C(Q, \mu)|^2 \int dc_n \, dc_{\bar{n}} \, dc_s \, \delta(c - c_n - c_{\bar{n}} - c_s) J_n(Q^2 c_n - m^2) J_{\bar{n}}(Q^2 c_{\bar{n}} - m^2) \\ &\quad \times \frac{Q^4}{4N_c (2\pi)^2} \sum_{X_s} \delta\left(c_s - \frac{1}{Q} \frac{k_s^+ k_s^-}{k_s^+ + k_s^-}\right) \langle 0 | \bar{Y}_{\bar{n}}(z^+) Y_n(z^-) | X_s \rangle \langle X_s | Y_n^\dagger(0) \bar{Y}_{\bar{n}}^\dagger(0) | 0 \rangle , \end{aligned} \quad (5.21)$$

where the jet functions (including an implicit spin-trace) are defined by:

$$J_n(Qk_n^+ - m^2, m, \mu) = \frac{1}{2\pi Q} \text{Disc} \left[i \int_{-\infty}^{\infty} dx e^{ik_n x} \langle 0 | T \left\{ \frac{\not{n}}{4} \chi_n(x) \bar{\chi}_{n,Q}(0) \right\} | 0 \rangle \right], \quad (5.22)$$

$$J_{\bar{n}}(Qk_{\bar{n}}^- - m^2, m, \mu) = \frac{-1}{2\pi Q} \text{Disc} \left[i \int_{-\infty}^{\infty} dy e^{ik_{\bar{n}} y} \langle 0 | T \left\{ \frac{\not{\bar{n}}}{4} \chi_{\bar{n},-Q}(0) \bar{\chi}_{\bar{n}}(y) \right\} | 0 \rangle \right]. \quad (5.23)$$

The substitution

$$c_n \rightarrow \frac{s' + m^2}{Q^2}, \quad c_{\bar{n}} \rightarrow \frac{s - s' + m^2}{Q^2}, \quad (5.24)$$

where $s = Qk_n^+ - m^2$ and $s' = Qk_{\bar{n}}^- - m^2$ is the off-shellness of the n - and \bar{n} -collinear jet (in expanded form). This leads to the final result which is given by:

$$\begin{aligned} \frac{1}{\sigma_0^i} \frac{d\sigma^i}{dc} &= Q H(Q, \mu) \int ds J_\tau(s, m, \mu) S_c(Q(c - 2\hat{m}^2) - \frac{s}{Q}, \mu), \\ H(Q, \mu) &= |C(Q, \mu)|^2, \\ J_\tau(s, m, \mu) &= \int ds' J_n(s', m, \mu) J_{\bar{n}}(s - s', m, \mu), \\ S_c(\ell, \mu) &= \frac{1}{N_c} \sum_{X_s} \delta\left(\ell - \frac{k_s^- k_s^+}{k_s^- + k_s^+}\right) \langle 0 | \bar{Y}_{\bar{n}} Y_n(0) | X_s \rangle \langle X_s | Y_n^\dagger \bar{Y}_{\bar{n}}^\dagger(0) | 0 \rangle. \end{aligned} \quad (5.25)$$

This means that we have achieved to write the cross-section as a product of three factors. These factors involve SCET matrix elements which can be determined separately. This will enable us to sum large logarithms of ratios of the characteristic scales (see Sec. 6.1).

Now let's examine this result in more detail and make first observations:

- As mentioned before the hard function is just the squared matching coefficient from SCET to QCD. Therefore it is universal for all e^+e^- event shapes. Results and detailed calculations are given in Sec. 6.2.1.
- The c-parameter jet function is a simple convolution of the hemisphere jet functions and therefore the same as for thrust. One could expect this since the assignment of the c-parameter in the n - and \bar{n} -collinear region is the same as for thrust and therefore these two event-shapes are the same in the kinematic region which the jet function accounts for. The detailed calculation can be found in Sec. 6.2.2.
- The soft function encodes all the soft radiation as well as soft cross-talk between the jets, thus it also gets non-perturbative contributions. In general the whole soft function is given by a convolution of a perturbative partonic soft function and a non-perturbative shape function (also called soft model function) [27, 33]:

$$S_c(l, \mu) = \int dl' S_c^{\text{part}}(\ell - \ell', \mu) S_c^{\text{mod}}(\ell'). \quad (5.26)$$

The used shape function and some connected issues are discussed in more detail in Sec. 6.4. In contrast to the corresponding thrust soft function the partonic c-parameter soft function cannot be calculated from the hemisphere soft function. We know that the soft function does not depend on the mass of primary heavy quarks (one can see this explicitly since the involved Wilson lines do not depend on the quark mass) but in higher orders gets a mass dependence from secondary heavy quarks. Therefore the massive c-parameter soft function at $\mathcal{O}(\alpha_s)$ should be the same as for the massless case [12]. More details concerning the calculation are given in Sec. 6.2.3.

6. Resummed Cross-Section

In this section we will derive the final form and all the contributions to the resummed SCET cross-section. We start by calculating the introduced hard, jet and soft function as well as their RG behavior. This will be used to resum large logarithms to next-to-next-to-leading-logarithmic (N²LL) accuracy.

To get a full description of the c -parameter cross-section we also need to include non-perturbative and kinematically power suppressed effects. Therefore we will add the so-called non-singular cross-section and later account for non-perturbative effects using the already mentioned shape function.

Furthermore we motivate and carry out explicit renormalon subtractions. This will increase the convergence of our perturbative series and thereby improve our analysis. In the end we will summarize the contributions to our cross-section formula and give details on the numerical implementation.

6.1. Large Log Resummation and the Renormalization Group

It is well known that in perturbative calculations of event shape distributions higher order contributions which should give small corrections are enhanced by logarithms of large ratios of the typical momentum scales [1, 3]. It is easy to see that if these logarithmic enhancement factors scale like $\ln \sim \alpha_s^{-1}$ they will spoil the perturbative series.

To counter this problem we can make use of the factorization theorem of Eq. (5.25) and standard renormalization group (RG) methods. Usually each cross-section factor contains the dynamics at a characteristic scale which is shown by the fact that the involved logarithms are ratios of this scale and the renormalization scale μ . Without any modification it is not possible to choose μ in a way to minimize all logs in the different cross-section factors. It becomes apparent that it is possible to write each of the cross-section factors as a so-called evolution kernel times a matching coefficient which is evaluated at some arbitrary matching scale μ_0 . The involved evolution factor, which is calculated by solving the corresponding RG equation, sums certain series of logarithms to all orders in perturbation theory. The argument of these resummed logarithms are ratios of μ and μ_0 while the arguments of the logarithms contained in the matching coefficient are ratios of μ_0 and the corresponding characteristic scale.

If one chooses the correct matching scale μ_0 one can minimize the logs contained in the mentioned matching coefficient while summing certain series of large logs with the evolution factor. It would be natural that this matching scale is similar to the corresponding characteristic scale but in general this is a non-trivial problem since these are c - and m -dependent. To see this we first look at $c \rightarrow c_{min}$ where several scales are present namely the c.o.m. energy Q , the invariant mass of the involved jets and the typical energy of the soft cross-talk between the jets¹⁰. Next we look at $c \rightarrow c_{max}(\hat{n})$ where we only find one typical scale which is Q . Between these two configurations we need a continuous transition which will be given in the form of so-called *profile functions* $\mu_0(c)$. They ensure that the logarithms contained in the matching coefficients stay small for different values of c and m and are discussed in more detail in Sec. 7.1.

In the following we will show how to calculate the evolution kernels in general. Explicit calculations will be done in Sec. 6.2.4.

First look at the hard function which satisfies the following RG equation:

$$\mu \frac{d}{d\mu} H(Q, \mu) = \gamma_H(Q, \mu) H(Q, \mu), \quad \gamma_H = \gamma_C + \gamma_C^\dagger, \quad (6.1)$$

¹⁰Of course there is also the non-perturbative scale Λ_{QCD} .

with γ_C the anomalous dimension of the Wilson coefficient. Now we introduce some convenient expressions for a general function F with an argument of dimension j . Let this function F fulfill some RG equation which is not specified at this point and define some perturbative coefficients:

$$\Gamma_F[\alpha_s(\mu)] = \sum_{i=0} \Gamma_{F,i} \left(\frac{\alpha_s(\mu)}{4\pi} \right)^{i+1}, \quad \gamma_F[\alpha_s(\mu)] = \sum_{i=0} \gamma_{F,i} \left(\frac{\alpha_s(\mu)}{4\pi} \right)^{i+1}, \quad (6.2)$$

as well as ω and K , which will play an important role in the evolution kernels:

$$\begin{aligned} \omega(\mu, \mu_0, \Gamma_F, j) &= \frac{2}{j} \int_{\alpha_s(\mu_0)}^{\alpha_s(\mu)} d\alpha \frac{\Gamma_F[\alpha]}{\beta[\alpha]}, \\ K(\mu, \mu_0, \Gamma_F, \gamma_F) &= 2 \int_{\alpha_s(\mu_0)}^{\alpha_s(\mu)} d\alpha \frac{\Gamma_F[\alpha]}{\beta[\alpha]} \int_{\alpha_s(\mu_0)}^{\alpha} \frac{d\alpha'}{\beta[\alpha']} + \int_{\alpha_s(\mu_0)}^{\alpha_s(\mu)} d\alpha \frac{\gamma_F[\alpha]}{\beta[\alpha]}. \end{aligned} \quad (6.3)$$

Note that we used the QCD beta function (see Sec. E.3 for explicit expressions and further information) which takes the form:

$$\mu \frac{d\alpha_s}{d\mu}(\mu) = \beta[\alpha_s(\mu)] = - \frac{\alpha_s^2(\mu)}{2\pi} \sum_{i=0} \beta_i \left(\frac{\alpha_s}{4\pi} \right)^i. \quad (6.4)$$

Now we can write down the general form of the anomalous dimension of the hard function (we will see that this holds true when doing explicit calculations in Sec. 6.2.4), which reads:

$$\gamma_H(Q, \mu) = - \Gamma_H[\alpha_s(\mu)] \ln \left(\frac{\mu^2}{Q^2} \right) + \gamma_H[\alpha_s(\mu)]. \quad (6.5)$$

Solving the RG equation of Eq. 6.1 by integrating from μ_H to μ yields:

$$\begin{aligned} H(Q, \mu) &= H(Q, \mu_H) \exp \left[\omega_H(\mu, \mu_H, \Gamma_H, 2) \ln \left(\frac{\mu_H^2}{Q^2} \right) + K_H(\mu, \mu_H, \Gamma_H, \gamma_H) \right] \\ &\equiv H(Q, \mu_H) U_H(Q, \mu_H, \mu). \end{aligned} \quad (6.6)$$

Now we have achieved the mentioned separation of the hard function into a matching coefficient at the hard scale μ_H and a factor which accounts for the μ -evolution which we call U_H .

Next we want to analyze the μ -evolution for the jet and the soft function. Their RG equations are given by [27]:

$$\mu \frac{d}{d\mu} J_{n,\bar{n}}(s, \mu) = \int ds' \gamma_{J_{n,\bar{n}}}(s-s') J_{n,\bar{n}}(s, \mu), \quad (6.7)$$

$$\mu \frac{d}{d\mu} S(\ell, \mu) = \int d\ell' \gamma_S(\ell-\ell') S(\ell, \mu). \quad (6.8)$$

Note that we have two types of RG behavior: local and convoluted. The former just depends on global constants, the latter is a convolution over anomalous dimensions, which depend on some kinematic variable, together with the involved function (for more details see [27]).

Since the RG equation for the jet function takes an analogous form as for the soft function we can do the calculations for both at the same time by looking again at a general function F with the following RG equation:

$$\mu \frac{d}{d\mu} F(t, \mu) = \int dt' \gamma_F(t-t', \mu) F(t', \mu). \quad (6.9)$$

The general form of the anomalous dimension is given by [27]:

$$\gamma_F(t-t', \mu) = -2\Gamma_F[\alpha_s(\mu)] \left\{ \frac{1}{j\kappa^j} \left[\frac{\mu^j \theta(t-t')}{t-t'} \right]_+ - \delta(t-t') \ln \left(\frac{\mu}{\kappa} \right) \right\} + \gamma_F[\alpha_s(\mu)] \delta(t-t') , \quad (6.10)$$

where j is the dimension of the argument of F and κ an arbitrary positive momentum scale (in the following we set $\kappa = \mu$). Actually it is convenient to look at this in Fourier space (we denote the Fourier transform of a function as $\mathcal{F}(f)(y) = \tilde{f}(y) = \int dt \exp(-ity) f(t)$ and use relations from Sec. B) where the last two equations are given by:

$$\mu \frac{d}{d\mu} \tilde{F}(y, \mu) = \tilde{\gamma}_F(y, \mu) \tilde{F}(y, \mu) , \quad (6.11)$$

$$\tilde{\gamma}_F(y, \mu) = \frac{2\Gamma_F[\alpha_s(\mu)]}{j} \ln(iy\mu^j e^{\gamma_E}) + \gamma_F[\alpha_s(\mu)] , \quad (6.12)$$

with $y \equiv y - i0$. Solving the RG equation by integrating from μ_0 to μ we get:

$$\begin{aligned} \tilde{F}(y, \mu) &= \exp[\omega_F(\mu, \mu_0, \Gamma_F, j) \ln(iy\mu_0^j e^{\gamma_E}) + K_F(\mu, \mu_0, \Gamma_F, \gamma_F)] \tilde{F}(y, \mu_0) \\ &\equiv \tilde{U}_F(y, \mu, \mu_0) \tilde{F}(y, \mu_0) , \end{aligned} \quad (6.13)$$

where again ω and K defined in Eq. (6.3) were used.

To get the evolution kernel in momentum space we calculate the inverse Fourier transform which is given by $\mathcal{F}^{-1}(\tilde{f})(t) = 1/(2\pi) \int dy \exp(iy) \tilde{f}(y)$. This yields:

$$U_F(t-t', \mu, \mu_0) = \frac{e^{K_F(e^{\gamma_E})\omega_F}}{\mu_0^j \Gamma(-\omega_F)} \left[\frac{(\mu_0^j)^{1+\omega_F} \theta(t-t')}{(t-t')^{1+\omega_F}} \right]_+ . \quad (6.14)$$

Now we have determined the general form of the involved evolution kernels. The explicit form of the ω_F and K_F will be given in Sec. 6.2.4.

Order of Log Resummation and Cross-Section Formula

In the first part of this subsection we discussed the principle idea of log resummation using RG methods and in this context the emergence of evolutions kernels. Since we only know a few orders of the perturbative expansion of the anomalous dimension and the involved matrix elements we can only resum series of logs to a corresponding order. How to consistently resum the most leading series of logarithms was clarified and reviewed in [34]. Furthermore there exist recipes in the SCET literature which specify the ingredients to achieve a certain log resummation (we adopt the conventions of [10]). These schemes and their ingredients are summarized in Tab. 2.

Overall we separated ordinary from log enhanced contributions, which were formally resummed in so-called evolution kernels. By the use of RG-methods we are able to calculate these expressions explicitly which subsequently will allow us to achieve a resummation of the three most important series of large logarithms to all orders in perturbation theory (therefore called next-to-next-to-leading logarithmic accuracy or simply N²LL). In the process we introduced several matching scales, namely the hard scale μ_H , the jet scale μ_J and the soft scale μ_S which should be similar to the physical scale of the corresponding cross-section factor. Details concerning these matching scales and the connected issue of profile functions will be discussed in Sec. 7.1. Involving all these improvements, the factorized cross-section formula from Eq. (5.25) can then be written as:

$$\begin{aligned} \frac{1}{\sigma_0^i} \frac{d\sigma^i}{dc} &= Q H(Q, \mu_H) U_H(Q, \mu_H, \mu) \int ds ds' U_J(s-s', \mu, \mu_J) J_\tau(s', m, \mu_J) \\ &\quad \times \int d\ell U_S\left(Qc - \frac{s+2m^2}{Q} - \ell, \mu, \mu_S\right) S_c(\ell, \mu_S) . \end{aligned} \quad (6.15)$$

	Γ_F	γ_F	Matching	Nonsingular
LL	1	0	0	0
NLL	2	1	0	0
N ² LL	3	2	1	1
N ³ LL _p	4_{pade}	3	2	2
NLL'	2	1	1	1
N ² LL'	3	2	2	2
N ³ LL' _p	4_{pade}	3	3	3

Table 2: Definition and ingredients for log resummation schemes (orders in α_s)

Since we now sum log enhanced terms which in ordinary (FO) perturbation theory would only contribute to higher orders we call this a *resummed perturbative expansion*.

6.2. Hard, Jet and Partonic Soft Function

In this subsection we will calculate different contributions to the perturbative part of the cross section formula given in Eq. (6.15). Therefore we calculate hard, jet and soft function defined in Eq. (5.25) to $\mathcal{O}(\alpha_s)$ and combine them with evolution kernels defined in the previous subsection.

6.2.1. Hard Function and Matching to QCD

We start by calculating the matching coefficient of SCET to QCD. The matching coefficient arises when we match the current in QCD to the current in SCET given by Eq. (5.3). The matching is realized by imposing that at a certain hard scale the matrix elements of the matched currents are the same, hence the matching coefficient gives the difference between these matrix elements order by order at the hard scale.

To calculate the matching coefficient one has to compute the renormalized QCD and SCET matrix elements and compare. The QCD matrix element was already calculated in Sec. 3.3 and the result is given in Eq. (3.58). As mentioned before leading SCET is not able to reproduce the complete mass structure of the full QCD result. This means that in the dijet region higher order mass effects are subleading in SCET what also results in an incomplete reproduction of the IR divergences which are multiplied by some powers of \hat{m} ¹¹. To cure this we match the SCET result to the leading order of the expanded QCD result (where all the IR divergences are reproduced), include some higher order mass dependence to the SCET results by shifting the threshold to the QCD threshold i.e. $c \rightarrow c + 2\hat{m}^4$ and account for residual subleading mass effects via contributions to the non-singular cross-section.

After the threshold shift it is easy to see that the tree level matrix element is the same for QCD and SCET which is why we only have to take the one loop matrix element into account.

To calculate the matching one has to properly expand the result of Eq. (3.58) for $m \ll Q$. We get

¹¹This should be interpreted in the sense of a Taylor expansion in \hat{m} .

(where $Q^2 \equiv Q^2 + i0$):

$$\begin{aligned} \langle \text{pp}' | \mathcal{J}_i^\mu | 0 \rangle_{\text{QCD}} |_{m^2 \ll Q^2} = & \Gamma_i^\mu \frac{\alpha_s(\mu) C_F}{4\pi} \left\{ -\frac{2}{\epsilon} - \frac{2}{\epsilon} \ln \left(\frac{m^2}{-Q^2} \right) - 4 - \ln \left(\frac{m^2}{-Q^2} \right) \right. \\ & \left. - 2 \ln \left(\frac{\mu^2}{-Q^2} \right) + \frac{\pi^2}{3} + \ln^2 \left(\frac{m^2}{-Q^2} \right) + \ln \left(\frac{m^2}{-Q^2} \right) \ln \left(\frac{-Q^2}{\mu^2} \right) \right\}. \end{aligned} \quad (6.16)$$

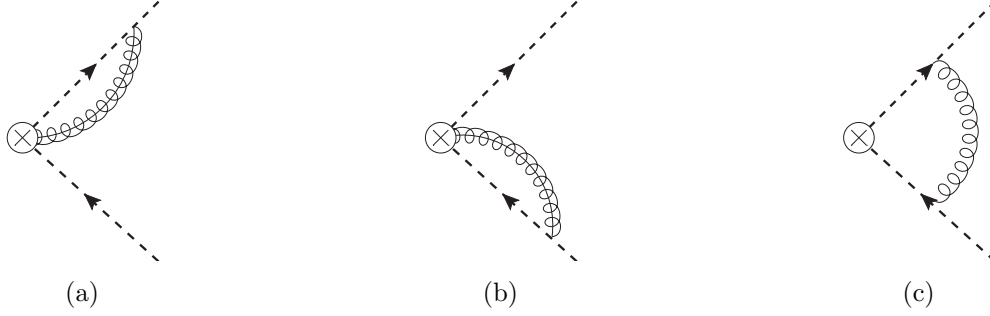


Figure 7: SCET diagrams contributing to the matching to $\mathcal{O}(\alpha_s)$

After expanding the QCD result we can calculate the corresponding SCET matrix elements by evaluating the diagrams in Fig. 7 (for details on the calculation see Sec. D.2) and applying the LSZ formula. Then the final SCET matrix element reads:

$$\begin{aligned} \langle \text{pp}' | J_i^\mu | 0 \rangle_{\text{SCET}} = & \Gamma_i^\mu \frac{\alpha_s(\mu) C_F}{4\pi} \left\{ \frac{2}{\epsilon^2} + \frac{1}{\epsilon} - \frac{2}{\epsilon} \ln \left(\frac{m^2}{-Q^2} \right) + \frac{2}{\epsilon} \ln \left(\frac{\mu^2}{-Q^2} \right) + \ln \left(\frac{\mu^2}{Q^2} \right) \right. \\ & \left. + \ln \left(\frac{Q^2}{m^2} \right) + \left[\ln \left(\frac{-Q^2}{\mu^2} \right) + \ln \left(\frac{m^2}{-Q^2} \right) \right]^2 + 4 + \frac{\pi^2}{6} \right\}. \end{aligned} \quad (6.17)$$

Now we can match the QCD and SCET matrix elements and get the defined matching coefficient:

$$\begin{aligned} \langle \text{pp}' | \mathcal{J}_i^\mu | 0 \rangle_{\text{QCD}} |_{m^2 \ll Q^2} = & C^0(Q, \mu) \langle \text{pp}' | J_i^\mu | 0 \rangle_{\text{SCET}} \\ \Rightarrow C^0(Q, \mu) = & 1 + \frac{\alpha_s(\mu) C_F}{4\pi} \left\{ -\frac{2}{\epsilon^2} - \frac{3}{\epsilon} - \frac{2}{\epsilon} \ln \left(\frac{\mu^2}{-Q^2 - i0} \right) \right. \\ & \left. - 3 \ln \left(\frac{\mu^2}{-Q^2 - i0} \right) - \ln^2 \left(\frac{\mu^2}{-Q^2 - i0} \right) - 8 + \frac{\pi^2}{6} \right\}. \end{aligned} \quad (6.18)$$

As the label “0” suggests the matching coefficient still needs to be renormalized¹². One can see this when calculating the diagrams with an IR regulator (for example a gluon mass or an off-shellness) so that just UV divergences which have to be renormalized remain. The renormalization is done with the matching coefficient counterterm $(Z_C - 1)$ which is the same as writing $C^0 = Z_C C$

$$Z_C(Q, \mu) = 1 - \frac{\alpha_s(\mu) C_F}{4\pi} \left\{ \frac{2}{\epsilon^2} + \frac{3}{\epsilon} + \frac{2}{\epsilon} \ln \left(\frac{\mu^2}{-Q^2 - i0} \right) \right\}. \quad (6.19)$$

The absolute square of the renormalized matching coefficient yields the final form of the hard function to $\mathcal{O}(\alpha_s)$ which reads:

$$H(Q, \mu) = |C(Q, \mu)|^2 = 1 + \frac{\alpha_s(\mu) C_F}{4\pi} \left\{ -6 \ln \left(\frac{\mu^2}{Q^2} \right) - 2 \ln^2 \left(\frac{\mu^2}{Q^2} \right) - 16 + \frac{7\pi^2}{3} \right\}. \quad (6.20)$$

¹²We choose here to renormalize the matching coefficient like it was done in [6] and not the current as in [26].

6.2.2. Jet Function

In this subsection we would like to calculate the thrust jet function with massive quarks to $\mathcal{O}(\alpha_s)$ which was first done in [27]. Since this function is a simple convolution of the two corresponding hemisphere jet functions we start by calculating them. Therefore we determine the diagrams in Fig. 8 and afterwards take the imaginary part. This will yield the hemisphere jet function as defined in Eq. (5.22) and in the following the thrust jet function.

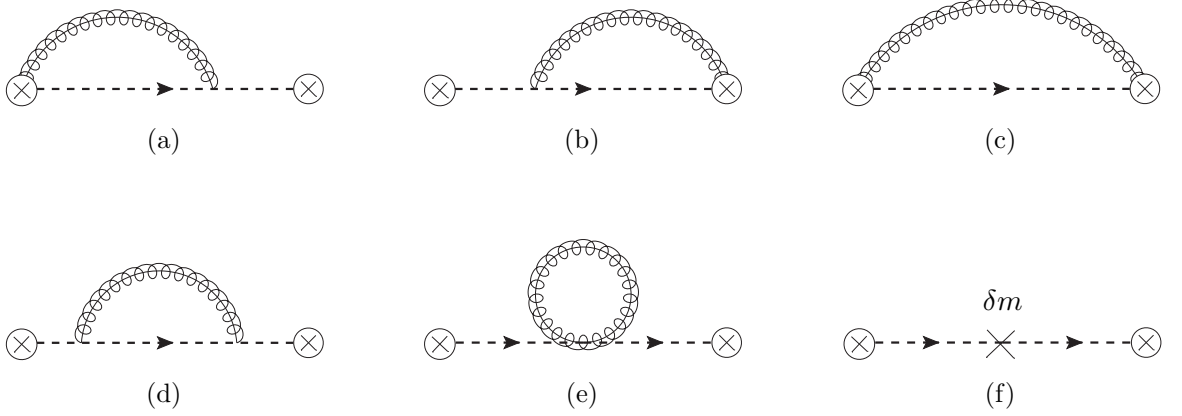


Figure 8: SCET diagrams contributing to the massive hemisphere jet function to $\mathcal{O}(\alpha_s)$

First one has to compute the trivial $\mathcal{O}(\alpha_s^0)$ diagram which is minus the propagator due to the definition of the jet function. Afterwards we determine the $\mathcal{O}(\alpha_s)$ diagrams which is done in Sec. D.1.1. For the sum of all contributions we then get:

$$\begin{aligned}
 J &= J_0 + J_a + J_b + J_c + J_d + J_e + J_f \\
 &= -i \frac{\not{n}}{2} \frac{Q}{s} \left\{ 1 + 2 \frac{m}{s} \delta m + \frac{\alpha_s C_F}{4\pi} \left[\frac{4}{\epsilon^2} + \frac{3}{\epsilon} + \frac{4}{\epsilon} \ln \left(\frac{\mu^2}{-s} \right) + 3 \ln \left(\frac{\mu^2}{-s} \right) + 2 \ln^2 \left(\frac{\mu^2}{-s} \right) \right. \right. \\
 &\quad \left. \left. - 2 \ln^2 \left(\frac{m^2}{-s} \right) + \ln \left(\frac{m^2}{-s} \right) \left(-4 \frac{m^2}{m^2 + s} + \frac{m^2(5m^2 + 6s)}{(m^2 + s)^2} \right) \right. \right. \\
 &\quad \left. \left. - 4 \text{Li}_2 \left(\frac{-s}{m^2} \right) + 8 + \pi^2 - \frac{s}{m^2 + s} \right] \right\}, \tag{6.21}
 \end{aligned}$$

where $s \equiv s + i0 = p^2 - m^2 + i0$ and we use some generic mass scheme defined by $m - m^{\text{pole}} = \delta m$. We know that the hemisphere jet function is given by:

$$J_{n,\bar{n}}(s, m, \mu) = \frac{1}{\pi Q} \text{Im} \left\{ i \text{Tr} \left(\frac{\not{n}}{4} J \right) \right\} \equiv \text{Im} \{ \hat{J} \}, \tag{6.22}$$

where it is easy to see that $\text{Tr}(\not{n}\not{n}) = 8$. Afterwards we take the imaginary part of \hat{J} , using relations of Sec. D.1.2. In the process we set $s \equiv s + i0 = \kappa^2 x + i0$ with x a dimensionless variable and $\kappa > 0$ a dummy scale to keep the right dimension. Without loss of generality we choose $\kappa = \mu$ which is very convenient. With this we get the bare hemisphere jet function to $\mathcal{O}(\alpha_s)$ which reads:

$$\begin{aligned}
 J_{n,\bar{n}}^0(s, m, \mu) &= \delta(s) - 2m\delta m \delta'(s) + \frac{\alpha_s(\mu)C_F}{4\pi} \left\{ \delta(s) \left(\frac{4}{\epsilon^2} + \frac{3}{\epsilon} + 2 \ln \left(\frac{m^2}{\mu^2} \right) + 8 + \pi^2 \right) \right. \\
 &\quad \left. - \frac{4}{\mu^2} \left[\frac{\mu^2 \theta(s)}{s} \right]_+ \left(\frac{1}{\epsilon} + \ln \left(\frac{m^2}{\mu^2} \right) + 1 \right) + \frac{8}{\mu^2} \left[\frac{\mu^2 \theta(s) \ln(s/\mu^2)}{s} \right]_+ \right. \\
 &\quad \left. + \theta(s) \left(\frac{s}{(m^2 + s)^2} - \frac{4}{s} \ln \left(1 + \frac{s}{m^2} \right) \right) \right\}. \tag{6.23}
 \end{aligned}$$

The renormalization of the jet function is given by [27]:

$$J_{n,\bar{n}}^0(s, m, \mu) = \int ds' Z_{J_{n,\bar{n}}}(s - s', \mu) J_{n,\bar{n}}(s', m, \mu), \quad (6.24)$$

which yields:

$$Z_{J_{n,\bar{n}}}(s - s', \mu) = \delta(s - s') + \frac{\alpha_s(\mu)C_F}{4\pi} \left\{ \delta(s - s') \left(\frac{4}{\epsilon^2} + \frac{3}{\epsilon} \right) - \frac{4}{\mu^2} \left[\frac{\mu^2 \theta(s)}{s} \right]_+ \right\}. \quad (6.25)$$

Now the renormalized hemisphere jet function follows immediately. The final expression we are interested in is the thrust jet function which is a simple convolution between the two hemisphere jet functions as given in Eq. (5.25) and therefore reads:

$$\begin{aligned} J_\tau(s, m, \mu) = \delta(s) + \frac{\alpha_s(\mu)C_F}{2\pi} & \left\{ \delta(s) \left(2 \ln \left(\frac{m^2}{\mu^2} \right) + 8 + \pi^2 \right) \right. \\ & - \frac{4}{\mu^2} \left[\frac{\mu^2 \theta(s)}{s} \right]_+ \left(\ln \left(\frac{m^2}{\mu^2} \right) + 1 \right) + \frac{8}{\mu^2} \left[\frac{\mu^2 \theta(s) \ln(s/\mu^2)}{s} \right]_+ \\ & \left. + \theta(s) \left(\frac{s}{(m^2 + s)^2} - \frac{4}{s} \ln \left(1 + \frac{s}{m^2} \right) \right) \right\}, \end{aligned} \quad (6.26)$$

where s is the typical off-shellness of the involved jets in expanded form.

6.2.3. Partonic Soft Function

The partonic soft function is defined in Eq. (5.25). We start by calculating the trivial tree level diagram which is given by a delta function and afterwards compute the diagrams of Fig. 9 (details concerning the diagrams are given in Sec. D.3) together with the delta function which imposes some kinematic constraints on radiated particles. The partonic soft function to $\mathcal{O}(\alpha_s)$ is then given by:

$$S_c^{part}(\ell, \mu) = \delta(\ell) + 16\pi\alpha_s(\mu)C_F\tilde{\mu}^{2\epsilon} \int \frac{d^d k}{(2\pi)^d} \delta\left(\ell - \frac{k^+ + k^-}{k^+ k^-}\right) \frac{\delta(k^2)}{k^+ k^-}. \quad (6.27)$$

The external particles (namely gluons) which carry the momentum k^μ are physical on-shell particles thus fulfill the on-shell condition for gluons $k^2 = 0$. Furthermore as physical particles they carry positive energy which overall results in the insertion of $(2\pi)\delta(k^2)\theta(k^0)^{13}$. Together with $d^d k = dk^+ dk^- d^{d-2} \vec{k}^\perp / 2$ we get:

$$\begin{aligned} \int \frac{d^d k}{(2\pi)^d} (2\pi)\delta(k^2)\theta(k^0) &= \frac{1}{2} \int \frac{dk^+ dk^-}{(2\pi)^2} \theta(k^+ + k^-) \int \frac{d^{d-2} \vec{k}^\perp}{(2\pi)^{d-3}} \delta(k^+ k^- - (k^\perp)^2) \\ &= \frac{1}{2} \int \frac{dk^+ dk^-}{(2\pi)^2} \theta(k^+ + k^-) \frac{\Omega_{\text{tot}}^{d-2}}{(2\pi)^{d-3}} \int_0^\infty dk^\perp (k^\perp)^{d-3} \delta(k^+ k^- - (k^\perp)^2) \\ &= \frac{2^{2\epsilon-4} \pi^{\epsilon-2}}{\Gamma(1-\epsilon)} \int dk^+ dk^- \theta(k^+ + k^-) \theta(k^+ k^-) \int dx x^{-\epsilon} \delta(x - k^+ k^-) \\ &= \frac{2^{2\epsilon-4} \pi^{\epsilon-2}}{\Gamma(1-\epsilon)} \int dk^+ dk^- \theta(k^+) \theta(k^-) (k^+ k^-)^{-\epsilon}, \end{aligned} \quad (6.28)$$

¹³We know that due to confinement gluons will never be physical onshell particles. The particles which are really produced e.g. hadrons are in fact massive and therefore not produced at this threshold. This gives rise to some subtleties which are discussed in Sec. 6.4 and 6.5.1.

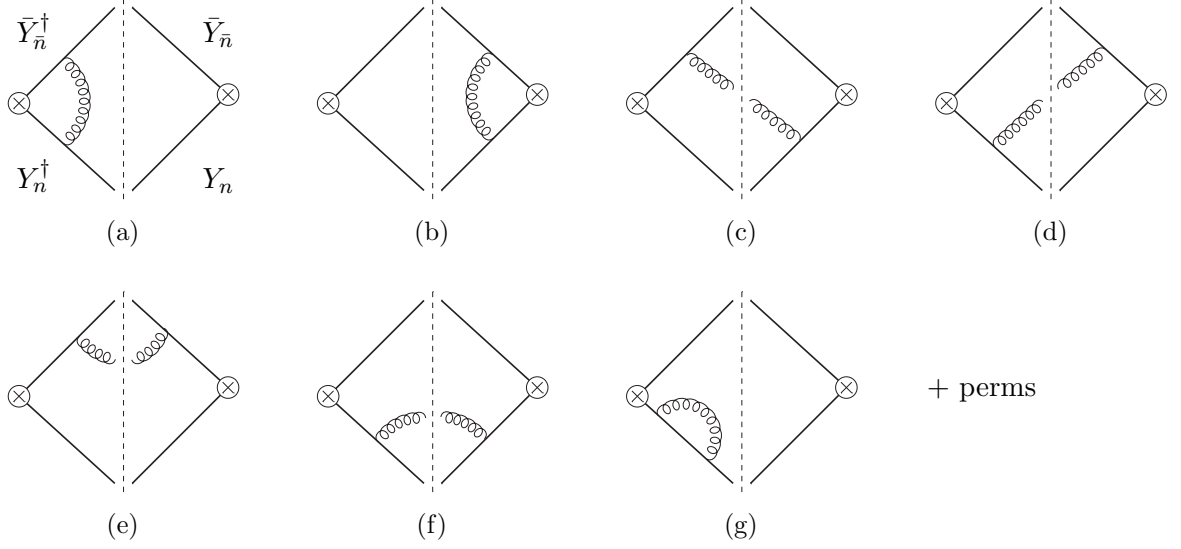


Figure 9: SCET diagrams contributing to the partonic c-parameter soft function to $\mathcal{O}(\alpha_s)$ (solid lines are Y-Wilson lines and the dashed line is the final state cut)

where we used that the diagrams do not depend on k^\perp and the substitution $(k^\perp)^2 \rightarrow x$. The total solid angle in $(d-2)$ -dimensions (we use $d = 4 - 2\epsilon$) is given by $\Omega_{\text{tot}}^{d-2} = \Omega_{\text{tot}}^{2-2\epsilon} = \frac{2\pi^{1-\epsilon}}{\Gamma(1-\epsilon)}$.

Using Eq. (6.28) it is easy to solve the integration in Eq. (6.27) and we get:

$$S_c^{\text{part}}(\ell, \mu) = \delta(\ell) + \frac{\alpha_s(\mu)C_F}{\pi} \frac{(\mu^2 e^{\gamma_E})^\epsilon}{\Gamma(1-\epsilon)} \ell^{-1-2\epsilon} B(\epsilon, \epsilon), \quad (6.29)$$

where $B(x, y)$ denotes the well known complete beta function.

To get the correct expansion in ϵ (in a distributional sense) we use a relation shown in Eq. (B.2). Again we used a positive dummy variable $\kappa > 0$ for rewriting $\ell = \kappa x$ which is later set to μ . Some manipulations yield the final form for the bare partonic soft function to $\mathcal{O}(\alpha_s)$. We obtain the renormalized soft function in analogy with the jet function - see Eq. (6.24). The counter term is given by:

$$Z_{S_c}(\ell - \ell', \mu) = \delta(\ell - \ell') + \frac{\alpha_s(\mu)C_F}{\pi} \left\{ -\frac{1}{\epsilon^2} \delta(\ell - \ell') + \frac{2}{\mu} \left[\frac{\mu \theta(\ell - \ell')}{\ell - \ell'} \right]_+ \frac{1}{\epsilon} \right\}. \quad (6.30)$$

Finally we arrive at the renormalized partonic c-parameter soft function to $\mathcal{O}(\alpha_s)$. Our result agrees with [12] and reads:

$$S_c^{\text{part}}(\ell, \mu) = \delta(\ell) + \frac{\alpha_s(\mu)C_F}{4\pi} \left\{ \pi^2 \delta(\ell) - \frac{16}{\mu} \left[\frac{\mu \theta(\ell) \ln(\ell/\mu)}{\ell} \right]_+ \right\}. \quad (6.31)$$

6.2.4. Anomalous Dimensions and Evolution Kernels

Next we use our general analysis of Sec. 6.1 and determine the involved evolution kernels. Therefore we need the anomalous dimension of the hard, jet and soft function to first order which can be obtained from results of the previous subsection. With this it is possible to derive the K and ω 's to leading-log (LL) order. To get the desired N²LL resummation we use anomalous dimensions to 3-loop order from massless calculations (see Tab. 3). This is possible since anomalous dimensions are connected to the UV behavior of the corresponding quantity and therefore insensitive to masses.

We start by looking at the SCET to QCD matching coefficient and its renormalization scale dependence:

$$\mu \frac{d}{d\mu} C^0(Q, \mu) = 0 \quad (6.32)$$

$$\Rightarrow \mu \frac{d}{d\mu} Z_C(Q, \mu) C(Q, \mu) = (\mu \frac{d}{d\mu} Z_C) C(Q, \mu) + Z_C(Q, \mu) (\mu \frac{d}{d\mu} C(Q, \mu)) = 0 \quad (6.33)$$

$$\Rightarrow \gamma_C(Q, \mu) = -Z_C(Q, \mu)^{-1} \mu \frac{d}{d\mu} Z_C(Q, \mu) . \quad (6.34)$$

Using Eq. (6.19) and $\gamma_H = \gamma_C + \gamma_C^\dagger$ we get the anomalous dimension of the hard function to first order which reads:

$$\gamma_H(Q, \mu) = \frac{\alpha_s(\mu)}{4\pi} \left(-8C_F \ln \left(\frac{\mu^2}{Q^2} \right) - 12C_F \right) + \mathcal{O}(\alpha_s^2) \Rightarrow \Gamma_{H,0} = -8C_F, \gamma_{H,0} = -12C_F . \quad (6.35)$$

To derive the anomalous dimension of the jet and soft function we use that the calculation is in complete analogy with the hard function case if we Fourier transform (see Sec. B for details on the Fourier transform of distributions):

$$\tilde{\gamma}_J(y, \mu) = \frac{\alpha_s(\mu)}{4\pi} \left(8C_F \ln(iy\mu^2 e^{\gamma_E}) + 6C_F \right) + \mathcal{O}(\alpha_s^2) \Rightarrow \Gamma_{J,0} = 8C_F, \gamma_{J,0} = 6C_F, \quad (6.36)$$

$$\tilde{\gamma}_S(y, \mu) = \frac{\alpha_s(\mu)}{2 \cdot 4\pi} \left(-8C_F \ln(iy\mu e^{\gamma_E}) \right) + \mathcal{O}(\alpha_s^2) \Rightarrow \Gamma_{S,0} = -8C_F, \gamma_{S,0} = 0 . \quad (6.37)$$

To sum series of non-leading logarithms we need higher order anomalous dimensions. The expressions and references are summarized in Tab. 3 and given below.

F	j	$\Gamma_F[\alpha_s]$	$\gamma_{F,0}$	$\gamma_{F,1}$	Ref.
H	2	$-2\Gamma^{\text{cusp}}$	$\gamma_{H,0}$	$\gamma_{H,1}$	[35]
$J_{n,\bar{n}}$	2	$2\Gamma^{\text{cusp}}$	$\gamma_{J,0}$	$\gamma_{J,1}$	[35, 36]
S_c	1	$-2\Gamma^{\text{cusp}}$	$\gamma_{S,0}$	$\gamma_{S,1}$	(6.47)

Table 3: Coefficients for the anomalous dimension - defined in Eq. (6.12)

All the anomalous dimensions have a cusp term (proportional to $\ln \mu$ and associated with Sudakov double logarithms) which is proportional to the QCD cusp anomalous dimension [35]:

$$\Gamma^{\text{cusp}}[\alpha_s] = \sum_{i=0} \Gamma_i^{\text{cusp}} \left(\frac{\alpha_s}{4\pi} \right)^i, \quad (6.38)$$

$$\begin{aligned} \Gamma_0^{\text{cusp}} &= \frac{16}{3}, & \Gamma_1^{\text{cusp}} &= \frac{1072}{9} - \frac{16}{3}\pi^2 - \frac{160}{27}n_f, \\ \Gamma_2^{\text{cusp}} &= 1960 - \frac{2144}{9}\pi^2 + \frac{176}{15}\pi^4 + 352\zeta_3 + \left(-\frac{5104}{27} + \frac{320}{27}\pi^2 - \frac{832}{9}\zeta_3 \right) n_f - \frac{64}{81}n_f^2. \end{aligned} \quad (6.39)$$

Furthermore the non-cusp anomalous dimensions are given by:

$$\gamma_{H,1} = -\frac{7976}{27} - \frac{136}{9}\pi^2 + \frac{736}{3}\zeta_3 + \left(\frac{1040}{81} + \frac{16}{9}\pi^2 \right) n_f, \quad (6.40)$$

$$\gamma_{J,1} = \frac{7220}{27} + \frac{8}{3}\pi^2 - \frac{704}{3}\zeta_3 - \left(\frac{968}{81} + \frac{16}{27}\pi^2 \right) n_f, \quad (6.41)$$

$$\gamma_{S,1} = -\gamma_{H,1} - 2\gamma_{J,1}. \quad (6.42)$$

These are the ingredients we need for calculating the K and ω 's to N²LL (see Sec. E.1).

Consistency Checks

The general form of the anomalous dimension of the hard, jet and soft function reads:

$$\gamma_H(\mu) = \Gamma_H[\alpha_s(\mu)] \ln \left(\frac{\mu^2}{Q^2} \right) + \gamma_H[\alpha_s(\mu)] , \quad (6.43)$$

$$\tilde{\gamma}_J(\mu) = \Gamma_J[\alpha_s(\mu)] \ln (iy\mu^2 e^{\gamma_E}) + \gamma_J[\alpha_s(\mu)] , \quad (6.44)$$

$$\tilde{\gamma}_S(\mu) = 2\Gamma_S[\alpha_s(\mu)] \ln (iyQ\mu e^{\gamma_E}) + \gamma_S[\alpha_s(\mu)] . \quad (6.45)$$

This can be used to formulate some consistency relations for the anomalous dimension. We know that the full cross-section must be independent of the renormalization scale, thus the following relation holds:

$$\mu \frac{d}{d\mu} (H\tilde{J}\tilde{S}) = [\gamma_H(\mu) + 2\tilde{\gamma}_J(y, \mu) + \tilde{\gamma}_S(y, \mu)](H\tilde{J}\tilde{S}) = 0 , \quad (6.46)$$

Note that the factor 2 in front of the jet anomalous dimension arises because we are using the hemisphere mass jet function which involves a factor of 1/2 compared to thrust.

By using $\ln(iy\mu^2 e^{\gamma_E}) = \ln(\mu/Q) + \ln(iy\mu Q e^{\gamma_E})$ one can simply compare the coefficients of the different contributions. From Eq. (6.46) we get:

$$\gamma_H[\alpha_s(\mu)] + 2\gamma_J^{\text{hemi}}[\alpha_s(\mu)] + \gamma_S^c[\alpha_s(\mu)] = 0 , \quad (6.47)$$

$$\Gamma_H[\alpha_s(\mu)] = -\Gamma_J^{\text{hemi}}[\alpha_s(\mu)] = \Gamma_S^c[\alpha_s(\mu)] . \quad (6.48)$$

These relations can be used for consistency checks of the anomalous dimensions or in our case to determine the soft function anomalous dimension.

6.3. Non-Singular Cross-Section

In this subsection we determine the non-singular contributions to the SCET cross-section. The non-singular c-parameter distribution includes terms which are power suppressed in the SCET power counting parameter λ . When deriving the factorization theorem we completely ignore these contributions since we are working in the dijet limit where the power suppression works well. Since we are interested in a description which is applicable in a wide range of the c-parameter we need to include contributions which might become more important with increasing c. Note that at this point additional corrections suppressed in higher orders of m/Q which we encountered in the matching procedure (see Sec. 6.2.1) will enter as well.

The non-singular cross-section is given by the FO result minus the SCET cross-section expanded to $\mathcal{O}(\alpha_s)$ and all scales set equal. The singular plus non-singular cross-section therefore consistently reproduces the FO result when going to the far tail region. The non-singular cross-section is given by:

$$\frac{1}{\sigma_0^i} \frac{d\sigma_{\text{ns}}^i}{dc} = \frac{1}{\sigma_0^i} \frac{d\sigma_{\text{QCD}}^i}{dc} - \frac{1}{\sigma_0^i} \frac{d\sigma_{\text{SCET}}^i}{dc} , \quad (6.49)$$

where the full QCD cross section at some scale μ was given in Eq. (3.67). The unresummed SCET

cross-section evaluated at the scale $\mu = \mu_h = \mu_j = \mu_s$ reads:

$$\frac{1}{\sigma_0^i} \frac{d\sigma_{\text{SCET}}^i}{dc} = \delta(c - c_{\min}) + \frac{\alpha_s(\mu)C_F}{2\pi} \left\{ g^\delta(\hat{m})\delta(c - c_{\min}) + g^+(\hat{m}) \left[\frac{\theta(c - c_{\min})}{c - c_{\min}} \right]_+ + g^{\text{nd}}(c, \hat{m})\theta(c - c_{\min}) \right\}, \quad (6.50)$$

$$g^\delta(\hat{m}) = 2\ln^2(\hat{m}^2) + \ln(\hat{m}^2) + \frac{4\pi^2}{3}, \quad (6.51)$$

$$g^+(\hat{m}) = -4(1 + \ln(\hat{m}^2)), \quad (6.52)$$

$$g^{\text{nd}}(c, \hat{m}) = -\frac{4}{c - c_{\min}} \ln \left(1 + \frac{c - c_{\min}}{\hat{m}^2} \right) + \frac{c - c_{\min}}{(c - c_{\min} + \hat{m}^2)^2}, \quad (6.53)$$

and can be computed by using the results from Sec. 6.2. With this we are able to calculate the contributions to the non-singular cross-section which has the known distributional and non-distributional structure:

$$\frac{1}{\sigma_0^i} \frac{d\sigma_{\text{ns}}^i}{dc} = f_{\text{ns}}^{0,i}(\hat{m})\delta(c - c_{\min}) + \frac{\alpha_s(\mu)C_F}{2\pi} \left\{ f_{\text{ns}}^{\delta,i}(\hat{m})\delta(c - c_{\min}) + f_{\text{ns}}^{+,i}(\hat{m}) \left[\frac{\theta(c - c_{\min})}{c - c_{\min}} \right]_+ + f_{\text{ns}}^{\text{nd},i}(c, \hat{m})\theta(c - c_{\min}) \right\}. \quad (6.54)$$

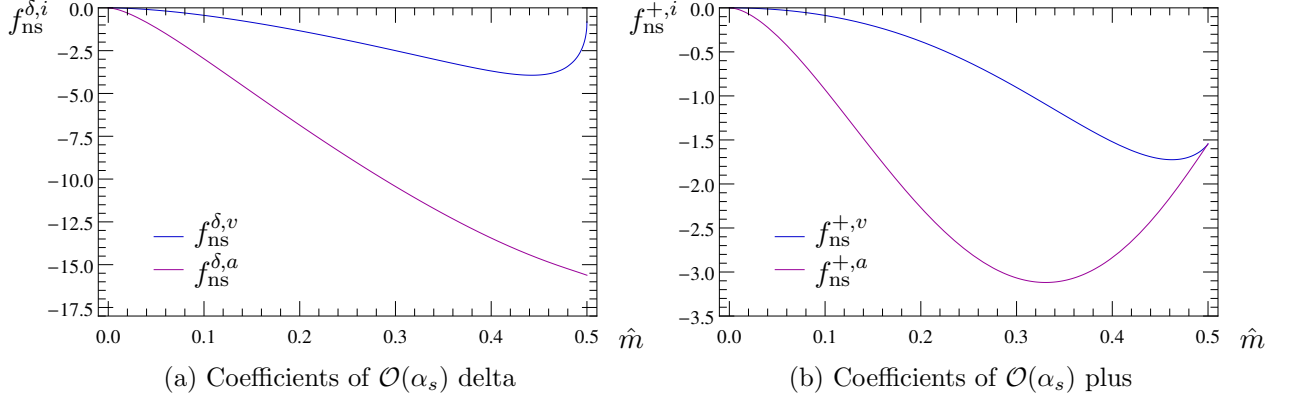
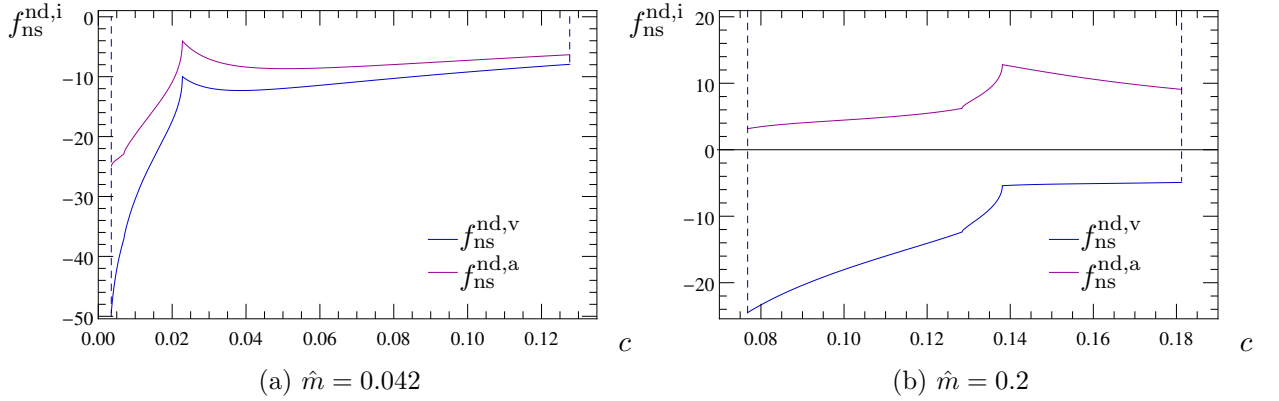
Since the analytic form of the $\mathcal{O}(\alpha_s)$ FO delta function coefficient is not yet known the coefficient for the non-singular delta function is given numerically. It is plotted in Fig. 10a and we provide numerical values for different masses \hat{m} in Tab. 4. Using $v = \sqrt{1 - 4\hat{m}^2}$ and the coefficient c_m^i , which was defined in Eq. (3.13), the tree level delta and the one-loop plus distribution coefficient (plotted in Fig. 10b) read:

$$f_{\text{ns}}^{0,v}(\hat{m}) = \frac{2\hat{m}^2}{1+v}(v^2 + v - 2), \quad f_{\text{ns}}^{0,a}(\hat{m}) = \frac{-4\hat{m}^2}{1+v}(v^2 + v + 1), \quad (6.55)$$

$$f_{\text{ns}}^{+,i}(\hat{m}) = 8\ln\left(\frac{1+v}{2}\right) - 16\hat{m}^2\ln\left(\frac{1+v}{2\hat{m}}\right) + 4(1-v) + 4(c_m^i - 1) \left[2(1 - 2\hat{m}^2)\ln\left(\frac{1-v}{2m}\right) - v \right]. \quad (6.56)$$

\hat{m}	$f_{\text{ns}}^{\delta,v}$	$f_{\text{ns}}^{\delta,a}$
0.0	0	0
0.1	-0.437282	-2.9748
0.2	-1.34044	-6.85046
0.3	-2.49863	-10.4324
0.4	-3.68759	-13.446
0.5	-0.812396	-15.6168

Table 4: Coefficient of $\mathcal{O}(\alpha_s)$ delta function for different \hat{m}

Figure 10: Coefficients for the $\mathcal{O}(\alpha_s)$ distributional non-singular cross-sectionFigure 11: Coefficients for the $\mathcal{O}(\alpha_s)$ non-distributional non-singular cross-section

Note that the coefficients for the distributional part vanish for $\hat{m} \rightarrow 0$. This is the expected behavior since these parts arise from the m/Q suppressed terms. The $\mathcal{O}(\alpha_s)$ non-distributional non-singular cross-section is plotted for different masses in Fig. 11. It is given by:

$$f_{\text{ns}}^{\text{nd},i}(c, \hat{m}) = f_{\text{ndiv}}^i(c, \hat{m}) - g^{\text{nd}}(c, \hat{m}), \quad (6.57)$$

where the coefficient function f_{ndiv}^i is defined in Eq. (3.52) as the radiative FO cross-section minus its singular behavior. If this subtraction is not done carefully one might suffer from numerical instabilities due to large cancellations. See Sec. 3.2.2 for a discussion how to expand the radiative FO result in the threshold limit which allows to cancel the divergent terms explicitly.

6.4. Non-Perturbative Corrections

The measurement of QCD observables (especially event-shapes) is done by detecting hadrons and specifying their kinematic properties. However, up to this point our discussion only involves perturbative contributions at the parton level. To get results which are comparable with experiment we need to account for non-perturbative hadronization effects. Due to their power suppression (in powers of Q) they are known in the literature as *power corrections*. Note that in the following we assume the final state hadrons to be massless and therefore do not discuss hadron mass effects which would introduce an additional difficulty (for more details see [31]).

One of the most popular approaches on treating hadronization effects in QCD is called the *dispersive approach*¹⁴. Using this method the impact of power corrections on the mean value of event shape

¹⁴Sometimes also called *renormalon approach* or the *effective coupling model*.

variables was investigated and it was determined that the leading effect corresponds to an additive power correction. It involves a universal quantity which is of order Λ_{QCD}/Q times a calculable coefficient specific for each event shape. Furthermore in the region which is far away from the dijet configuration it was shown that the leading power correction shifts the differential distribution by the same amount (for a brief review see [37]).

In the effective field theory where several scales are involved one encounters three types of power corrections [10]. Except for the ones we already know from QCD there also exist power corrections enhanced by the soft scale (called “type 1”). Since they are of order $\Lambda_{\text{QCD}}/\mu_S \sim \Lambda_{\text{QCD}}/(Qc)$ these terms play a very important role in the peak region where $Qc \sim \Lambda_{\text{QCD}}$.

A very general framework of treating power corrections which we will also adopt for our analysis involves the usage of so-called *shape* or *model functions*. It was already mentioned in Sec. 5.3 that the full soft function also contains non-perturbative parts which can be implemented by a convolution of the perturbative partonic soft function and the non-perturbative soft model function [27, 33]:

$$S_c(\ell, \mu) = \int d\ell' S_c^{\text{part}}(\ell - \ell', \mu) S_c^{\text{mod}}(\ell'). \quad (6.58)$$

For the region far away from the peak i.e. $Qc \gg \Lambda_{\text{QCD}}$ where the soft function receives perturbative and non-perturbative contributions one can perform an operator product expansion (OPE) for the soft function. The OPE is given by [10]:

$$S_c(\ell, \mu) = S_c^{\text{part}}(\ell, \mu) - \frac{dS_c^{\text{part}}(\ell, \mu)}{d\ell} \bar{\Omega}_1^c + \dots, \quad (6.59)$$

which involves the leading non-perturbative c-parameter matrix element $\bar{\Omega}_1^c$. This matrix element which represents the leading “type 1” power correction is proportional to a universal matrix element common to all event-shapes [38]. Therefore it is related to the corresponding thrust matrix element (defined in [10]) through the relation [31]:

$$\bar{\Omega}_1^c = \frac{\pi}{4} \bar{\Omega}_1^\tau. \quad (6.60)$$

It is easy to see in Eq. (6.59) that the OPE which is valid in the tail region is consistent with a simple shift in the soft function argument $S_c^{\text{part}}(\ell - \bar{\Omega}_1^c, \mu)$ which was observed earlier for the dispersive approach in QCD. Imposing a normalization condition $\int d\ell' S_c^{\text{mod}}(\ell', \mu) = 1$, using the above OPE and expanding Eq. (6.58) for $\ell' \ll \ell$ in the tail region one finds:

$$\bar{\Omega}_1^c = \int d\ell \ell S_c^{\text{mod}}(\ell). \quad (6.61)$$

Similar to the leading power correction higher order type 1 corrections are related to higher moments of the model function i.e. $\bar{\Omega}_i^c = \int d\ell \ell^i S_c^{\text{mod}}(\ell)$ [10]. In the peak region which corresponds to $Qc \sim \Lambda_{\text{QCD}}$ higher corrections play an increasingly important role, hence higher moments have to be included when approaching the peak.

After this general analysis of the shape function we should think about how it is realized in practice. Usually it was setup as a physically reasonable function involving a few parameters which then were fit to experimental data. An alternative approach is provided by the ansatz of [39] where one uses an infinite linear combination of basis functions:

$$F^{\text{mod}}(\ell, \lambda, p, \{c_i\}) = \frac{1}{\lambda} \left[\sum_{n=0}^N c_n f_n\left(p, \frac{\ell}{\lambda}\right) \right]^2. \quad (6.62)$$

The basis functions read (involving Legendre polynomials P_n):

$$f_n(p, x) = \sqrt{\frac{(2n+1)x^p(1+p)^{1+p}}{\Gamma(1+p)}} \exp\left(-\frac{1+p}{2}x\right) P_n(y(p, x)) ,$$

$$y(p, x) = 1 - 2 \exp(-(1+p)x) \sum_{i=0}^p \left[\frac{(1+p)^i}{\Gamma(i+1)} x^i \right] . \quad (6.63)$$

With $\sum_i c_i^2 = 1$ this function is normalized to 1, fulfills $F^{\text{mod}}(0) = 0$ is positive definite and has support for $\ell \geq 0$. Furthermore for $N < \infty$ the parameter λ represents the width of the function, which could be seen in Eq. (6.63). The advantage of this kind of shape function is that it is independent of a specific choice for the parametrization which allows us to study the model dependence in a more systematic way. Such a shape function was used for the analysis of [10] which was chosen to be:

$$S_\tau^{\text{mod}}(\ell, \lambda) = F^{\text{mod}}(\ell, \lambda, 3, \{c_0 = 1, c_{i \geq 1} = 0\}) . \quad (6.64)$$

This analysis was carried out in the tail region where $\bar{\Omega}_1^\tau$ is the dominant power correction. Although the argumentation only applies for the tail region we can still use the same shape function. Since we are interested in a qualitative analysis of mass effects to the c-parameter distribution it is sufficient to use a model which is at least physically reasonable for the investigated c-parameter range. The shape function used in the mentioned analysis where $\lambda = 0.5$ was chosen definitely satisfies this requirement.

Non-Singular

The power corrections to the non-singular cross-section will be treated by a convolution with the same shape function as for the singular case [10]:

$$\frac{d\sigma_{\text{ns}}}{dc} = \int d\ell \frac{d\sigma_{\text{ns}}}{dc} \left(c - \frac{\ell}{Q}, \mu_{\text{ns}} \right) S_c^{\text{mod}}(\ell) . \quad (6.65)$$

Since we implement the power corrections the same way for the singular and non-singular part we achieve that in the far tail region the sum of these two contributions give exactly the full FO result. This includes that the above relation fulfills the OPE of Eq. (6.59) which as we know leads to the shift of the FO result known from QCD. Therefore the above defined implementation leads to a consistent description in the region far from the peak where the non-singular contributions are important.

6.5. Renormalons, $\overline{\text{MS}}$ Mass and Gap

It is known that the perturbative series we use to describe cross-sections and other physical quantities is in general a divergent asymptotic series [40]. One tool for probing high order effects is the insertion of so-called bubble chains. For instance if there is a virtual gluon in the one or two-loop diagram it is always possible to insert one or several massless quark loops into this virtual gluon line. These diagrams give the leading contribution to higher orders of the perturbative series. If one now investigates the high order asymptotic behavior of this series one will find a factorial growth (a standard example to study is the correlation function of two vector currents [41]).

The sum of the perturbative series might be defined using the so-called Borel transform. Usually one then finds poles in the complex plane of the Borel parameter which corresponds to factorial

divergences of the perturbative series, for example from bubble chain diagrams. Some of these poles which we call IR renormalons arise since the integration over virtual loop momenta also involves contributions from very low momentum transfers which give rise to non-perturbative corrections of the perturbative results [42]. To recover the “sum” of the original series one has to perform the inverse borel transform where these poles introduce ambiguities of order Λ_{QCD}/Q . These ambiguities should cancel with a corresponding ambiguity in non-perturbative contributions. If one correctly separates non-perturbative contributions from the perturbative series one can make this cancellation explicit order by order and thereby remove the renormalon. This should improve the convergence of the series significantly.

6.5.1. Gap

In the case of the partonic soft function one finds a renormalon which is related to the fact that the partonic threshold at $\ell = 0$ is unphysical [10]. This leading renormalon should cancel with the leading power correction $\bar{\Omega}_1^c$. By defining the leading power correction in an appropriate scheme one can induce explicit subtractions which remove the renormalon in the partonic soft function.

To achieve this let's consider a so-called gapped soft function (we follow [10, 33]). In contrast to the shape function discussed in the earlier discussion we now look at a shape function with support only for $\ell \geq \Delta \sim \Lambda_{\text{QCD}}$ where the so-called gap Δ represents the energy needed to produce two light hadrons. Then the relation of Eq. (6.61) reads:

$$\bar{\Omega}_1^c = \Delta + \int d\ell \ell S_c^{\text{mod}}(\ell), \quad (6.66)$$

where Δ now contains the complete renormalon dependence of the power correction. Next we split the gap in a non-perturbative $\bar{\Delta}$ and a perturbative part δ where each term depends on μ_S and a new subtraction scale R :

$$\Delta = \bar{\Delta}(R, \mu_S) + \delta(R, \mu_S). \quad (6.67)$$

With δ containing the renormalon we can make the cancellation explicit and define the renormalon free leading power correction:

$$\Omega_1^c(R, \mu_S) = \bar{\Omega}_1^c - \delta^c(R, \mu_S) = \bar{\Delta}(R, \mu_S) + \int d\ell \ell S_c^{\text{mod}}(\ell). \quad (6.68)$$

Note that the non-perturbative parameter $\bar{\Delta}$ has to be determined from experimental data. This is done by fitting in the tail-region where Ω_1^c is the dominant power correction which is directly connected to $\bar{\Delta}$. A suitable definition for $\delta(R, \mu_s)$ is given by [33, 43]:

$$\delta^c(R, \mu) = R e^{\gamma_E} \left[\frac{d}{d \ln(iy)} \ln \left(\tilde{S}_c^{\text{part}}(y, \mu) \right) \right]_{y=(iR e^{\gamma_E})^{-1}}, \quad (6.69)$$

where $\tilde{S}_c^{\text{part}}(y, \mu)$ is the position space partonic soft function. It can be calculated using Eq. (6.31) and relations from Sec. B which yields:

$$\tilde{S}_c^{\text{part}}(y, \mu) = 1 + \frac{\alpha_s(\mu) C_F}{4\pi} \left(-\frac{\pi^2}{3} - 8 \ln^2(iy e^{\gamma_E} \mu) \right). \quad (6.70)$$

Furthermore we define the perturbative series of δ as:

$$\delta^c(R, \mu) = R e^{\gamma_E} \sum_{i=1} \delta_i^c(R, \mu_s) \left(\frac{\alpha_s(\mu_s)}{4\pi} \right)^i \equiv \sum_i \hat{\delta}_i(R, \mu). \quad (6.71)$$

Using the log structure of the partonic soft function (which we know through the anomalous dimension) and the first non-log term which is given by $s_1^c = -C_F\pi^2/3$ (compare with thrust $s_1^\tau = -C_F\pi^2$) one can compute the first and second coefficient of the above series:

$$\begin{aligned}\delta_1^c(R, \mu_s) &= 2\Gamma_{s,0}L_{\mu R} = -21.3333L_{\mu R} , \\ \delta_2^c(R, \mu_s) &= 2s_1^c\beta_0 + \gamma_{s,1} + 2\Gamma_{s,1}L_{\mu R} + 2\beta_0\Gamma_{s,0}L_{\mu R}^2 = 85.1619 - 147.374L_{\mu R} - 163.556L_{\mu R}^2 ,\end{aligned}\tag{6.72}$$

where $L_{\mu R} = \ln(\mu_s/R)$ and for the numerical values we used $n_f = 5$. Then the full $\mathcal{O}(\alpha_s)$ soft function reads:

$$\begin{aligned}S(\ell, \mu_s) &= \int d\ell' S_c^{\text{part}}(\ell - \ell' - \delta, \mu_s) S_c^{\text{mod}}(\ell' - \bar{\Delta}) \\ &= \int d\ell' \left\{ S_c^{\text{part}}(\ell - \ell', \mu_s) - \hat{\delta}_1 \left[\frac{d}{dk} S_c^{\text{part}}(k, \mu_s) \right]_{k=\ell-\ell'} \right\} S_c^{\text{mod}}(\ell' - \bar{\Delta}) ,\end{aligned}\tag{6.73}$$

where the perturbative and non-perturbative contributions are now indeed separately free of the leading renormalon [31]. Note that in the process of our renormalon subtraction we introduced an additional dependence on the subtraction scale R . It would be natural to expect $R \sim 1\text{GeV}$ [10] but since we want to avoid large logarithms in the δ coefficients we would like to have $R \sim \mu_s \gg 1\text{GeV}$. To resolve this issue the fit for $\bar{\Delta}$ is carried out at some scales $R_\Delta, \mu_\Delta \sim 1\text{GeV}$ and afterwards evolved to the appropriate scale to avoid large logarithms. How this evolution in μ and R is achieved to N²LL accuracy is discussed in Sec. E.2 (based on [44, 45]).

6.5.2. $\overline{\text{MS}}$ Mass

It was already mentioned in one of the previous subsections that when measuring QCD observables one always uses properties of hadrons. The pole mass defined as the position of the full propagator pole corresponds to the mass of an asymptotically free particle. Since quarks are never asymptotically free due to confinement the pole mass is not a physical quantity, hence one can suggest other mass definitions. As shown in [42] the pole mass receives corrections sensitive to long distance physics which give rise to an IR renormalon. Because of these corrections the pole mass introduces an intrinsic order Λ_{QCD}/m ambiguity. This ambiguity, in contrast to the other renormalons, is not compensated by a non-perturbative matrix element but rather by the same ambiguity in the corresponding matrix element.

By switching to a so-called short distance mass [46, 47] one can get a mass definition which is free of this dependence on non-perturbative physics and thereby get rid of the mentioned renormalon. The short distance mass we will use for this analysis is the so-called $\overline{\text{MS}}$ -mass $\overline{m}(\mu)$ which is related to the pole mass at one loop by [48]:

$$\hat{m} \equiv \hat{m}^{\text{pole}} = \hat{\overline{m}}(\mu) + \delta\hat{\overline{m}}(\mu) ,\tag{6.74}$$

$$\delta\hat{\overline{m}}(\mu) = \frac{\alpha_s(\mu)C_F}{\pi} \hat{\overline{m}}(\mu) \left[1 - \frac{3}{2} \ln \left(\frac{\overline{m}(\mu)}{\mu} \right) \right] + \mathcal{O}(\alpha_s^2) .\tag{6.75}$$

In order to switch to the above defined $\overline{\text{MS}}$ mass we implement the relation given in Eq. (6.74) into our cross-section formula and expand up to $\mathcal{O}(\alpha_s)$. The renormalon is contained in the only mass dependent quantity which is the jet function. This is why one should implement the scheme change already at the level of the jet function. However, we shift the SCET threshold to the full QCD threshold which introduces an additional mass dependence. Although this additional mass dependence is formally subleading in SCET it is the reason why we do this scheme change on the level of the cross-section. For these terms we also use μ_J as the renormalon subtraction scale.

6.6. Final Result

In the previous subsections we calculated the singular resummed (N²LL) c-parameter cross-section in SCET, the non-singular c-parameter cross-section, included a way of treating non-perturbative effects and improved the convergence of our perturbative series by renormalon subtractions.

These are all the ingredients we want to include in our analysis of mass effects to the c-parameter cross-section. The final formula for the massive c-parameter cross section using quantities calculated before reads:

$$\frac{d\sigma^i}{dc} = \frac{d\sigma_s^i}{dc} + \frac{d\sigma_{ns}^i}{dc}, \quad i = a, v. \quad (6.76)$$

The resummed singular partonic c-parameter cross-section is given by Eq. (6.15). Convolution with a model and renormalon subtraction yields:

$$\begin{aligned} \frac{1}{\sigma_0^i} \frac{d\sigma_s^i}{dc} = & Q H(Q, \mu_H) U_H(Q, \mu_H, \mu) \int ds ds' U_J(s - s', \mu, \mu_J) J_\tau(s', \bar{m}(\mu_J), \mu_J) \\ & \times \int d\ell d\ell' U_S \left(Q(c - \bar{c}_{\min}) - \frac{s}{Q} - \ell, \mu, \mu_S \right) S_c^{\text{mod}}(\ell' - \bar{\Delta}) \\ & \times \left\{ S_c^{\text{part}}(\ell - \ell', \mu_S) - \delta'(\ell - \ell') \left[\hat{\delta}_1(R, \mu_S) + 4\hat{m}(\mu_J) \left(1 - 2\hat{m}^2(\mu_J) \right) Q \delta\hat{m}(\mu_J) \right] \right\} \\ & + \mathcal{O}(\alpha_s^2), \end{aligned} \quad (6.77)$$

where we defined the c-threshold using the $\overline{\text{MS}}$ mass $\bar{c}_{\min} = 2\hat{m}^2(\mu_J)(1 - \hat{m}^2(\mu_J))$. Furthermore the non-singular partonic c-parameter cross-section is given by Eq. (6.54). With the appropriate renormalon subtraction we get:

$$\begin{aligned} \frac{1}{\sigma_0^i} \frac{d\sigma_{ns}^i}{dc} = & \left\{ f_{ns}^{0,i}(\hat{m}) + \left[\frac{d}{d\mu} f_{ns}^{0,i}(\mu) \right]_{\mu=\hat{m}} \delta\hat{m} + \frac{\alpha_s(\mu) C_F}{2\pi} f_{ns}^{\delta,i}(\hat{m}) \right\} Q S_c^{\text{mod}}(Q(c - \bar{c}_{\min}) - \bar{\Delta}) \\ & - \left\{ \hat{\delta}_1(R, \mu_S) + 4\hat{m}(\mu_J) \left(1 - 2\hat{m}^2(\mu_J) \right) Q \delta\hat{m}(\mu_J) \right\} f_{ns}^{0,i}(\hat{m}) Q \left[\frac{d}{d\ell} S_c^{\text{mod}}(\ell) \right]_{\ell=Q(c-\bar{c}_{\min})-\bar{\Delta}} \\ & + \frac{\alpha_s(\mu) C_F}{2\pi} \int d\ell \left\{ f_{ns}^{+,i}(\hat{m}) \left[\frac{\theta(c - \bar{c}_{\min} - \frac{\ell}{Q})}{c - \bar{c}_{\min} - \frac{\ell}{Q}} \right]_+ + f_{ns}^{\text{nd},i}(c - \frac{\ell}{Q}, \hat{m}) \right\} S_c^{\text{mod}}(\ell - \bar{\Delta}) \\ & + \mathcal{O}(\alpha_s^2). \end{aligned} \quad (6.78)$$

As mentioned before we are interested in an analysis of the mass effects contributing to the c-parameter cross-section. Therefore we want to compare the massive with the corresponding massless distribution which can be obtained by taking the massless limit or from [12].

Importance of Singular and Non-Singular Contributions

Up to now we never talked about the relative importance of the singular and the non-singular cross-section contributions. In fact the non-singular contributions also contain large logarithms which are never resummed due to the absence of a subleading factorization theorem. If the non-singular contributions are really suppressed w.r.t. the singular contributions the thereby introduced error should be comparably small. In this subsection we want to clarify the importance of the non-singular contributions for the whole range of the C-parameter¹⁵. For this we compare singular and

¹⁵Note that in analogy with Eq. (7.1) we changed back to the C-parameter which fulfills $C = 6c$.

non-singular contributions while using input, such as profile functions and physical constants, from Sec. 7.

In Fig. 12 the singular and the non-singular massless differential cross-section is plotted. Actually it is sufficient and illustrative to only look at the massless case since the massive case shows the same behavior.

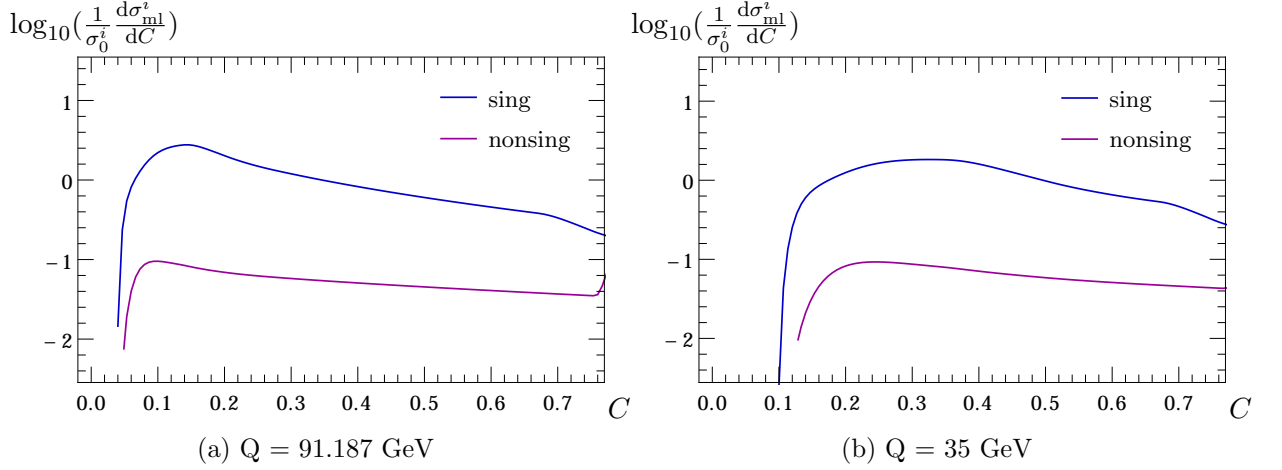


Figure 12: Comparison of the singular and non-singular massless differential cross-section with default profiles for NLL'.

When looking at the mentioned plots one can clearly see that the singular terms are the leading contribution to the differential C-parameter cross-section. In fact the singular terms seem to dominate the non-singular terms by one magnitude for the whole C-parameter tail region which is the region of interest (for the massless case at $Q = 91.187 \text{ GeV}$ the tail region is approximately given by $0.2 \lesssim C \lesssim 0.7$; see Sec. 7.1). As mentioned before the massive cross-section shows the same behavior and is therefore not discussed in further detail.

7. Analysis

In this section we want to analyze the obtained results and draw first conclusions. For this we introduce the mentioned profile functions and propose a generalization to the massive case. Afterwards we look at different applications and compare the massive against the massless results.

Since we intend to do a numerical analysis we also need numerical values for the physical constants which appear in our cross-section formula. In the following we will use [10]:

$$\begin{aligned} m_Z &= 91.187 \text{ GeV} & \Gamma_Z &= 2.4952 \text{ GeV} & \theta_w &= \sin^{-1}(\sqrt{0.23119}) \\ \alpha_s(m_Z) &= 0.118 & \alpha(m_Z) &= (127.925)^{-1} \end{aligned}$$

7.1. Profile Function

In Sec. 6.1 we saw that it is possible to resum certain logs to all orders in perturbation theory using standard RG methods. In the process the non-trivial problem of finding suitable matching scales which are c - and \hat{m} -dependent arose. To account for this one uses so-called *profile functions*.

For our analysis of mass effects in the c -parameter cross-section we will adapt the profiles of the massless analysis used in [12]. In the following we will try to motivate their general behavior and how to use variations of these profiles to estimate theoretical errors. Furthermore we switch back to the C -parameter (in Sec. 2 we substituted $c = C/6$) which changes the differential cross-section as follows:

$$\frac{1}{\sigma_0} \frac{d\sigma}{dC} = \frac{1}{6\sigma_0} \frac{d\sigma}{dc} \Big|_{c=C/6} \quad (7.1)$$

The factorization formula given in Eq. (6.15) involves three different scales which are responsible for avoiding large logarithms. They are called the hard scale μ_H , the jet scale μ_J and the soft scale μ_S . Their natural scaling in the peak, tail and far-tail region is given by [10, 12]:

$$\begin{aligned} \text{peak:} & \quad \mu_H \sim Q, & \mu_J & \sim \sqrt{\Lambda_{QCD} Q}, & \mu_S & \sim \Lambda_{QCD} \\ \text{tail:} & \quad \mu_H \sim Q, & \mu_J & \sim Q\sqrt{\frac{C}{6}}, & \mu_S & \sim Q\frac{C}{6} \\ \text{far-tail:} & \quad \mu_H = \mu_J = \mu_S \sim Q \end{aligned} \quad (7.2)$$

Here the scaling in the peak region is connected to non-perturbative physics and the scaling in the far-tail region is required to produce the FO result. Furthermore the scaling in the tail-region is determined by the contributions involved in the factorization theorem where the corresponding logs should be small:

- hard scale: In the hard function, which is given in Eq. (6.20), we only find one type of log. It will be small if $\mu_H \sim Q$.
- jet scale: When looking at the massive thrust jet function, given in Eq. (6.26), one can see that it involves two different types of logarithms which corresponds to two possible scale choices. When taking the convolution with the soft function into account the scaling $\mu_J^2 \sim Q^2(c - c_{\min})$ or $\mu_J^2 \sim Q^2(c - c_{\min} + \hat{m}^2)$ minimizes one of the logs. For the massless case the scalings become the same which reads $\mu_J \sim Q\sqrt{c} = Q\sqrt{C/6}$.
- soft scale: By investigating the soft function, given in Eq. (6.31), and the involved logarithms we observe that the soft scale should scale like $\mu_S \sim Q(c - c_{\min})$. In the massless case this corresponds to $\mu_S \sim Qc = QC/6$.

The aim is now to choose smooth and continuous functions which satisfy these constraints. In Fig. 13a one can see the chosen profiles and the different regions.

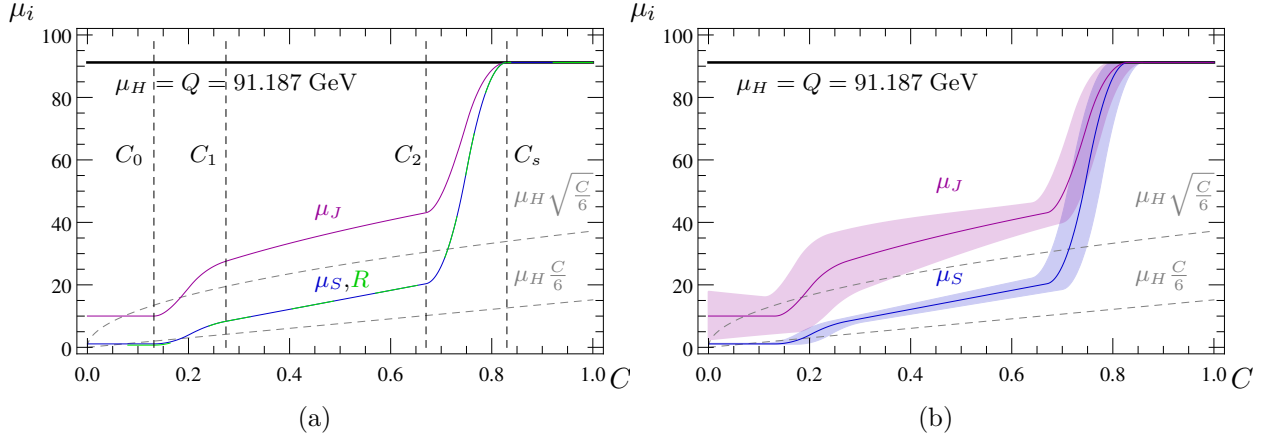


Figure 13: (a) Profile functions for the scales μ_H , $\mu_J(C)$, $\mu_S(C)$ and $R(C)$ with default parameters. (b) Bands of profile variations for the scales $\mu_J(C)$ and $\mu_S(C)$

In the following we will introduce the profile function for the soft scale $\mu_S(C)$. It will be used to define the profile function for the jet scale and serve as a prototype for $R(C)$. All profile functions are restricted by the following statements:

- From 0 to $C_0 = n_0/Q$ we are in the peak region where non-perturbative effects are dominant and a clear scale separation is mandatory. To ensure a gap subtraction which is not zero we also demand a non-zero difference of $\mu_0 = \mu_S(0)$ and $R_0 = R(0)$.
- Between $C_1 = n_1/Q$ and C_2 one is in the tail region where the scales should follow their natural scaling determined by the involved logarithms (they are plot as gray dashed lines).
- For $C > C_s$ we are in the far-tail region where all the scales are equal to the hard scale.

In between these regions we use a transition function (it is discussed in more detail in [12] and in the following we call it ζ function) which ensures a continuous and continuously differentiable transition. Therefore this function needs four arguments, namely the value of the profile function and its first derivative at each endpoint¹⁶. In fact the explicit form of this function is not important as long as it fulfills the above relations and provide some kind of natural transition between the mentioned regions. Using this we can write the profile function for the soft scale $\mu_S(C)$ as:

$$\mu_S(C) = \begin{cases} \mu_0 & 0 \leq C < C_0 \\ \zeta(\mu_0, 0; 0, \mu_H r) & C_0 \leq C < C_1 \\ C \mu_H r & C_1 \leq C < C_2 \\ \zeta(0, \mu_H r; \mu_H, 0) & C_2 \leq C < C_s \\ \mu_H & C_s \leq C \end{cases}, \quad (7.3)$$

where r denotes the slope of the profile function in the canonical region and $\mu_H = e_H Q$ the hard scale involving a variation parameter e_H . When constructing the profile functions one uses parameters to determine general features. One varies these parameters to estimate theoretical errors of the obtained results [10, 12]. The parameters, their default values and variation ranges are given in Tab. 5. The resulting variation bands for the soft and jet scale are shown in Fig. 13b which later are implemented through a random scan with 500 random parameter configurations.

Using the already defined quantities we can write down the profile function for the remaining scales

¹⁶To get a unique notation we attach straight lines to each endpoint and continue them to 0. Then the four arguments denote the corresponding properties of these straight lines at $C = 0$.

parameter	default value	range of values
μ_0	1.1 GeV	1.0 to 1.3 GeV
R_0 ¹⁷	0.7 GeV	0.6 to 0.9 GeV
n_0	12 GeV	10 to 16 GeV
n_1	25 GeV	22 to 28 GeV
C_2 ¹⁸	0.67	0.64 to 0.70
C_s	0.83	0.80 to 0.86
r	0.33	0.29 to 0.38
e_J	0	-0.5 to 0.5
e_H	1	0.5 to 2.0
n_s	0	-1, 0, 1

Table 5: Theory parameters, their default values and variations

which are given by:

$$\mu_J(C) = \begin{cases} [1 + e_J(C_s - C)^2] \sqrt{\mu_H \mu_S} & C \leq C_s \\ \mu_H & C > C_s \end{cases}, \quad (7.4)$$

$$R(C) = \begin{cases} R_0 & 0 \leq C < C_0 \\ \zeta(R_0, 0; 0, \mu_H r) & C_0 \leq C < C_1 \\ \mu_S(C) & C \geq C_1 \end{cases}. \quad (7.5)$$

To account for errors in the non-singular contributions we also vary the scale choice of μ_{ns} which is given by:

$$\mu_{\text{ns}}(C) = \begin{cases} \frac{1}{2}(\mu_H + \mu_J(C)) & n_s = 1 \\ \mu_H & n_s = 0 \\ \frac{1}{2}(3\mu_H - \mu_J(C)) & n_s = -1 \end{cases}. \quad (7.6)$$

Furthermore we choose the renormalization scale to be $\mu = \mu_J(C)$.

Generalization to the Massive Case

In principle it would be possible to use the massless profiles for this analysis. We know that the distribution gets shifted when increasing $\hat{m} = m/Q$. One might observe that at some point the profile functions would stop representing the three different C-parameter regions, namely peak, tail and far-tail region. To assure good log-resummation we need to generalize the profile functions to the massive case.

The idea behind the proposed generalization is that the range between the minimal C-parameter and the 3-particle maximal C-parameter changes depending on the mass. Our massive profiles are

¹⁷To ensure that the gap subtraction is not zero in the peak region we vary μ_0 and R_0 in a correlated way so that $\mu_0 - R_0 = \text{const.}$

¹⁸For very small $Q = Q_0$ it happens that $C_1 = C_2$. To ensure continuous profile functions and a continuous transition to small Q we set $C_2 = C_1$ for $Q \leq Q_0$.

then just a linear mapping of the massless profiles to this new range. The values of the profile functions at some C -parameter values are then associated with $\tilde{C}(C, \hat{m})$ which is given by:

$$\tilde{C}(C, \hat{m}) = 6 c_{\min}(\hat{m}) + \frac{c_{\text{top}}(\hat{m}) - c_{\min}(\hat{m})}{c_{\text{top}}(0) - c_{\min}(0)} C = 6 c_{\min}(\hat{m}) + 8 \left[c_{\text{top}}(\hat{m}) - c_{\min}(\hat{m}) \right] C, \quad (7.7)$$

involving quantities already known from Eq. (3.41) and (3.43). This means that for $\hat{m} > 0$ this mapping results in squeezing and afterwards shifting the profile functions to bigger values of C .

Remark: For the massive case one should also look at the jet scale in the canonical region. We already mentioned that in the massive case there are two possible scale choices. In a more advanced analysis one should also consider both alternatives.

7.2. Initial $b\bar{b}$ -Pair Production

In this subsection we will look into the production of an initial $b\bar{b}$ -pair. The cross-section involves vector and axial-vector contributions, hence is given by (for the massive or the massless case):

$$\frac{1}{\sigma_0} \frac{d\sigma}{dC} = \sum_{i=v,a} \frac{\sigma_0^i}{\sigma_0} \left[\frac{1}{\sigma_0^i} \frac{d\sigma_s^i}{dC} + \frac{1}{\sigma_0^i} \frac{d\sigma_{\text{ns}}^i}{dC} \right], \quad (7.8)$$

involving quantities of Eq. (6.77) and (6.78). First we check the convergence of the massive and the massless case which means that we expect the error band¹⁹ to shrink when increasing the order of log resummation. Afterwards we compare massive against massless case and discuss the results.

The massless study [12], from which we adopted the profile functions, uses the so-called *prime* counting. This is the reason why we will also use this counting for our analysis, which means that we will analyze the differential cross-section with LL and NLL' resummation. Although the analysis does not differ significantly from the unprimed analysis (NLL and N²LL) the primed results yield smaller error bands and are therefore the better choice.

In the following we will only discuss the tail region. Since we only included the first moment of the shape function our results are not suitable to treat the peak and because of the strong change of the profiles slope (which leads to an unphysical kink) we also will not discuss the far-tail region.

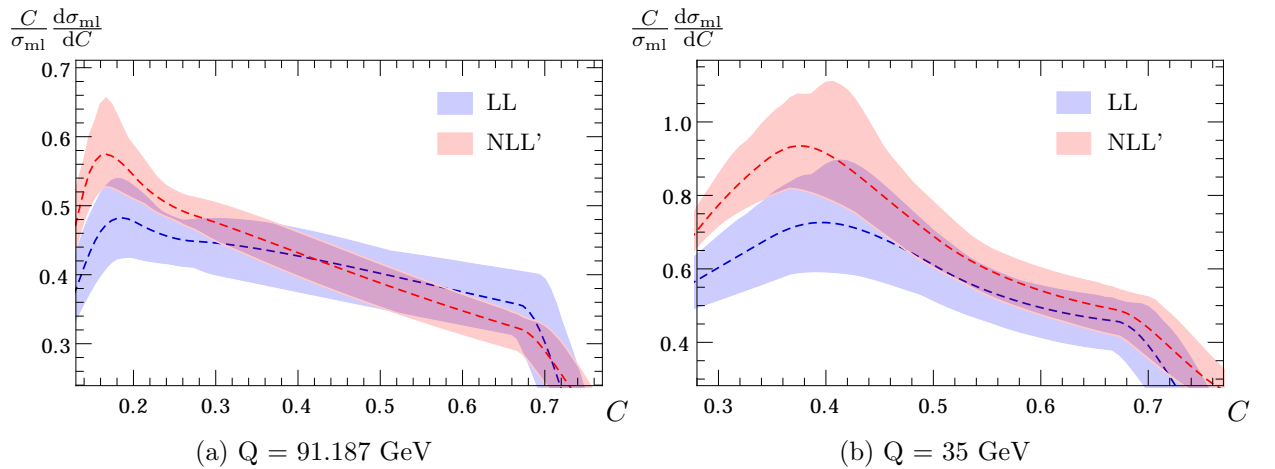


Figure 14: Massless differential cross-section with default profiles and bands due to profile variations for LL and NLL' resummation.

¹⁹Here we refer to an error estimate which is obtained by variations of the profiles which is non-Gaussian.

First we look at the massless case. The convergence of the massless differential cross-section with LL and NLL' resummation is shown in Fig. 14. Although no big effect, the convergence can be seen for both used center of mass (c.o.m.) energies. The fact that the NLL' band is not enclosed by the LL band is caused by the $\mathcal{O}(\alpha_s)$ matrix elements. These terms are only next-to-leading-order (NLO) in the perturbative series and can therefore yield sizable corrections.

Next we look at the massive case. Therefore we switch to the generalized profile functions and afterwards determine the hierarchy between the mass (in this case $\bar{m}_b(\bar{m}_b) = 4.2$ GeV) and the involved profile functions. Up to now when concerned with the running of different cross-section contributions we always considered a scale hierarchy like $\Lambda_{\text{QCD}} \ll m < \mu_S < \mu_J < \mu_H \sim Q$ (in analogy with [13] we will call this situation scenario IV), hence 5 flavor running was used for all factors of the cross-section formula. For low enough Q , at some point, the hierarchy will change to $\Lambda_{\text{QCD}} \ll \mu_S < m < \mu_J < \mu_H \sim Q$ (scenario III). Since the soft function evolution, which starts at the soft scale and ends at the jet scale, now crosses the mass scale we have to adapt the soft function evolution. The details of this problem and how to treat it is discussed in [13–15]. In our analysis we will only look at the region of scenario IV and therefore always use 5 flavor running.

In Fig. 15 one can see the hierarchy of the scales as well as the boundary between scenario III and IV for different c.o.m. energies. In addition the convergence of the differential cross-section with LL and NLL' resummation for the massive case is shown. If one compares with the massless plots one can see that the massive cross-section shows a very similar convergence behavior.

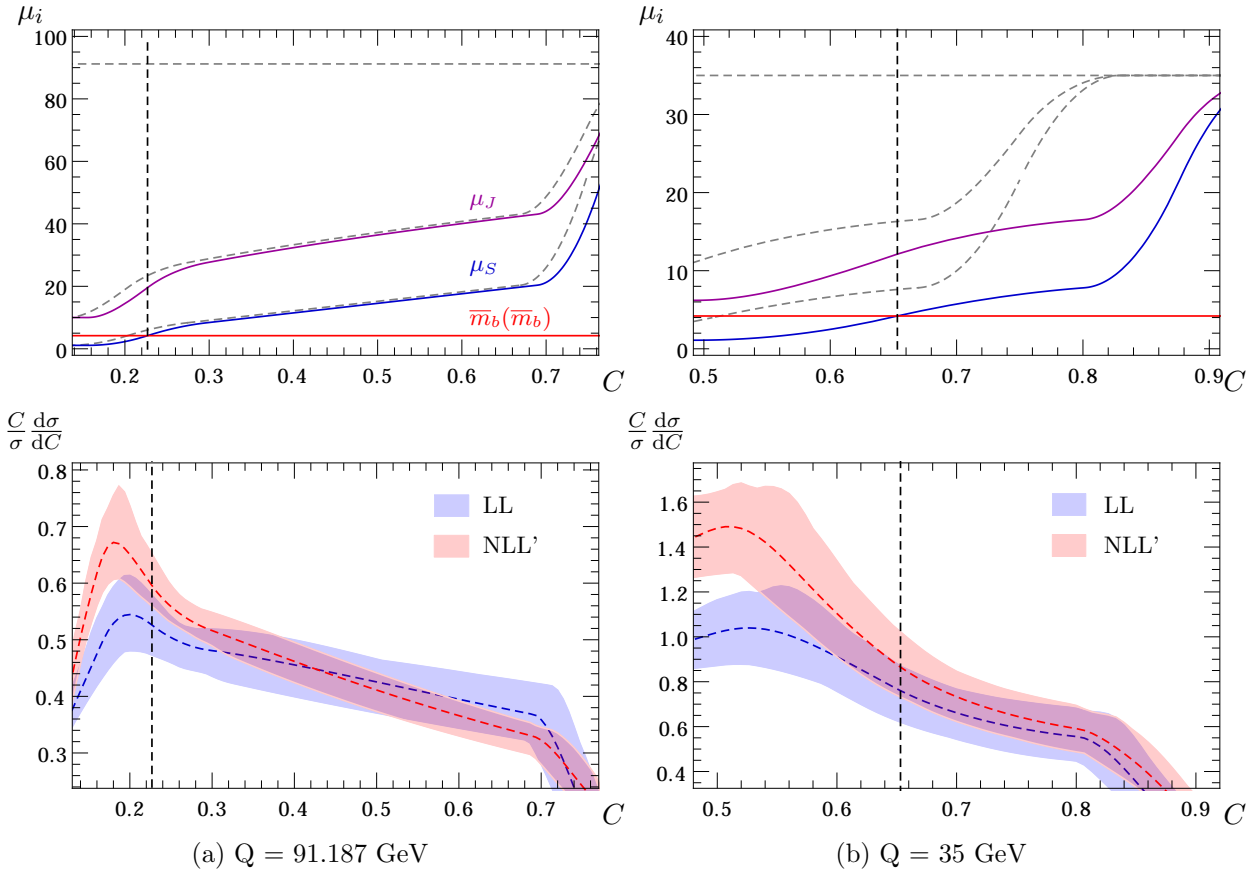


Figure 15: (top) Profile functions for the massive and the massless (gray dashed) case together with the bottom mass $\bar{m}_b(\bar{m}_b) = 4.2$ GeV which determines the boundary between Scenario III and IV. (bottom) Massive ($\bar{m}_b(\bar{m}_b) = 4.2$ GeV) differential cross-section with default profiles and bands due to profile variations for LL and NLL'.

Now we will compare the massless and the massive differential cross-section with NLL' resummation. This is shown in Fig. 16 where one can see a significant effect for a lower c.o.m. energy. This reflects

the mass sensitivity of the massive C-parameter which is mainly given by a shift of the distribution. At this point one should mention that experimentally this *tagged* $b\bar{b}$ -production cross-section is difficult to measure which is why experimental results involve big errors. This might disqualify the tagged $b\bar{b}$ -production cross-sections for a precise determination of fundamental parameters.

Remark: Furthermore one would face the problem that experimental data sets are only available for the original definition of the C-parameter given in Eq. (2.5). For this observable, which is certainly much less sensitive to the quark mass, the exact mass dependence is not known.

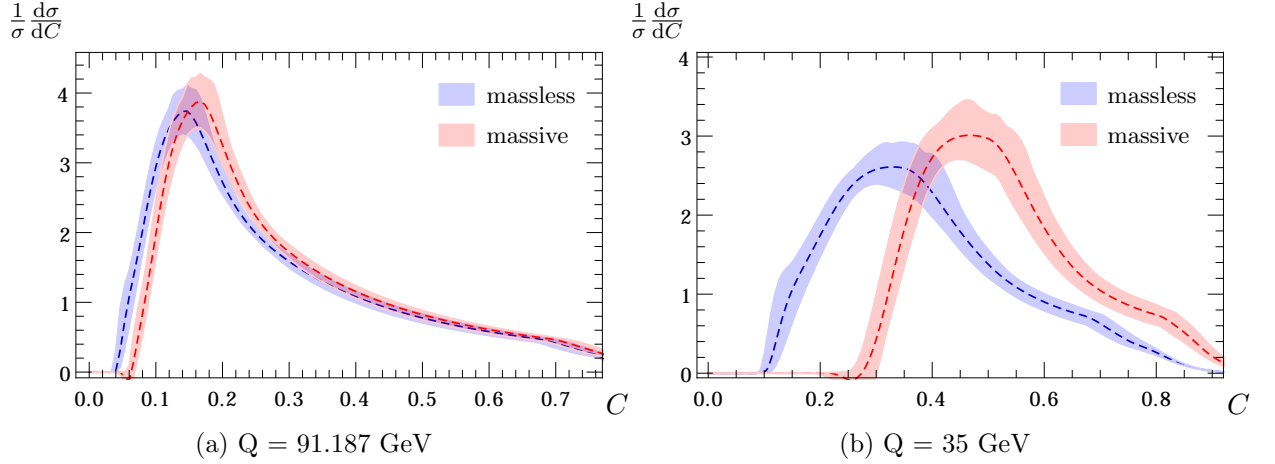


Figure 16: Comparison of the massless and the massive ($\bar{m}_b(\bar{m}_b) = 4.2$ GeV) differential cross-section with default profiles and bands due to profile variations for NLL'.

However, the high mass sensitivity of the massive C-parameter can be used to determine the relation between the experimentally measured top quark mass parameter and a theoretically well-defined short-distance mass. As argued in [49] the experimental value of the top quark mass, which is determined with the help of Monte Carlo generators, is theoretically not well defined. A comparison of Monte Carlo generated cross-section data with analytic results is needed to clarify this issue and allow for a precise and theoretically well-defined top quark mass determination. The results obtained in this thesis are a first step to such an analysis.

Up to now we only treated initial bottom quark production while imposing the scale hierarchy of scenario IV. To get results for $t\bar{t}$ -production we have to overcome some subtleties which are explained in more detail for the case of thrust in [15]:

- It was already mentioned that for bigger values of $\hat{m} = m/Q$ the hierarchy of the scales might not comply with scenario IV, hence we have to implement a consistent way of treating different scenarios.
- As we know, the jet function allows for two different scale choices which are given by $\mu_J^2 \sim Q^2(c - c_{\min})$ and $\mu_J^2 \sim Q^2(c - c_{\min} + \hat{m}^2)$. For small masses, where the two scales are similar, no problem will arise, but for big masses no scale choice will allow to resum both logarithms. Since $\hat{m} = m/Q$ is usually bigger when looking at $t\bar{t}$ -production one faces this problem much earlier. It can be seen when looking at the involved logarithms that this issue becomes critical for the region where $(c - c_{\min}) \sim \hat{m}^2$, which can be treated by introducing another effective field theory called bHQET.

A more detailed discussion on how to generalize the obtained result for $t\bar{t}$ -production is beyond the scope of this work.

7.3. All Flavor Production

The analysis of [12] which should determine the value of $\alpha_s(m_Z)$ uses experimental data at c.o.m. energies between 35 and 207 GeV. In this subsection we want to clarify whether one should expect that bottom mass effects play a significant role in this analysis.

Remark: For the mentioned analysis, since it considers massless partons, the original definition of the C-parameter was used. When we analyze the effect of a massive bottom quark to the massive C-parameter all-flavor production cross-section, we cannot quantify the effect on the corresponding original C-parameter cross-section. However, since the original C-parameter is much less sensitive to the mass of the initial quark-pair we can use our results as an upper bound.

For the all-flavor production cross-section we consider the following two cases of produced quarks:

- 5 massless (3 down-type; 2 up-type)
- 4 massless (2 down-type; 2 up-type) plus one massive (down-type; $\overline{m}_b(\overline{m}_b) = 4.2$ GeV)

For the correct normalization we define the all flavor born cross-section as:

$$\sigma_0^{(5)} = 3\sigma_0^d + 2\sigma_0^u, \quad (7.9)$$

involving the up- and down-type massless born cross-sections defined by Eq. (3.15). The all flavor production cross-section is then given by (with implicit summation over vector and axial-vector):

$$\frac{d\sigma}{dC} = 2(\sigma_0^u + \sigma_0^d) \left[\frac{1}{\sigma_0} \frac{d\sigma_s}{dC} + \frac{1}{\sigma_0} \frac{d\sigma_{ns}}{dC} \right]_{ml} + \sigma_0^d \left[\frac{1}{\sigma_0} \frac{d\sigma_s}{dC} + \frac{1}{\sigma_0} \frac{d\sigma_{ns}}{dC} \right]_{ml/m} \quad (7.10)$$

These pre-factors can be used to estimate the impact on the final cross-section. Actually at $Q = m_Z$ the up- and the down-type born cross-section are roughly the same. Furthermore we know from the previous subsection that at this c.o.m. energy the mass effects are not very big and therefore we expect almost no change. For $Q = 35$ GeV the up-type born cross-section is almost 4 times larger than the down-type born cross-section. Taking this into account means that the massive contributions are suppressed by almost a factor of ten. Although the impact on the single flavor production cross-section at this energy is big we expect these effects to counter each other. This is why we do not expect a very large impact of the bottom mass to the final all flavor production cross-section.

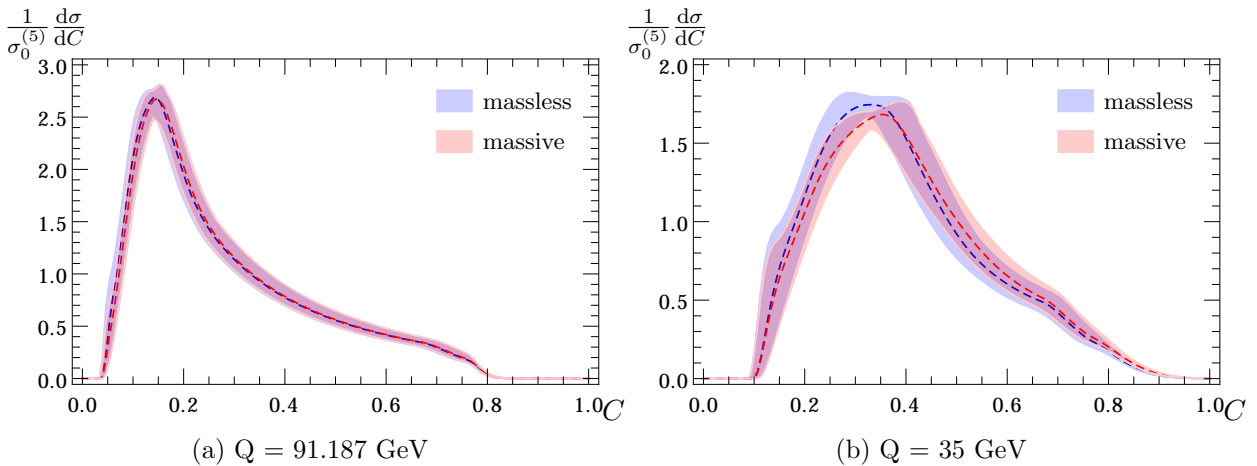


Figure 17: Comparison of the 5 massless and the 4 massless plus 1 massive ($\overline{m}_b(\overline{m}_b) = 4.2$) differential cross-section with default profiles and bands due to profile variations for NLL'

In Fig. 17 one can see the all flavor production cross-section with either a massless or massive bottom quark. As anticipated, the effect of a massive bottom quark is not very large. At NLL' the massless and massive result are still compatible.

This means that, at this level, the analysis of [12] is not influenced by bottom quark mass effects. Since a much higher resummation order (N^3LL') is used in [12], it is hard to estimate the effect on the full analysis. However, since the original C-parameter is much less sensitive to parton masses one should still expect no large effect.

8. Outlook

Since its introduction in the early 1980s the C-parameter was investigated in several event-shape studies. The usual approach is to consider massless partons. However for a number of cases mass effects cannot be neglected. Therefore the question at hand was how mass effects influence the C-parameter differential cross-section.

To answer this we first computed the full QCD result to $\mathcal{O}(\alpha_s)$ which before was only accessible through a parton level Monte Carlo generator. Furthermore we derived the SCET factorization theorem for the massive C-parameter, computed the involved factors to $\mathcal{O}(\alpha_s)$ and resummed large logarithms to N²LL accuracy. Afterwards non-perturbative power corrections were included by convoluting the perturbative cross-section with a shape function. To improve the convergence of the perturbative series we switched to the $\overline{\text{MS}}$ short-distance mass and removed the leading renormalon in the soft function. As a practical application, primary bottom quark mass-effects at different c.o.m. energies for tagged $b\bar{b}$ and all-flavor production were investigated.

Up to now we always considered a scale hierarchy like $\Lambda_{\text{QCD}} \ll m < \mu_S < \mu_J < \mu_H \sim Q$ (scenario IV) which is why $n_f = 5$ was used for the running of all cross-section factors. In addition we encountered unresummed large logarithms in the region where $(c - c_{\min}) \sim \hat{m}^2$ which is called the bHQET region. It was already anticipated that for smaller c.o.m. energy or bigger masses (as in a study of top quark mass effects) the hierarchy can change and also the bHQET-region can no longer be ignored. This

As mentioned before, one of the future applications of this works findings is to investigate the relation between the Monte Carlo top quark mass parameter m_t^{MC} and a theoretically well defined top quark mass. This investigation should clarify how this MC parameter can be used as a theoretical input and whether the given error estimates which are comparably small are valid. To answer these questions a more general treatment of mass effects (as in [13–15]), which is based on the results presented in this work, is needed.

A. Radiative Contribution to the FO result

A.1. Reduction of Elliptic Integrals to Legendre's Normal Form

In this subsection we will describe the details on how to reduce the elliptic integrals given in Eq. (3.35) to Legendre's normal form. The general form of the involved integrals is given by (note that we replace x_3 with y):

$$\int_{y_m}^{\tilde{y}} dy \mathcal{F}_i(y, c, \hat{m}), \quad i = a, v, \quad (\text{A.1})$$

with

$$\mathcal{F}_i(y, c, \hat{m}) = \frac{f_i(y, c, \hat{m})}{\sqrt{(y - y_0)(y - y_1)(y - y_2)(y - y_3)}}, \quad (\text{A.2})$$

and $y_0 \geq y_1 \geq y_2 \geq y_3$

$$y_0 = \frac{1}{1 + c}, \quad y_1 = y_p, \quad y_2 = y_m, \quad y_3 = 0.$$

Now our aim is to express the integrals in Eq. (A.1) in terms of (incomplete) Legendre elliptic integrals which were defined in Eq. (3.45). In the following we present a step-by-step recipe how to do the reduction. Therefore we follow [23] and adapt the expressions to the ones involved in our calculation.

1. The first step is to do a partial fractional decomposition of $f(y, c, \hat{m})$. In general this yields a polynomial in y and several fractions with simpler denominator:

$$\mathcal{F}(y, c, \hat{m}) = \sum_i a_i(c, \hat{m}) \frac{y^i}{z} + \sum_{j,k} b_j(c, \hat{m}) \frac{1}{[y - c_k(c, \hat{m})]^j z}. \quad (\text{A.3})$$

2. Next one has to do a substitution. The form of this substitution is determined by the properties of the y_i 's and the integration bounds. For our case it is given by:

$$y \rightarrow \frac{y_2(y_1 - y_3) - y_3(y_1 - y_2)y}{(y_1 - y_3) - (y_1 - y_2)y} = \frac{y_1 y_2}{y_1 - (y_1 - y_2)y}. \quad (\text{A.4})$$

Note that in [23] they use $y \rightarrow y^2$ which turns out to be not very convenient. It is much better to use this substitution and a different form of the standard integrals where one has to substitute $y^2 \rightarrow y$.

3. Some of the integrals (the ones involving y^0, y^1) are already in the right form and yield elliptic integral expressions (one just has to rearrange the parts conveniently, for example:)

$$\begin{aligned} \int_0^{\sin^2 \theta} dy \frac{y}{\sqrt{y(1-y)(1-my)}} &= \frac{1}{m} \int_0^{\sin^2 \theta} dy \left\{ \frac{1}{\sqrt{y(1-y)(1-my)}} - \sqrt{\frac{1-my}{y(1-y)}} \right\} \\ &= \frac{2}{m} \left\{ F(\theta, m) - E(\theta, m) \right\}. \end{aligned} \quad (\text{A.5})$$

For the remaining integrals one has to use a recursive *reduction formula*. In the following we show how to derive these kind of formulas. In fact after the substitution of step 1 all the remaining integrals look like:

$$\frac{1}{(1 - ny)^k \sqrt{y(1-y)(1-my)}} = \frac{1}{(1 - ny)^k z}. \quad (\text{A.6})$$

Now we use $z^2 = b_3(1 - ny)^3 + b_2(1 - ny)^2 + b_1(1 - ny) + b_0$, calculate the coefficients b_i and take the derivative with respect to y . This yields:

$$\begin{aligned} \frac{d}{dy} \left[(1 - ny)^k z \right] &= \frac{n}{z} \left\{ k(1 - ny)^{k-1} z^2 + (1 - ny)^k \frac{dz^2}{dy} \right\} \\ &= \frac{n}{z} \left\{ b_3 \left(k + \frac{3}{2} \right) (1 - ny)^{k+2} + b_2 (k + 1) (1 - ny)^{k+1} \right. \\ &\quad \left. + b_1 \left(k + \frac{1}{2} \right) (1 - ny)^k + b_0 k (1 - ny)^{k-1} \right\}. \end{aligned} \quad (\text{A.7})$$

For example the first reduction formula ($k = -1$, the next would be $k = -2$) is achieved by integrating this expression from 0 to $\sin^2(\theta)$:

$$\begin{aligned} &\int_0^{\sin^2 \theta} dy \frac{1}{(1 - ny)^2 z} \\ &= \frac{1}{b_0} \left\{ \frac{1}{n} \frac{\sin \theta \cos \theta \sqrt{1 - m \sin^2 \theta}}{1 - n \sin^2 \theta} + \frac{b_3}{2} \int_0^{\sin^2 \theta} dy \frac{1 - ny}{z} - b_1 \Pi(n; \theta, m) \right\} \\ &= \frac{1}{b_0} \left\{ \frac{1}{n} \frac{\sin \theta \cos \theta \sqrt{1 - m \sin^2 \theta}}{1 - n \sin^2 \theta} + b_3 \left(1 - \frac{n}{k} \right) F(\theta, m) + b_3 \frac{n}{k} E(\theta, m) - b_1 \Pi(n; \theta, m) \right\}. \end{aligned} \quad (\text{A.8})$$

This yields a recursive reduction of integrals of the form (A.6) and therewith of all remaining integrals.

A.2. Radiative FO Result in Legendre's Normal Form

When applying the reduction procedure presented in the previous subsection one arrives at results involving expressions of the form:

$$\begin{aligned} \tilde{\mathcal{F}}_i(c, \hat{m}, \theta) &= c_i(c, \hat{m}) + f_i(c, \hat{m}) F(\theta, m) + e_i(c, \hat{m}) E(\theta, m) \\ &\quad + p_{n,i}(c, \hat{m}) \Pi(n; \theta, m) + p_{h,i}(c, \hat{m}) \Pi(h; \theta, m). \end{aligned} \quad (\text{A.9})$$

Therein we have five c-parameter and mass dependent coefficients as well as one elliptic modulus and two characteristics. To write them in an effective way we define the following expressions:

$$y_h = \frac{c - 2\hat{m}^2(1 - \hat{m}^2)}{c - 2\hat{m}^2}, \quad (\text{A.10})$$

$$\xi = \sqrt{1 + 16\hat{m}^2 + 32\hat{m}^4 - 8c(1 + 2\hat{m}^2)^2}, \quad (\text{A.11})$$

$$\xi_2 = \sqrt{(1 + \xi)^2 - 16(c - 2\hat{m}^2)^2}. \quad (\text{A.12})$$

Then the involved characteristics are given by:

$$n = 1 - \frac{y_2}{y_1} = \frac{2\xi}{1 + \xi + 4c - 8m^2}, \quad (\text{A.13})$$

$$h = \frac{y_h(y_1 - y_2)}{y_1(y_h - y_2)} = \frac{2\xi}{1 + \xi - 4c + 8m^2}, \quad (\text{A.14})$$

as well as the elliptic modulus:

$$m = \frac{y_0(y_1 - y_2)}{y_1(y_0 - y_2)} = \frac{n h}{\xi}. \quad (\text{A.15})$$

Now only the lengthy expressions for the coefficients are missing. We present them for the vector and axial-vector separately.

Vector Case:

$$\begin{aligned}
 c_v(c, \hat{m}) = & \frac{\xi \sin(2\theta)}{2(1+c)^3 \sqrt{\xi_2^2 - 2\xi(1 - \cos(2\theta))}} \left\{ 4 \right. \\
 & + \frac{2[\xi_2^2 - 2(1 - \cos(2\theta))\xi]}{(c - 2\hat{m}^2)^2(4c + \cos(2\theta)\xi - 8\hat{m}^2 + 1)} \left[c(3 + 5c) + 2(-2 - c + 7c^2)\hat{m}^2 \right. \\
 & \quad \left. + 2(-1 - 6c + 7c^2)\hat{m}^4 + 8(1 + c^2)\hat{m}^6 \right] \\
 & - \frac{128(c+1)^4 \hat{m}^6 (1 + 2\hat{m}^2)(-4c + 8\hat{m}^2 + \xi + 1)(\xi_2^2 - 2(1 - \cos(2\theta))\xi)}{\xi_2^2(c - 2\hat{m}^2)^2(-4c + 8\hat{m}^2 + \xi - 1)(-4c + \cos(2\theta)\xi + 8\hat{m}^2 + 1)} \\
 & - \frac{(1 + 2\hat{m}^2)[\xi_2^2 - 2(1 - \cos(2\theta))\xi]}{(c - 2\hat{m}^2)(4c + \cos(2\theta)\xi - 8\hat{m}^2 + 1)^2} \left[3 + 26c + 32c^2 + 3\cos(2\theta)\xi \right. \\
 & \quad \left. + 6c\cos(2\theta)\xi - 4(13 + 28c + 3\cos(2\theta)\xi)\hat{m}^2 + 16(7 + c)\hat{m}^4 \right] \left. \right\}, \tag{A.16}
 \end{aligned}$$

$$\begin{aligned}
 f_v(c, \hat{m}) = & \frac{16}{(c+1)^2(c - 2\hat{m}^2)^2[c + 2(\hat{m}^2 - 1)\hat{m}^2]\xi_2} \left\{ -c^2(-1 + c^2) \right. \\
 & - 2c(2 - 2c + 3c^3)\hat{m}^2 - 2(-2 + 8c - 7c^2 - 2c^3 + 7c^4)\hat{m}^4 \\
 & - 4(-4 + 8c - 5c^2 - 4c^3 + 3c^4)\hat{m}^6 - 8(-3 + c + 5c^2 + 4c^3 + c^4)\hat{m}^8 \\
 & - 8(2 - 15c - 7c^2 + 3c^3)\hat{m}^{10} - 8(13 + 12c + 5c^2 + 2c^3)\hat{m}^{12} - 32(-2 + c^2)\hat{m}^{14} \left. \right\}, \tag{A.17}
 \end{aligned}$$

$$\begin{aligned}
 e_v(c, \hat{m}) = & \frac{8(-1 + 4c - 8\hat{m}^2 - \xi)}{(c+1)^2(c - 2\hat{m}^2)^2(1 + 4c - 8\hat{m}^2 - \xi)\xi_2} \left\{ 3c^2(1 + 2c) \right. \\
 & + 2c(-4 - 3c + 8c^2)\hat{m}^2 + 2(2 - 7c + 2c^2 + 14c^3)\hat{m}^4 + 4(5 - 11c + 6c^3)\hat{m}^6 \\
 & \left. + 8(8 + 12c + 9c^2 + 2c^3)\hat{m}^8 + 32(-2 + c^2)\hat{m}^{10} \right\}, \tag{A.18}
 \end{aligned}$$

$$\begin{aligned}
 p_{n,v}(c, \hat{m}) = & \frac{4(1 + 4c - 8\hat{m}^2 - \xi)}{(1+c)^3(c - 2\hat{m}^2)^3\xi_2} \left\{ -c^2(2 + c + 2c^2) + 2c(4 - 3c + 8c^2 + 2c^3)\hat{m}^2 \right. \\
 & + 2(-4 + 21c - 23c^2 + 13c^3 + 15c^4)\hat{m}^4 + 4(-11 + 34c - 16c^2 - 10c^3 + 9c^4)\hat{m}^6 \\
 & \left. + 4(-27 + 49c + 21c^2 - 13c^3 + 2c^4)\hat{m}^8 + 16(-7 + 3c + 7c^2 + c^3)\hat{m}^{10} \right\}, \tag{A.19}
 \end{aligned}$$

$$\begin{aligned}
 p_{h,v}(c, \hat{m}) = & \frac{8\hat{m}^4(4c - 8\hat{m}^2 + \xi - 1)}{(c - 2\hat{m}^2)^3[c + 2\hat{m}^2(\hat{m}^2 - 1)]\xi_2} \left\{ c^2 + 10c^2\hat{m}^2 + 4(-1 - 5c + 3c^2)\hat{m}^4 \right. \\
 & \left. - 4(-2 + 3c)\hat{m}^6 + 4(1 + 2c)\hat{m}^8 + 16\hat{m}^{10} \right\}. \tag{A.20}
 \end{aligned}$$

Axial-Vector Case:

$$\begin{aligned}
 c_a(c, \hat{m}) = & \frac{\xi \sin(2\theta)}{2(1+c)^3 \sqrt{\xi_2^2 - 2\xi(1 - \cos(2\theta))}} \left\{ 4 \right. \\
 & + \frac{2[\xi_2^2 - 2(1 - \cos(2\theta))\xi]}{(c - 2\hat{m}^2)^2(4c + \cos(2\theta)\xi - 8\hat{m}^2 + 1)} \left[c(3 + 5c) + 4(-1 - 3c + c^2)\hat{m}^2 \right. \\
 & \quad \left. - 2(-3 + 20c + 11c^2)\hat{m}^4 - 4(-7 + 2c + 5c^2)\hat{m}^6 \right] \\
 & - \frac{128(c+1)^4 \hat{m}^6 (1 - 4\hat{m}^2)(-4c + 8\hat{m}^2 + \xi + 1)(\xi_2^2 - 2(1 - \cos(2\theta))\xi)}{\xi_2^2(c - 2\hat{m}^2)^2(-4c + 8\hat{m}^2 + \xi - 1)(-4c + \cos(2\theta)\xi + 8\hat{m}^2 + 1)} \\
 & - \frac{(1 + 2\hat{m}^2)^2[\xi_2^2 - 2(1 - \cos(2\theta))\xi]}{(c - 2\hat{m}^2)(4c + \cos(2\theta)\xi - 8\hat{m}^2 + 1)^2} \left[3 + 26c + 32c^2 + 3\xi \cos(2\theta) \right. \\
 & \quad \left. + 6c\xi \cos(2\theta) - 4(13 + 28c + 3\xi \cos(2\theta))\hat{m}^2 + 16(7 + c)\hat{m}^4 \right] \left. \right\}, \tag{A.21}
 \end{aligned}$$

$$\begin{aligned}
 f_a(c, \hat{m}) = & \frac{16}{(c+1)^2(c - 2\hat{m}^2)^2[c + 2(\hat{m}^2 - 1)\hat{m}^2]\xi_2} \left\{ -c^2(-1 + c^2) \right. \\
 & + 2c(-2 - c + 2c^3)\hat{m}^2 + 2(2 + 4c + c^2 - 14c^3 + 17c^4)\hat{m}^4 \\
 & + 8(-1 + 2c + 9c^2 - 19c^3 + 2c^4)\hat{m}^6 + 8(-3 - 13c + 36c^2 + 12c^3 + 2c^4)\hat{m}^8 \\
 & + 8(8 - 39c - 51c^2 + 5c^3)\hat{m}^{10} + 8(15 + 74c + 9c^2 + 4c^3)\hat{m}^{12} \\
 & \left. + 16(-21 - 10c + 5c^2)\hat{m}^{14} + 192\hat{m}^{16} \right\}, \tag{A.22}
 \end{aligned}$$

$$\begin{aligned}
 e_a(c, \hat{m}) = & \frac{8(-1 + 4c - 8\hat{m}^2 - \xi)}{(c+1)^2(c - 2\hat{m}^2)^2(1 + 4c - 8\hat{m}^2 - \xi)\xi_2} \left\{ 3c^2(1 + 2c) - 8c(1 + 4c + 2c^2)\hat{m}^2 \right. \\
 & - 2(-2 - 33c - 24c^2 + 34c^3)\hat{m}^4 - 4(9 + 10c - 52c^2 + 8c^3)\hat{m}^6 \\
 & \left. - 8(-5 + 43c + 19c^2 + 4c^3)\hat{m}^8 - 80(-2 - 2c + c^2)\hat{m}^{10} - 192\hat{m}^{12} \right\}, \tag{A.23}
 \end{aligned}$$

$$\begin{aligned}
 p_{n,a}(c, \hat{m}) = & \frac{4(1 + 4c - 8\hat{m}^2 - \xi)}{(1+c)^3(c - 2\hat{m}^2)^3\xi_2} \left\{ -c^2(2 + c + 2c^2) + 2c(4 + 3c + 15c^2)\hat{m}^2 \right. \\
 & - 2(4 + 3c + 41c^2 - 21c^3 + 17c^4)\hat{m}^4 - 4(-1 - 15c + 55c^2 - 33c^3 + 18c^4)\hat{m}^6 \\
 & - 4(-7 - 69c + 111c^2 - 43c^3 + 4c^4)\hat{m}^8 - 8(13 - 61c + 43c^2 + 5c^3)\hat{m}^{10} \\
 & \left. + 64(-5 + c)\hat{m}^{12} \right\}, \tag{A.24}
 \end{aligned}$$

$$\begin{aligned}
 p_{h,a}(c, \hat{m}) = & \frac{8\hat{m}^4(4c - 8\hat{m}^2 + \xi - 1)}{(c - 2\hat{m}^2)^3[c + 2\hat{m}^2(\hat{m}^2 - 1)]\xi_2} \left\{ c^2 - 4c^2\hat{m}^2 - 4(1 - 3c + 6c^2)\hat{m}^4 \right. \\
 & \left. + 28c\hat{m}^6 - 4(-5 + 4c)\hat{m}^8 - 40\hat{m}^{10} \right\}. \tag{A.25}
 \end{aligned}$$

B. Distributions and useful Identities

In this section we intend to give the definition of the involved plus distributions and some relations we need to derive our results. The ordinary (log-)plus distribution is defined via the integral with

a suitable test function $f(x)$. For $m \geq 0$ we define it as:

$$\int_0^\Delta dx \left[\frac{\theta(x) \ln^m(x)}{x} \right]_+ f(x) = \int_0^\Delta dx \ln^m(x) \left[\frac{f(x) - f(0)}{x} \right] + f(0) \frac{\ln^{m+1}(\Delta)}{m+1}. \quad (\text{B.1})$$

Involving these plus and a delta distribution one can write down the useful relation which was used in the ϵ expansion of the soft function. For the dimensionless variable x it reads:

$$\frac{\theta(x)}{x^{1+a\epsilon}} = -\frac{1}{a\epsilon} \delta(x) + \left[\frac{\theta(x)}{x} \right]_+ - a\epsilon \left[\frac{\theta(x) \ln(x)}{x} \right]_+ + \frac{a^2 \epsilon^2}{2} \left[\frac{\theta(x) \ln^2(x)}{x} \right]_+ + \mathcal{O}(\epsilon^3). \quad (\text{B.2})$$

Furthermore we use the so-called fractional plus distributions. Together with $0 \neq \omega < 1$ they are defined as [27]:

$$\int_0^\Delta dx \left[\frac{\theta(x)}{x^{1+\omega}} \right]_+ f(x) = \int_0^\Delta dx \left[\frac{f(x) - f(0)}{x^{1+\omega}} \right] - f(0) \frac{\Delta^{-\omega}}{\omega}. \quad (\text{B.3})$$

Remark: One can also define them involving the non-distributional integral for some value ω where it exists and afterwards analytically continue to some other value of ω .

Now we can define the fractional log-plus distributions as derivatives of the fractional plus distribution, defined in Eq. B.3, which reads:

$$\begin{aligned} \int_0^\Delta dx \left[\frac{\theta(x) \ln^m(x)}{x^{1+\omega}} \right]_+ f(x) &= \left(-\frac{d}{d\omega} \right)^m \int_0^\Delta dx \left[\frac{\theta(x)}{x^{1+\omega}} \right]_+ f(x) \\ &= \int_0^\Delta \ln^m(x) \left[\frac{f(x) - f(0)}{x^{1+\omega}} \right] - \frac{f(0)}{\omega^{1+m}} \Gamma[1+m, \omega \ln(\Delta)]. \end{aligned} \quad (\text{B.4})$$

Fourier Transform

In the calculation of evolution kernels and anomalous dimensions it is sometimes convenient to take the Fourier transform of a function which involves plus distributions. To calculate the Fourier transform of the ordinary (log-)plus distributions we take the Fourier transform of Eq. (B.2) and identify the different terms:

$$\begin{aligned} \mathcal{F}\left(\frac{\theta(x)}{x^{1+a\epsilon}}\right)(y) &= \int_0^\infty dx e^{-i\xi x} \frac{1}{x^{1+a\epsilon}} \\ &= -\frac{1}{a\epsilon} - \ln(iye^{\gamma_E}) - a\epsilon \left\{ \frac{\pi^2}{12} + \ln^2(iye^{\gamma_E}) \right\} \\ &\quad + \frac{a^2 \epsilon^2}{2} \left\{ -\frac{1}{3} \ln^3(iye^{\gamma_E}) - \frac{\pi^2}{6} \ln(iye^{\gamma_E}) - \frac{2}{3} \zeta_3 \right\} + \mathcal{O}(\epsilon^3). \end{aligned} \quad (\text{B.5})$$

To calculate the Fourier transform of fractional (log-)plus distributions one has to calculate it for some ω where the Fourier transform exists and again analytically continue to the real value.

C. Massive SCET Feynman Rules

In this section we give the $\mathcal{O}(\lambda^0)$ Feynman rules one can derive from the massive SCET Lagrangian (see Eq. (4.12), they can also be found in [28, 50]). In the following we consider all gluon momenta outgoing.

$$\text{---} \overline{\psi} \text{---} \xrightarrow{p} \text{---} \psi \text{---} = i \frac{\not{p}}{2p^2 - m^2 + i0} \quad (\text{C.1})$$


$$= (ig_s T^A \tilde{\mu}^\epsilon) n_\mu \frac{\not{n}}{2} \quad (\text{C.2})$$

$$\begin{aligned}
& \text{Diagram: A vertical chain of circles with a wavy line on top labeled } \mu, A. \text{ Two horizontal dashed lines with arrows labeled } p \text{ and } p' \text{ enter from the left and right respectively.} \\
& = (ig_s T^A \tilde{\mu}^\epsilon) \left[n_\mu + \frac{\gamma_\mu^\perp (\not{p}^\perp + m)}{\bar{n} \cdot p} + \frac{(\not{p}'^\perp - m) \gamma_\mu^\perp}{\bar{n} \cdot p'} \right. \\
& \quad \left. - \frac{(\not{p}'^\perp - m)(\not{p}^\perp + m)}{\bar{n} \cdot p \bar{n} \cdot p'} \bar{n}_\mu \right] \frac{\not{n}}{2} \\
& = V_\mu^A(p, p', m)
\end{aligned} \tag{C.3}$$

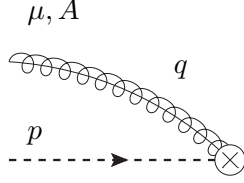
$$\begin{aligned}
& \text{Diagram: A V-shaped loop of fermions. The left leg has momentum p and indices μ, A. The right leg has momentum q and indices ν, B. The bottom vertex connects to two external horizontal dashed lines with momenta p' and p respectively.} \\
= & \frac{ig_s^2 T^A T^B \tilde{\mu}^{2\epsilon}}{\bar{n} \cdot (p - q)} \left[\gamma_\mu^\perp \gamma_\nu^\perp - \frac{\gamma_\mu^\perp (\not{p}^\perp + m)}{\bar{n} \cdot p} \bar{n}_\nu - \frac{(\not{p}'^\perp - m) \gamma_\nu^\perp}{\bar{n} \cdot p'} \bar{n}_\mu \right. \\
& \quad \left. + \frac{(\not{p}'^\perp - m)(\not{p}^\perp + m)}{\bar{n} \cdot p \bar{n} \cdot p'} \bar{n}_\mu \bar{n}_\nu \right] \frac{\not{n}}{2} \\
& + \frac{ig_s^2 T^B T^A \tilde{\mu}^{2\epsilon}}{\bar{n} \cdot (q + p')} \left[\gamma_\nu^\perp \gamma_\mu^\perp - \frac{\gamma_\nu^\perp (\not{p}^\perp + m)}{\bar{n} \cdot p} \bar{n}_\mu - \frac{(\not{p}'^\perp - m) \gamma_\mu^\perp}{\bar{n} \cdot p'} \bar{n}_\nu \right. \\
& \quad \left. + \frac{(\not{p}'^\perp - m)(\not{p}^\perp + m)}{\bar{n} \cdot p \bar{n} \cdot p'} \bar{n}_\mu \bar{n}_\nu \right] \frac{\not{n}}{2} \\
= & W_{\mu\nu}^{AB}(p, p', q, m)
\end{aligned} \tag{C.4}$$

Wilson Line Feynman Rules

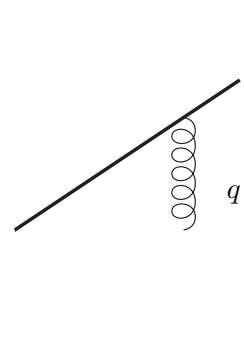
We also give the Feynman rules for the used collinear and soft Wilson lines involving a single gluon. They are derived via the momentum space expressions of these Wilson lines.



$$= g_s \frac{T^A \bar{n}_\mu}{q^- + i0} \tilde{\mu}^\epsilon \quad (\text{C.5})$$



$$= -g_s \frac{T^A n_\mu}{q^+ + i0} \tilde{\mu}^\epsilon \quad (\text{C.6})$$



$$= \left\{ \begin{array}{ll} g_s \frac{T^A n_\mu}{q^+ + i0} \tilde{\mu}^\epsilon & Y_n \\ -g_s \frac{T^A n_\mu}{q^+ + i0} & Y_n^\dagger \\ g_s \frac{\bar{T}^A \bar{n}_\mu}{q^- + i0} & \bar{Y}_{\bar{n}} \\ -g_s \frac{\bar{T}^A \bar{n}_\mu}{q^- + i0} \tilde{\mu}^\epsilon & \bar{Y}_{\bar{n}}^\dagger \end{array} \right. \quad (\text{C.7})$$

D. Details on Hard-, Jet- and partonic Soft-Function Calculation

D.1. Jet Function

D.1.1. Diagrams

In this subsection we will present details concerning the calculation of the massive hemisphere jet function diagrams. The calculation which we repeat here was first done in [27]. As one can see in Fig. 8 we have six nontrivial contributions where the last one accounts for the mass counterterm which is needed in the one loop computation. Note that we will only show details on the calculation of the first contribution which should serve as a guiding principle for the other calculations. Furthermore one already knows a lot about the appearing diagrams (at least their gamma structure) since they are essentially the same as for the renormalization of SCET [6].

The first diagram is given by (define $s \equiv s + i0 = p^2 - m^2 + i0$ and use SCET power counting):

$$\begin{aligned} J_a &= i \frac{\not{p}}{2} \frac{p^-}{p^2 - m^2 + i0} \int \frac{d^d q}{(2\pi)^d} V_\mu^A(p - q, p, m) i \frac{\not{p}}{2} \frac{p^- - q^-}{(p - q)^2 - m^2 + i0} \left(g_s \frac{T^B \bar{n}_\nu}{q^- + i0} \tilde{\mu}^\epsilon \right) \frac{-i g^{\mu\nu} \delta^{AB}}{q^2 + i0} \\ &= -8\pi\alpha_s(\mu) C_F \frac{\not{p}}{2} \frac{Q}{s} \mu^{2\epsilon} \int \frac{d^d q}{(2\pi)^d} \frac{Q - q^-}{(q^- + i0)((p - q)^2 - m^2 + i0)(q^2 + i0)} \end{aligned} \quad (\text{D.1})$$

$$\equiv -8\pi\alpha_s(\mu) C_F \frac{\not{p}}{2} \frac{Q}{s} I_a(s, m^2, \mu). \quad (\text{D.2})$$

To solve the integral denoted as $I_a(s, m^2, \mu)$ we use a relation which we already know from Eq. (6.28):

$$\frac{d^d q}{(2\pi)^d} = \frac{2^{-d} \pi^{-1-\frac{d}{2}}}{\Gamma(\frac{d-2}{2})} (q^\perp)^{d-3} dq^+ dq^- dq^\perp. \quad (\text{D.3})$$

Exploiting the SCET power counting we get:

$$I_a(s, m^2, \mu) = \frac{2^{-d} \pi^{-1-\frac{d}{2}} \mu^{4-d}}{\Gamma(\frac{d-2}{2})} \int dq^\perp (q^\perp)^{d-3} dq^- \frac{Q - q^-}{q^- + i0} \quad (D.4)$$

$$\times \frac{-1}{(Q - q^-)q^-} \int dq^+ \left\{ \left[q^+ - \frac{s - p^+ q^- - (q^\perp)^2 + i0}{Q - q^-} \right] \left[q^+ - \frac{(q^\perp)^2 - i0}{q^-} \right] \right\}^{-1}.$$

Of course we know from Cauchy's theorem that if all poles lie in one complex half-plane the integral will give zero. To get a non-zero result of the above q^+ integral we have to impose some bounds on the q^- integral which are realized by the theta functions $\theta(Q - q^-)$ and $\theta(q^-)$. Now we can carry out the integration using Cauchy's theorem and afterwards do the regular q^\perp integration. This yields:

$$I_a(s, m^2, \mu) = \frac{2^{-d} \pi^{-1-\frac{d}{2}} \mu^{4-d}}{\Gamma(\frac{d-2}{2})} \int_0^Q dq^- \frac{2\pi i (1 - q^-/Q)}{q^- + i0} \int_0^\infty dq^\perp \frac{(q^\perp)^{d-3}}{(q^\perp)^2 - \frac{s q^- - p^+ (q^-)^2}{Q}}$$

$$= \frac{-i 2^{-d} \pi^{1-\frac{d}{2}} \mu^{4-d} \csc(\frac{d\pi}{2})}{\Gamma(\frac{d-2}{2})} \int_0^Q dq^- \frac{(1 - q^-/Q)}{q^- + i0} \left(\frac{p^+ (q^-)^2 - q^- s}{Q} \right)^{\frac{d}{2}-2}. \quad (D.5)$$

With the substitution $q^-/Q \rightarrow z$ and SCET power counting we get:

$$I_a(s, m^2, \mu) = \frac{-i 2^{-d} \pi^{1-\frac{d}{2}} (\frac{\mu}{\sqrt{-s}})^{4-d} \csc(\frac{d\pi}{2})}{\Gamma(\frac{d-2}{2})} \int_0^1 dz z^{\frac{d}{2}-3} (1-z) \left(1 - \frac{s+m^2}{s} z \right)^{\frac{d}{2}-2}$$

$$= -i 2^{-d} \pi^{1-\frac{d}{2}} (\frac{\mu}{\sqrt{-s}})^{4-d} \csc(\frac{d\pi}{2}) {}_2\tilde{F}_1\left(2 - \frac{d}{2}, \frac{d}{2} - 2; \frac{d}{2}; \frac{s+m^2}{s}\right), \quad (D.6)$$

where ${}_2\tilde{F}_1(a, b; c; z) = {}_2F_1(a, b; c; z)/\Gamma(b)$ denotes the regularized Gauss hypergeometric function. Now we set $d = 4 - 2\epsilon$ and expand for small ϵ using the *Mathematica* package *HypExp* [51]:

$$I_a(s, m^2, \mu) = \frac{-i}{16\pi^2} \left\{ \frac{1}{\epsilon^2} + \frac{1}{\epsilon} \left[1 + \ln\left(\frac{\mu^2}{-s}\right) \right] + 2 + \frac{\pi^2}{12} - \frac{m^2}{m^2 + s} \ln\left(\frac{m^2}{-s}\right) + \frac{1}{2} \ln^2\left(\frac{\mu^2}{-s}\right) \right.$$

$$\left. + \ln\left(\frac{\mu^2}{-s}\right) - \text{Li}_2\left(1 - \frac{m^2}{-s}\right) \right\} + \mathcal{O}(\epsilon). \quad (D.7)$$

Finally we use some relations involving dilogs and logs:

$$\text{Li}_2\left(1 - \frac{1}{x}\right) = -\frac{1}{2} \ln^2(x) - \text{Li}_2(1 - x), \quad (D.8)$$

$$\text{Li}_2(1 - x) = \frac{1}{6} \pi^2 - \ln(x) \ln(1 - x) - \text{Li}_2(x), \quad (D.9)$$

which together with $x = \frac{-s}{m^2}$ yields the final result for the integral. With this and the expression from Eq. (D.2) we can write down the result for the first diagram of the jet function which reads:

$$J_a = \frac{i\alpha_s(\mu)C_F}{4\pi} \frac{Q}{s} \frac{\not{n}}{2} \left\{ \frac{2}{\epsilon^2} + \frac{2}{\epsilon} \left[1 + \ln\left(\frac{\mu}{-s}\right) \right] + 4 + \frac{\pi^2}{2} - \frac{2m^2}{m^2 + s} \ln\left(\frac{m^2}{-s}\right) - \ln^2\left(\frac{m^2}{-s}\right) \right.$$

$$\left. + 2 \ln\left(\frac{m^2}{-s}\right) \ln\left(\frac{m^2 + s}{-s}\right) - 2\text{Li}_2\left(\frac{-s}{m^2}\right) + 2 \ln\left(\frac{\mu^2}{-s}\right) + \ln^2\left(\frac{\mu^2}{-s}\right) \right\} + \mathcal{O}(\epsilon).$$

The other contributions are given by:

$$J_b = J_a , \quad (D.11)$$

$$J_c = 0 , \quad (D.12)$$

$$\begin{aligned} J_d &= i \frac{\not{p}}{2} \frac{p^-}{p^2 - m^2 + i0} \int \frac{d^d q}{(2\pi)^d} V_\mu^A(p - q, p, m) i \frac{\not{p}}{2} \frac{p^- - q^-}{(p - q)^2 - m^2 + i0} V_\nu^B(p, p - q, m) \\ &\quad \times \frac{-ig^{\mu\nu} \delta^{AB}}{q^2 + i0} i \frac{\not{p}}{2} \frac{p^-}{p^2 - m^2 + i0} \\ &= 4\pi\alpha_s(\mu) C_F \frac{\not{p}}{2} \frac{Q^2}{s^2} \tilde{\mu}^{2\epsilon} \int \frac{d^d q}{(2\pi)^d} \frac{p^- - q^-}{((p - q)^2 - m^2 + i0)(q^2 + i0)} \left\{ \frac{(d - 2)((p - q)^2 - m^2)}{(p^- - q^-)^2} \right. \\ &\quad \left. + \frac{(d - 2)(p^2 - m^2)}{(p^-)^2} - \frac{2dm^2 + 2(d - 2)p \cdot (p - q)}{p^-(p^- - q^-)} \right\} + \text{Terms} \propto (\text{even } \# \text{ of } \gamma) . \end{aligned} \quad (D.13)$$

Note that from Eq. (6.22) (and the trace therein) we know that only expressions with an odd number of gamma matrices will contribute to the jet function. The remaining contributions are given by²⁰:

$$\begin{aligned} J_e &= \frac{1}{2} i \frac{\not{p}}{2} \frac{p^-}{p^2 - m^2 + i0} \int \frac{d^d q}{(2\pi)^d} W_{\mu\nu}^{AB}(p, p, q, m) \frac{-ig^{\mu\nu} \delta^{AB}}{q^2 + i0} i \frac{\not{p}}{2} \frac{p^-}{p^2 - m^2 + i0} \\ &= -4\pi\alpha_s(\mu) C_F \frac{\not{p}}{2} \frac{Q^2}{s^2} \tilde{\mu}^{2\epsilon} \int \frac{d^d q}{(2\pi)^d} \frac{(d - 2)}{(q^2 + i0)(p^- + q^-)} . \end{aligned} \quad (D.14)$$

Now we sum up the last two contributions (note that the tadpole cancels one term in J_d) and get two integrals:

$$\begin{aligned} J_d + J_e &= 4\pi\alpha_s(\mu) C_F \frac{\not{p}}{2} \frac{Q^2}{s^2} \\ &\quad \times \left\{ \left[\frac{(d - 2)s}{(p^-)^2} \bar{n}_\mu - \frac{2(d - 2)}{p^-} p_\mu \right] \tilde{\mu}^{2\epsilon} \int \frac{d^d q}{(2\pi)^d} \frac{p^\mu - q^\mu}{((p - q)^2 - m^2 + i0)(q^2 + i0)} \right. \\ &\quad \left. - \left[\frac{2dm^2}{p^-} \right] \tilde{\mu}^{2\epsilon} \int \frac{d^d q}{(2\pi)^d} \frac{p^\mu}{((p - q)^2 - m^2 + i0)(q^2 + i0)} \right\} . \end{aligned} \quad (D.15)$$

These two integrals can be solved using Feynman parameters. Expanding in small ϵ yields:

$$\begin{aligned} J_d + J_e &= \frac{i\alpha_s(\mu) C_F}{4\pi} \frac{Q}{s} \frac{\not{p}}{2} \left\{ \frac{m^2}{s} \left[\frac{6}{\epsilon} + 6 \ln \left(\frac{\mu^2}{m^2} \right) + 8 \right] \right. \\ &\quad \left. - \left[\frac{1}{\epsilon} + \ln \left(\frac{\mu^2}{-s} \right) - \frac{m^2(5m^2 + 6s)}{(m^2 + s)^2} \ln \left(\frac{m^2}{-s} \right) + \frac{s}{m^2 + s} \right] \right\} . \end{aligned} \quad (D.16)$$

The last remaining term is the one including the mass counter term. We use a generic mass scheme which is defined via $m - m^{\text{pole}} = \delta m$ (later we switch to the $\overline{\text{MS}}$ -mass scheme, see Sec. 6.5.2) The contribution is given by:

$$\begin{aligned} J_f &= i \frac{\not{p}}{2} \frac{p^-}{p^2 - m^2 + i0} \left(-i \frac{\not{p}}{2} \frac{2m(\delta m^{\text{pole}} + \delta m)}{p^-} \right) i \frac{\not{p}}{2} \frac{p^-}{p^2 - m^2 + i0} \\ &= \frac{i\alpha_s(\mu) C_F}{4\pi} \frac{Q}{s^2} \frac{\not{p}}{2} 2m(\delta m^{\text{pole}} + \delta m) , \end{aligned} \quad (D.17)$$

²⁰Note that J_e involves a symmetry factor for the gluon loop.

where the $\mathcal{O}(\alpha_s)$ pole mass counterterm is given by [27]:

$$\delta m^{\text{pole}} = -m \frac{\alpha_s(\mu) C_F}{4\pi} \left[\frac{3}{\epsilon} + 3 \ln \left(\frac{m^2}{\mu^2} \right) + 4 \right]. \quad (\text{D.18})$$

Now one can observe that there are again some cancellations in the sum of the last three contributions. They are given by:

$$\begin{aligned} J_d + J_e + J_f = & - \frac{i\alpha_s(\mu) C_F}{4\pi} \frac{Q}{s} \frac{\not{p}}{2} \left[\frac{1}{\epsilon} + \ln \left(\frac{\mu^2}{-s} \right) - \frac{m^2(5m^2 + 6s)}{(m^2 + s)^2} \ln \left(\frac{m^2}{-s} \right) + \frac{s}{m^2 + s} \right] \\ & + i \frac{Q}{s^2} \frac{\not{p}}{2} 2m\delta m. \end{aligned} \quad (\text{D.19})$$

To complete this calculation we need to include zero bin subtractions. They can be computed by taking the diagrams which involve a collinear gluon and impose usoft power counting. All of them give zero, hence the sum of all contributing diagrams is given by Eq. (6.21).

D.1.2. Imaginary Part

When evaluating the jet function one needs to compute the different contributing diagrams which was done in the previous subsection and afterwards take the imaginary part. Using $s \equiv s + i0 = \kappa^2 x + i0$ with the dimensionless variable x and a dummy scale $\kappa > 0$ (to keep the right dimension) we can write:

$$\begin{aligned} \hat{J} = & - \frac{1}{\pi} \frac{1}{s + i0} - 2m\delta m \frac{1}{\pi} \frac{1}{s^2 + i0} \\ & - \frac{\alpha_s C_F}{4\pi} \left\{ \frac{1}{\pi} \frac{1}{s + i0} \left[\frac{4}{\epsilon^2} + \frac{3}{\epsilon} + \frac{4}{\epsilon} \ln \left(\frac{\mu^2}{\kappa^2} \right) + 2 \ln^2 \left(\frac{\mu^2}{\kappa^2} \right) + 2 \ln^2 \left(\frac{m^2}{\kappa^2} \right) + 3 \ln \left(\frac{\mu^2}{\kappa^2} \right) + 8 + \pi^2 \right] \right. \\ & + \frac{4}{\pi} \frac{1}{s + i0} \ln \left(\frac{-s - i0}{\kappa^2} \right) \left[-\frac{1}{\epsilon} - \ln \left(\frac{\mu^2}{\kappa^2} \right) - \ln \left(\frac{m^2}{\kappa^2} \right) - \frac{3}{4} \right] + \frac{4}{\pi} \frac{1}{s + i0} \ln^2 \left(\frac{-s - i0}{\kappa^2} \right) \\ & - \frac{4}{\pi} \frac{1}{s + i0} \text{Li}_2 \left(\frac{-s - i0}{m^2} \right) + \frac{4}{\pi} \frac{1}{s + i0} \ln \left(\frac{m^2}{-s - i0} \right) \ln \left(1 + \frac{s + i0}{m^2} \right) - \frac{1}{s + m^2 + i0} \\ & \left. + \frac{1}{\pi} \frac{m^2(m^2 + s)}{s(s + m^2)^2} \ln \left(\frac{m^2}{-s - i0} \right) \right\}, \end{aligned} \quad (\text{D.20})$$

where \hat{J} was defined in Eq. (6.22). To take the imaginary part of this expression we use relations given in [27]. They involve plus distributions (which are defined in Sec. B) and read:

$$\frac{1}{\pi} \text{Im} \left\{ \frac{1}{s + i0} \right\} = \frac{1}{\kappa^2} (-\delta(x)) = -\delta(s), \quad (\text{D.21})$$

$$\frac{1}{\pi} \text{Im} \left\{ \frac{\ln(-x - i0)}{s + i0} \right\} = - \left[\frac{\theta(x)}{x} \right]_+ \frac{1}{\kappa^2}, \quad (\text{D.22})$$

$$\frac{1}{\pi} \text{Im} \left\{ \frac{\ln^2(-x - i0)}{s + i0} \right\} = \left(\frac{\pi^2}{3} \delta(x) - 2 \left[\frac{\theta(x) \ln(x)}{x} \right]_+ \right) \frac{1}{\kappa^2}, \quad (\text{D.23})$$

$$\frac{1}{\pi} \text{Im} \left\{ \frac{1}{s+i0} \text{Li}_2 \left(\frac{-s-i0}{m^2} \right) \right\} = -\frac{1}{s} \ln \left(\frac{-s}{m^2} \right) \theta(-m^2-s), \quad (\text{D.24})$$

$$\begin{aligned} \frac{1}{\pi} \text{Im} \left\{ \frac{1}{s+i0} \ln \left(\frac{m^2}{-s-i0} \right) \ln \left(1 + \frac{s+i0}{m^2} \right) \right\} \\ = \frac{1}{s} \ln \left(\frac{m^2}{-s} \right) \theta(-m^2-s) + \frac{1}{\kappa^2} \left[\frac{\theta(x)}{x} \right]_+ \ln \left(1 + \frac{s}{m^2} \right), \end{aligned} \quad (\text{D.25})$$

$$\begin{aligned} \frac{1}{\pi} \text{Im} \left\{ \frac{m^2(m^2+s)}{s(s+m^2)^2} \ln \left(\frac{m^2}{-s-i0} \right) \right\} \\ = -\delta(s) \ln \left(\frac{m^2}{\kappa^2} \right) + \frac{1}{\kappa^2} \left[\frac{\theta(x)}{x} \right]_+ - \frac{\theta(s)s}{(s+m^2)^2} + m^2 \ln \left(\frac{m^2}{-s} \right) \delta'(s+m^2). \end{aligned} \quad (\text{D.26})$$

Since we are working within an s integration (this can be seen in the factorization theorem) the following identities also hold:

$$\int ds \left[-\text{Im} \left\{ \frac{1}{s+m^2+i0} \right\} - m^2 \ln \left(\frac{m^2}{-s} \right) \delta'(s+m^2) \right] = 0, \quad (\text{D.27})$$

$$\int ds \left[-\frac{4}{\kappa^2} \left[\frac{\kappa^2 \theta(s)}{s} \right]_+ \ln \left(1 + \frac{s}{m^2} \right) \right] = \int ds \left[-\frac{4}{s} \ln \left(1 + \frac{s}{m^2} \right) \theta(s) \right]. \quad (\text{D.28})$$

Using the above relations as well as Eq. (D.20) and (6.22) we can determine the hemisphere jet function. Afterwards we set $\kappa = \mu$ and simplify the expression which yields the final result given in Eq. (6.23).

D.2. Hard Function

As promised in Sec. 6.2.1 we intend to give details on the calculation of the SCET matrix element used for matching SCET on QCD. To get the physical matrix element one has to evaluate the diagrams of Fig. 7. We start with the first diagram (omit spinors, use SCET power counting and the on-shell relation):

$$\begin{aligned} H_a &= \int \frac{d^d q}{(2\pi)^d} V_\alpha^A(p, p-q, m) i \not{q} \frac{p^- - q^-}{2(p-q)^2 - m^2 + i0} \left(g_s \frac{T^B \bar{n}_\beta}{q^- + i0} \tilde{\mu}^\epsilon \right) \Gamma_i^\mu \frac{-i g^{\alpha\beta} \delta^{AB}}{q^2 + i0} \\ &= 8\pi i \alpha_s(\mu) C_F \Gamma_i^\mu I_a(0, m^2, \mu), \end{aligned} \quad (\text{D.29})$$

where I_a is the integral known from the first diagram of the jet function defined in Eq. (D.2). In the previous subsection it was determined for a non-zero off-shellness. It is easy to adapt it for zero off-shellness by starting with Eq. (D.6). By performing the same substitution as in the previous calculation we get:

$$\begin{aligned} I_a(0, m^2, \mu) &= \frac{-i 2^{-d} \pi^{1-\frac{d}{2}} \tilde{\mu}^{4-d} \csc(\frac{d\pi}{2})}{\Gamma(\frac{d-2}{2})} \int_0^1 dz \frac{(1-z)}{z} [(Qp^+) z^2]^{\frac{d}{2}-2} \\ &= \frac{-i 2^{-d} \pi^{1-\frac{d}{2}} \csc(\frac{d\pi}{2})}{\Gamma(\frac{d-2}{2})} \left(\frac{\mu^2 \exp(\gamma_E)}{m^2 4\pi} \right)^{2-\frac{d}{2}} B(d-4, 2). \end{aligned} \quad (\text{D.30})$$

Next we set $d = 4 - 2\epsilon$ and expand for small ϵ . Then Eq. (D.29) reads:

$$H_a = \Gamma_i^\mu \frac{\alpha_s(\mu) C_F}{4\pi} \left\{ \frac{1}{\epsilon^2} + \frac{1}{\epsilon} \left[2 + \ln \left(\frac{\mu^2}{m^2} \right) \right] + \frac{1}{2} \ln^2 \left(\frac{\mu^2}{m^2} \right) + 2 \ln \left(\frac{\mu^2}{m^2} \right) + 4 + \frac{\pi^2}{12} \right\}. \quad (\text{D.31})$$

The remaining two diagrams are given by:

$$H_b = H_a, \quad (D.32)$$

$$\begin{aligned} H_c &= \int \frac{d^d q}{(2\pi)^d} (ig_s T^A \tilde{\mu}^\epsilon) n_\alpha \frac{\not{q}}{2} i \frac{\not{q}}{2} \frac{p^- + q^-}{(p+q)^2 - m^2 + i0} \Gamma_i^\mu i \frac{\not{q}}{2} \frac{-p'^+ + q^+}{(p-q)^2 - m^2 + i0} \\ &\quad \times (ig_s T^A \tilde{\mu}^\epsilon) \bar{n}_\beta \frac{\not{q}}{2} \frac{-ig^{\alpha\beta} \delta^{AB}}{q^2 + i0} \\ &= 0. \end{aligned} \quad (D.33)$$

Here one can see that the third diagram vanishes when using standard methods like Feynman parameters. To get the physical matrix elements we have to multiply a factor of $(Z_\psi^{\text{OS}})^{-1/2}$ (see Eq. (3.57)) per external leg which yields to the final result of the SCET matrix element given in Eq. (6.17).

D.3. Partonic Soft Function

In this subsection we will give details on the evaluation of the different contributions to the $\mathcal{O}(\alpha_s)$ partonic soft function. These diagrams are shown in Fig. 9 and involve Y-Wilson lines (introduced in Sec. 4.3.2) as well as a final state cut. The partonic soft function is given by (see Eq. (5.25); with color indices):

$$S_c(\ell, \mu) = \frac{1}{N_c} \sum_{X_s} \delta\left(\ell - \frac{k_s^- k_s^+}{k_s^- + k_s^+}\right) \langle 0 | \bar{Y}_n^{cd} Y_n^{ce}(0) | X_s \rangle \langle X_s | Y_n^{\dagger ef} \bar{Y}_n^{\dagger df}(0) | 0 \rangle. \quad (D.34)$$

Using SCET Feynman rules the diagrams are given by:

$$\begin{aligned} S_a &= \int \frac{d^d q}{(2\pi)^d} \left(-g_s \frac{\bar{T}^A \bar{n}_\mu}{q^- + i0} \tilde{\mu}^\epsilon \right) \frac{-ig^{\mu\nu} \delta^{AB}}{q^2 + i0} \left(g_s \frac{T^B n_\nu}{q^+ - i0} \tilde{\mu}^\epsilon \right) \\ &= 2ig_s^2 \bar{T}^A T^A \tilde{\mu}^\epsilon \int \frac{d^d q}{(2\pi)^d} \frac{1}{(q^- + i0)(q^+ - i0)(q^2 + i0)} = 0, \end{aligned} \quad (D.35)$$

$$S_b = S_a. \quad (D.36)$$

The next diagrams involve real radiation which is why we apply Cutkosky's rule and later impose an on-shell condition (see Eq. (6.28)). Furthermore the delta function which implements kinematic constraints on the final state gluon is included. We use $T_{de}^A \bar{T}_{de}^A = -T_{de}^A T_{ed}^A = -N_c C_F$ and get:

$$\begin{aligned} S_c &= \int \frac{d^d k_s}{(2\pi)^4} \delta\left(\ell - \frac{k_s^- k_s^+}{k_s^- + k_s^+}\right) \delta^{ef} \left(-g_s \frac{\bar{T}_{df}^A \bar{n}_\mu}{k_s^- + i0} \tilde{\mu}^\epsilon \right) (2\pi) \delta(k_s^2) g^{\mu\nu} \delta^{AB} \left(-g_s \frac{T_{ce}^B n_\nu}{k_s^+ - i0} \tilde{\mu}^\epsilon \right) \delta^{cd} \\ &= 2g_s^2 N_c C_F \tilde{\mu}^{2\epsilon} \int \frac{d^d k_s}{(2\pi)^4} \delta\left(\ell - \frac{k_s^- k_s^+}{k_s^- + k_s^+}\right) \frac{(2\pi) \delta(k_s^2)}{(k_s^+ - i0)(k_s^- + i0)}, \end{aligned} \quad (D.37)$$

$$S_d = S_c. \quad (D.38)$$

The remaining contributions evaluate to zero:

$$S_e = S_g \propto \bar{n} \cdot \bar{n} = 0, \quad (D.39)$$

$$S_f = S'_g \propto n \cdot n = 0. \quad (D.40)$$

This concludes the determination of the diagrams contributing to the partonic soft function. In the end we have two non-zero contributions given in Eq. (D.37) and (D.38) which are plugged in the soft function definition in Eq. (6.27) to yield the final result of Eq. (6.31).

E. Evolution

E.1. Anomalous Dimensions and Evolution Kernels

In Sec. 6.2.4 all the ingredients for the N²LL K and ω were given. One can obtain the full expression by correctly expanding the defining equation given in Eq. (6.3). Our result agrees with [10] and reads:

$$\begin{aligned}\omega^{\text{N}^3\text{LL}}(\mu, \mu_0, \Gamma, j) &= \frac{2}{j} \int_{\alpha_s(\mu_0)}^{\alpha_s(\mu)} d\alpha \frac{\Gamma[\alpha]}{\beta[\alpha]} \\ &= \frac{\Gamma_0}{\beta_0 j} \left[-\ln(r) + \frac{\alpha_s(\mu_0)}{4\pi} \left(\frac{\beta_1}{\beta_0} - \frac{\Gamma_1}{\Gamma_0} \right) (r-1) + \frac{1}{2} \left(\frac{\alpha_s(\mu_0)}{4\pi} \right)^2 \left(\frac{\beta_2}{\beta_0} + \frac{\beta_1 \Gamma_1}{\beta_0 \Gamma_0} - \frac{\beta_1^2}{\beta_0^2} - \frac{\Gamma_2}{\Gamma_0} \right) (r^2-1) \right. \\ &\quad \left. + \frac{1}{3} \left(\frac{\alpha_s(\mu_0)}{4\pi} \right)^3 \left(\frac{\beta_1^3}{\beta_0^3} - \frac{2\beta_1 \beta_2}{\beta_0^2} + \frac{\beta_3}{\beta_0} - \frac{\beta_1^2 \Gamma_1}{\beta_0^2 \Gamma_0} + \frac{\beta_2 \Gamma_1}{\beta_0 \Gamma_0} + \frac{\beta_1 \Gamma_2}{\beta_0 \Gamma_0} - \frac{\Gamma_3}{\Gamma_0} \right) (r^3-1) \right],\end{aligned}\quad (\text{E.1})$$

$$\begin{aligned}K^{\text{N}^2\text{LL}}(\mu, \mu_0, \Gamma, \gamma) - \omega^{\text{N}^2\text{LL}}(\mu, \mu_0, \gamma, 2) &= 2 \int_{\alpha_s(\mu_0)}^{\alpha_s(\mu)} d\alpha \frac{\Gamma[\alpha]}{\beta[\alpha]} \int_{\alpha_s(\mu_0)}^{\alpha} \frac{d\alpha'}{\beta[\alpha']} \\ &= \frac{\Gamma_0}{2\beta_0^2} \left[\frac{4\pi}{\alpha_s(\mu_0)} \left(\frac{1}{r} + \ln(r) - 1 \right) + \left(\frac{\Gamma_1}{\Gamma_0} - \frac{\beta_1}{\beta_0} \right) \left[r - 1 - \ln(r) \right] - \frac{\beta_1}{2\beta_0} \ln^2(r) \right. \\ &\quad \left. + \frac{\alpha_s(\mu_0)}{4\pi} \left[\left(\frac{\Gamma_1 \beta_1}{\Gamma_0 \beta_0} - \frac{\beta_1^2}{\beta_0^2} \right) \left[r - 1 - r \ln(r) \right] - B_2 \ln(r) + \left(\frac{\Gamma_2}{\Gamma_0} - \frac{\Gamma_1 \beta_1}{\Gamma_0 \beta_0} + B_2 \right) \frac{(r^2-1)}{2} \right. \right. \\ &\quad \left. \left. + \left(\frac{\Gamma_2}{\Gamma_0} - \frac{\Gamma_1 \beta_1}{\Gamma_0 \beta_0} \right) (1-r) \right] \right].\end{aligned}\quad (\text{E.2})$$

where the $B_2 = \beta_1^2/\beta_0^2 - \beta_2/\beta_0$ and $r = \alpha_s(\mu)/\alpha_s(\mu_0)$ which depends on the 4-loop running coupling.

E.2. R-Evolution

In Sec. 6.5.1 we introduced the non-perturbative gap parameter $\bar{\Delta}(R, \mu_S)$. Furthermore we observed that to avoid large logarithms we need to know how this parameter evolves in R and μ_S . An overview about this was already given in [10]. The two corresponding RG equations are defined as:

$$\begin{aligned}\mu \frac{d\bar{\Delta}(R, \mu)}{d\mu} &= -R \gamma_{\bar{\Delta}}^{\mu}[\alpha_s(\mu)], & \gamma_{\bar{\Delta}}^{\mu}[\alpha_s(\mu)] &= \sum_{i=0} \gamma_{\bar{\Delta},i}^{\mu} \left(\frac{\alpha_s(\mu)}{4\pi} \right)^{i+1}, \\ R \frac{d\bar{\Delta}(R, R)}{dR} &= -R \gamma_{\bar{\Delta}}^R[\alpha_s(\mu)], & \gamma_{\bar{\Delta}}^R[\alpha_s(\mu)] &= \sum_{i=0} \gamma_{\bar{\Delta},i}^R \left(\frac{\alpha_s(\mu)}{4\pi} \right)^{i+1}.\end{aligned}\quad (\text{E.3})$$

From Eq. (6.71) it is straightforward to see that the μ evolution is completely governed by the anomalous dimension of the soft function which is why we encounter the known ω expression. Furthermore the R anomalous dimension is given by:

$$\gamma_{\bar{\Delta},0}^R = 0, \quad \gamma_{\bar{\Delta},1}^R = e^{\gamma_E} (2s_1^c \beta_0 + \gamma_{S,1}) = 152.422, \quad (\text{E.4})$$

where we used $s_1^c = -C_F \pi^2/3$ defined through Eq. (6.70) and for the numerical values $n_f = 5$. For the whole derivation of the R -evolution we refer to [44, 45]. The solution to the μ and R evolution

of $\bar{\Delta}$ to N²LL accuracy is given by:

$$\begin{aligned} \bar{\Delta}(R, \mu) = & \bar{\Delta}(R_0, \mu_0) - 2 R_0 e^{\gamma_E} \omega^{\text{NLL}}(R_0, \mu_0, \Gamma_S, 2) - 2 R e^{\gamma_E} \omega^{\text{NLL}}(\mu, R, \Gamma_S, 2) \\ & + \Lambda_{\text{QCD}}^{(2)} S_1 e^{i\pi b_1} \left[\Gamma(-b_1 - 1, -\frac{2\pi}{\beta_0 \alpha_s(R)}) - \Gamma(-b_1 - 1, -\frac{2\pi}{\beta_0 \alpha_s(R_0)}) \right], \end{aligned} \quad (\text{E.5})$$

where we used the known incomplete gamma function and:

$$\begin{aligned} b_1 = \frac{\beta_1}{2\beta_0^2}, \quad b_2 = \frac{\beta_1^2 - \beta_0 \beta_2}{4\beta_0^4}, \\ S_1 = \frac{\gamma_{\bar{\Delta},1}^R}{(2\beta_0)^2}. \end{aligned} \quad (\text{E.6})$$

Note that since ω is not exponentiated the NLL result is sufficient. Furthermore for $\Lambda_{\text{QCD}}^{(2)}$ we use [44]:

$$\Lambda_{\text{QCD}}^{(2)} = R_\Lambda \exp\left(-\frac{2\pi}{\beta_0 \alpha_s(R_\Lambda)}\right) \left(\frac{2\pi}{\beta_0 \alpha_s(R_\Lambda)}\right)^{b_1} \exp\left(\frac{b_2 \beta_0 \alpha_s(R_\Lambda)}{2\pi}\right), \quad (\text{E.7})$$

and choose $R_\Lambda = 100$ GeV.

E.3. Evolution of α_s and the $\overline{\text{MS}}$ Mass

In Sec. 6.1 we introduced the QCD beta function. For a review about its determinations and the original literature see [52]. The beta function is defined in the α_s -RG equation [48]:

$$\mu \frac{d\alpha_s}{d\mu}(\mu) = \beta[\alpha_s(\mu)] = -\frac{\alpha_s^2(\mu)}{2\pi} \sum_{i=0} \beta_i \left(\frac{\alpha_s}{4\pi}\right)^i, \quad (\text{E.8})$$

where the involved β_i 's read:

$$\begin{aligned} \beta_0 &= 11 - \frac{2}{3}n_f, \\ \beta_1 &= 102 - \frac{38}{3}n_f, \\ \beta_2 &= \frac{2857}{2} - \frac{5033}{18}n_f + \frac{325}{54}n_f^2, \\ \beta_3 &= \frac{149753}{6} + 3564\zeta_3 + \left(-\frac{1078361}{162} - \frac{6508}{27}\zeta_3\right)n_f + \left(\frac{50065}{162} + \frac{6472}{81}\zeta_3\right)n_f^2 + \frac{1093}{729}n_f^3. \end{aligned} \quad (\text{E.9})$$

The 4-loop evolution is then given by solving Eq. (E.8) iteratively. Using $\rho = 1 + \frac{\alpha_s(\mu_0)\beta_0}{2\pi} \ln(\mu/\mu_0)$ the evolution reads:

$$\begin{aligned} \frac{1}{\alpha_s(\mu)} = & \frac{\rho}{\alpha_s(\mu_0)} + \frac{\beta_1 \ln(\rho)}{4\pi\beta_0} + \frac{\alpha_s(\mu_0)}{\rho} \frac{1}{(4\pi\beta_0)^2} \left[(\beta_1^2 - \beta_0\beta_2)(1 - \rho) + \beta_1^2 \ln(\rho) \right] \\ & + \frac{\alpha_s(\mu_0)^2}{\rho^2} \frac{1}{(4\pi\beta_0)^3} \left[\frac{\beta_0^2\beta_3}{2}(\rho^2 - 1) + \beta_0\beta_1\beta_2(\log(\rho) + \rho - \rho^2) + \frac{\beta_1^3}{2}\{(1 - \rho^2)^2 - \log^2(\rho)\} \right], \end{aligned} \quad (\text{E.10})$$

which numerically agrees with the expression given in [10]. Furthermore in Sec. 6.5.2 we switched mass schemes to the $\overline{\text{MS}}$ mass which RG equation is given by: [48]:

$$\mu \frac{d\overline{m}}{d\mu}(\mu) = \overline{m}(\mu) \gamma_m[\alpha_s(\mu)] = -2\overline{m}(\mu) \sum_{i=0} \gamma_{m,i} \left(\frac{\alpha_s}{4\pi} \right)^{i+1}, \quad (\text{E.11})$$

with:

$$\begin{aligned} \gamma_{m,0} &= 4, \\ \gamma_{m,1} &= \frac{202}{3} - \frac{20}{9}n_f, \\ \gamma_{m,2} &= 1249 - \left(\frac{2216}{27} + \frac{160}{3}\zeta_3 \right)n_f - \frac{140}{81}n_f^2, \\ \gamma_{m,3} &= \frac{4603055}{162} - \frac{135680}{27}\zeta_3 - 8800\zeta_5 + \left(-\frac{91723}{27} - \frac{34192}{9}\zeta_3 + 880\zeta_4 + \frac{18400}{9}\zeta_5 \right)n_f \\ &\quad + \left(\frac{5242}{243} + \frac{800}{9}\zeta_3 - \frac{160}{3}\zeta_4 \right)n_f^2 + \left(-\frac{332}{243} + \frac{64}{27}\zeta_3 \right)n_f^3. \end{aligned} \quad (\text{E.12})$$

The 4-loop evolution of the $\overline{\text{MS}}$ mass is then given by solving Eq. (E.11) iteratively where one encounters the expression of Eq. (E.1). The 4-loop evolution is then given by:

$$\overline{m}(\mu) = \exp \left[-2 \omega^{\text{N}^3\text{LL}}(\mu, \mu_0, \gamma_m, 2) \right] \overline{m}(\mu_0). \quad (\text{E.13})$$

References

- [1] M. Dasgupta and G. P. Salam, “Event shapes in e^+e^- annihilation and deep inelastic scattering,” *J.Phys.* **G30** (2004) R143, [arXiv:hep-ph/0312283](#) [hep-ph].
- [2] S. Kluth, “Tests of Quantum Chromo Dynamics at e^+e^- Colliders,” *Rept.Prog.Phys.* **69** (2006) 1771–1846, [arXiv:hep-ex/0603011](#) [hep-ex].
- [3] S. Catani, L. Trentadue, G. Turnock, and B. Webber, “Resummation of large logarithms in e^+e^- event shape distributions,” *Nucl.Phys.* **B407** (1993) 3–42.
- [4] S. Catani and B. Webber, “Resummed C parameter distribution in e^+e^- annihilation,” *Phys.Lett.* **B427** (1998) 377–384, [arXiv:hep-ph/9801350](#) [hep-ph].
- [5] C. W. Bauer, S. Fleming, and M. E. Luke, “Summing Sudakov logarithms in $B \rightarrow X_s \gamma$ in effective field theory,” *Phys.Rev.* **D63** (2000) 014006, [arXiv:hep-ph/0005275](#) [hep-ph].
- [6] C. W. Bauer, S. Fleming, D. Pirjol, and I. W. Stewart, “An Effective field theory for collinear and soft gluons: Heavy to light decays,” *Phys.Rev.* **D63** (2001) 114020, [arXiv:hep-ph/0011336](#) [hep-ph].
- [7] C. W. Bauer and I. W. Stewart, “Invariant operators in collinear effective theory,” *Phys.Lett.* **B516** (2001) 134–142, [arXiv:hep-ph/0107001](#) [hep-ph].
- [8] C. W. Bauer, D. Pirjol, and I. W. Stewart, “Soft collinear factorization in effective field theory,” *Phys.Rev.* **D65** (2002) 054022, [arXiv:hep-ph/0109045](#) [hep-ph].
- [9] C. W. Bauer, S. Fleming, D. Pirjol, I. Z. Rothstein, and I. W. Stewart, “Hard scattering factorization from effective field theory,” *Phys.Rev.* **D66** (2002) 014017, [arXiv:hep-ph/0202088](#) [hep-ph].
- [10] R. Abbate, M. Fickinger, A. H. Hoang, V. Mateu, and I. W. Stewart, “Thrust at N^3LL with Power Corrections and a Precision Global Fit for $\alpha_s(m_Z)$,” *Phys.Rev.* **D83** (2011) 074021, [arXiv:1006.3080](#) [hep-ph].
- [11] R. Abbate, M. Fickinger, A. H. Hoang, V. Mateu, and I. W. Stewart, “Precision Thrust Cumulant Moments at N^3LL ,” *Phys.Rev.* **D86** (2012) 094002, [arXiv:1204.5746](#) [hep-ph].
- [12] A. H. Hoang, D. W. Kolodrubetz, V. Mateu, and I. W. Stewart. (*in preparation*).
- [13] S. Gritschacher, A. H. Hoang, I. Jemos, and P. Pietrulewicz, “Secondary Heavy Quark Production in Jets through Mass Modes,” *Phys.Rev.* **D88** (2013) 034021, [arXiv:1302.4743](#) [hep-ph].
- [14] P. Pietrulewicz, S. Gritschacher, A. H. Hoang, I. Jemos, and V. Mateu, “Variable Flavor Number Scheme for Final State Jets in Thrust,” [arXiv:1405.4860](#) [hep-ph].
- [15] M. Butenschön, B. Dehnadi, A. H. Hoang, and V. Mateu. (*in preparation*).
- [16] R. K. Ellis, D. Ross, and A. Terrano, “The Perturbative Calculation of Jet Structure in e^+e^- Annihilation,” *Nucl.Phys.* **B178** (1981) 421.
- [17] G. Parisi, “Super Inclusive Cross-Sections,” *Phys.Lett.* **B74** (1978) 65.
- [18] J. F. Donoghue, F. Low, and S.-Y. Pi, “Tensor Analysis of Hadronic Jets in Quantum Chromodynamics,” *Phys.Rev.* **D20** (1979) 2759.
- [19] E. Gardi and L. Magnea, “The C parameter distribution in e^+e^- annihilation,” *JHEP* **0308** (2003) 030, [arXiv:hep-ph/0306094](#) [hep-ph].
- [20] K. Chetyrkin, J. H. Kuhn, and A. Kwiatkowski, “QCD corrections to the e^+e^- cross-section and the Z boson decay rate: Concepts and results,” *Phys.Rept.* **277** (1996) 189–281.

- [21] R. Mertig, M. Bohm, and A. Denner, “FEYN CALC: Computer algebraic calculation of Feynman amplitudes,” *Comput.Phys.Commun.* **64** (1991) 345–359.
- [22] B. Ioffe, “Associated Production of gluonic jets in heavy mesons in e^+e^- annihilation,” *Phys.Lett.* **B78** (1978) 277.
- [23] A. Erdélyi, *Higher Transcendental Functions, Vol. 2*. McGraw-Hill, 1953.
- [24] R. K. Ellis and G. Zanderighi, “Scalar one-loop integrals for QCD,” *JHEP* **0802** (2008) 002, [arXiv:0712.1851 \[hep-ph\]](#).
- [25] J. Jersak, E. Laermann, and P. Zerwas, “Electroweak Production of Heavy Quarks in e^+e^- Annihilation,” *Phys.Rev.* **D25** (1982) 1218.
- [26] S. Fleming, A. H. Hoang, S. Mantry, and I. W. Stewart, “Jets from massive unstable particles: Top-mass determination,” *Phys.Rev.* **D77** (2008) 074010, [arXiv:hep-ph/0703207 \[hep-ph\]](#).
- [27] S. Fleming, A. H. Hoang, S. Mantry, and I. W. Stewart, “Top Jets in the Peak Region: Factorization Analysis with NLL Resummation,” *Phys.Rev.* **D77** (2008) 114003, [arXiv:0711.2079 \[hep-ph\]](#).
- [28] A. K. Leibovich, Z. Ligeti, and M. B. Wise, “Comment on quark masses in SCET,” *Phys.Lett.* **B564** (2003) 231–234, [arXiv:hep-ph/0303099 \[hep-ph\]](#).
- [29] A. V. Manohar and I. W. Stewart, “The Zero-Bin and Mode Factorization in Quantum Field Theory,” *Phys.Rev.* **D76** (2007) 074002, [arXiv:hep-ph/0605001 \[hep-ph\]](#).
- [30] C. W. Bauer, S. P. Fleming, C. Lee, and G. F. Sterman, “Factorization of e^+e^- Event Shape Distributions with Hadronic Final States in Soft Collinear Effective Theory,” *Phys.Rev.* **D78** (2008) 034027, [arXiv:0801.4569 \[hep-ph\]](#).
- [31] V. Mateu, I. W. Stewart, and J. Thaler, “Power Corrections to Event Shapes with Mass-Dependent Operators,” *Phys.Rev.* **D87** (2013) 014025, [arXiv:1209.3781 \[hep-ph\]](#).
- [32] C. Nishi, “Simple derivation of general Fierz-like identities,” *Am.J.Phys.* **73** (2005) 1160–1163, [arXiv:hep-ph/0412245 \[hep-ph\]](#).
- [33] A. H. Hoang and I. W. Stewart, “Designing gapped soft functions for jet production,” *Phys.Lett.* **B660** (2008) 483–493, [arXiv:0709.3519 \[hep-ph\]](#).
- [34] L. G. Almeida, S. D. Ellis, C. Lee, G. Sterman, I. Sung, *et al.*, “Comparing and counting logs in direct and effective methods of QCD resummation,” *JHEP* **1404** (2014) 174, [arXiv:1401.4460 \[hep-ph\]](#).
- [35] T. Becher, M. Neubert, and B. D. Pecjak, “Factorization and Momentum-Space Resummation in Deep-Inelastic Scattering,” *JHEP* **0701** (2007) 076, [arXiv:hep-ph/0607228 \[hep-ph\]](#).
- [36] T. Becher and M. Neubert, “Toward a NNLO calculation of the $\bar{B} \rightarrow X_s \gamma$ decay rate with a cut on photon energy. II. Two-loop result for the jet function,” *Phys.Lett.* **B637** (2006) 251–259, [arXiv:hep-ph/0603140 \[hep-ph\]](#).
- [37] B. Webber, “Renormalon phenomena in jets and hard processes,” *Nucl.Phys.Proc.Suppl.* **71** (1999) 66–75, [arXiv:hep-ph/9712236 \[hep-ph\]](#).
- [38] C. Lee and G. F. Sterman, “Universality of nonperturbative effects in event shapes,” *eConf* **C0601121** (2006) A001, [arXiv:hep-ph/0603066 \[hep-ph\]](#).
- [39] Z. Ligeti, I. W. Stewart, and F. J. Tackmann, “Treating the b quark distribution function with reliable uncertainties,” *Phys.Rev.* **D78** (2008) 114014, [arXiv:0807.1926 \[hep-ph\]](#).

- [40] M. Beneke, “Renormalons,” *Phys.Rept.* **317** (1999) 1–142, [arXiv:hep-ph/9807443](#) [hep-ph].
- [41] V. I. Zakharov, “QCD perturbative expansions in large orders,” *Nucl.Phys.* **B385** (1992) 452–480.
- [42] I. I. Bigi, M. A. Shifman, N. Uraltsev, and A. Vainshtein, “The Pole mass of the heavy quark. Perturbation theory and beyond,” *Phys.Rev.* **D50** (1994) 2234–2246, [arXiv:hep-ph/9402360](#) [hep-ph].
- [43] A. Jain, I. Scimemi, and I. W. Stewart, “Two-loop Jet-Function and Jet-Mass for Top Quarks,” *Phys.Rev.* **D77** (2008) 094008, [arXiv:0801.0743](#) [hep-ph].
- [44] A. H. Hoang, A. Jain, I. Scimemi, and I. W. Stewart, “Infrared Renormalization Group Flow for Heavy Quark Masses,” *Phys.Rev.Lett.* **101** (2008) 151602, [arXiv:0803.4214](#) [hep-ph].
- [45] A. H. Hoang, A. Jain, I. Scimemi, and I. W. Stewart, “R-evolution: Improving perturbative QCD,” *Phys.Rev.* **D82** (2010) 011501, [arXiv:0908.3189](#) [hep-ph].
- [46] A. Hoang, M. Smith, T. Stelzer, and S. Willenbrock, “Quarkonia and the pole mass,” *Phys.Rev.* **D59** (1999) 114014, [arXiv:hep-ph/9804227](#) [hep-ph].
- [47] M. Beneke, “A Quark mass definition adequate for threshold problems,” *Phys.Lett.* **B434** (1998) 115–125, [arXiv:hep-ph/9804241](#) [hep-ph].
- [48] K. Chetyrkin, J. H. Kuhn, and M. Steinhauser, “RunDec: A Mathematica package for running and decoupling of the strong coupling and quark masses,” *Comput.Phys.Commun.* **133** (2000) 43–65, [arXiv:hep-ph/0004189](#) [hep-ph].
- [49] A. H. Hoang and I. W. Stewart, “Top Mass Measurements from Jets and the Tevatron Top-Quark Mass,” *Nucl.Phys.Proc.Suppl.* **185** (2008) 220–226, [arXiv:0808.0222](#) [hep-ph].
- [50] I. W. Stewart, “Lecture on effective field theory.” Lecture notes, 2013. http://ocw.mit.edu/courses/physics/8-851-effective-field-theory-spring-2013/lecture-notes/MIT8_851S13_scetnotes.pdf. [Online; accessed 2014-05-26].
- [51] T. Huber and D. Maitre, “HypExp: A Mathematica package for expanding hypergeometric functions around integer-valued parameters,” *Comput.Phys.Commun.* **175** (2006) 122–144, [arXiv:hep-ph/0507094](#) [hep-ph].
- [52] A. Pich, “Review of α_s determinations,” *PoS ConfinementX* (2012) 022, [arXiv:1303.2262](#) [hep-ph].
- [53] D. Binosi and L. Theussl, “JaxoDraw: A Graphical user interface for drawing Feynman diagrams,” *Comput.Phys.Commun.* **161** (2004) 76–86, [arXiv:hep-ph/0309015](#) [hep-ph].

Acknowledgements

First I would like to thank Prof. Hoang for the countless discussions and helpful guidance throughout this work and also that he gave me the opportunity to write my thesis in the excellent environment of the particle physics group at the University of Vienna.

Furthermore I am deeply grateful to Dr. Vicent Mateu for taking the time to deal with my questions and confusions which, I assume, was not always easy. Although it is not official, he clearly took the part of being the second supervisor of this thesis for which I want to thank him.

Also I would like to thank all the members of the particle physics group for providing such a personal and motivated environment. I especially enjoyed the lunch and coffee breaks which I shared with Bahman, Daniel, Piotr and Vicent. The mixture of serious discussions and funny conversations was always relaxing and very refreshing.

Of course I would also like to thank my other colleagues and friends. On purpose I will not write down a list of names because I could never think of a complete list. The people I am talking about hopefully know that I will always be thankful for the wonderful time we spent together.

Lastly I would like to thank my family for encouraging me to follow my interests. I am especially indebted to my parents for their lifelong support which made it possible to write this thesis.

Curriculum Vitae

Personal Data

Last Name:	Preißer
First Name:	Moritz
Place of Birth:	Salzburg (Austria)
Nationality:	Austria
E-mail:	moritz.preisser@gmail.com

Education

since 2012	Master program in Physics at University of Vienna
2012	Bachelor of Science (with distinction) Bachelor Thesis: “The Relativistic Hydrogen Atom” Supervisor: ao. Univ.-Prof. Dr. Bernhard Baumgartner
2009 - 2012	Bachelor program in Physics at University of Vienna
2008	Matura at Höhere Technische Bundeslehranstalt Salzburg - Bauwesen

Other Skills

Language Skills	German (native), English (fluent)
Programming Skills	C, C++, Ruby, Fortran (basic), Python (basic), \LaTeX , Mathematica